Doctoral Thesis

Theses at NTNU, 2008:38

Jostein Bakkeheim

Improved Transient Performance by Lyapunov-based Reset of Dynamic Controllers

NTNU
Norwegian University of
Science and Technology
Thesis for the degree of
philosophiae doctor
Faculty of Information Technology, Mathematics and
Electrical Engineering
Department of Engineering Cybernetics

NTNU
Norwegian University of
Science and Technology

Jostein Bakkeheim

Improved Transient Performance by Lyapunov-based Reset of Dynamic Controllers

Thesis for the degree of philosophiae doctor

Trondheim, April 2008

Norwegian University of
Science and Technology
Faculty of Information Technology, Mathematics and Electrical Engineering
Department of Engineering Cybernetics

Summary

Many control applications implemented in the industry are optimized for use in normal conditions. However, special or extreme conditions may occur, i.e. sudden changes in the environmental parameters or the controller set-points. These incidents may lead to unsatisfactory performance of the closed-loop system. A dynamic controller may, in the first place, interpret this as measurement noise to be ignored, as a result of being optimized for steady-state noise performance. Adaptive controllers are often designed in order to achieve asymptotic stability (AS) requirements, hence the transient performance may only be satisfactory for slow varying environmental parameters and controller set-points.

In this thesis, a framework for improving controller performance in such situations is presented, followed by three application examples.

The framework is presenting a controller strategy using a Lyapunov-based resetting mechanism, changing one or more of the controller states to a different value when an extreme situation is detected. The controller states are reset to a different value if this leads to a drop in the Lyapunov function value. An appropriately selected Lyapunov function is expected to lead to a controller with increased transient performance. In this way, the Lyapunov function is used both as a part in the controller algorithm and as a tool for proving stability for the whole controller system.

The system performance may then be divided into two separate regimes, having two separate sets of specifications and tuning variables being decoupled from each other. Performance close to steady-state, being one of the regimes, is typically tuned in order to handle normal conditions. In the other regime, however, a separate part of the controller is having a fast reacting performance, triggered by sudden changes in the environmental parameters or the controller set-points. This regime is referred to as the systems transient regime. The fast reacting performance in this regime typically leads to reduced measurement noise suppressions, but if appropriately tuned, this will only be triggered when severe changes in the environmental parameters or the controller set-points is measured. In this way, the steady-state noise performance of the overall controller system may be improved, without reducing the transient performance.

The main challenge encountered developing a controller using this strategy, is the search for a suitable Lyapunov function needed in the resetting strategy. One problem is to find a Lyapunov function, another is to make sure this is a suitable measure for the system's transient energy. The first problem may be solved in some situations where development of the dynamic controller also yields a Lyapunov function for the closed-loop system. The other problem is only briefly discussed. Optimization theory is, however, being motivated as a promising solution, tried out on a simple example system.

A fast observer is needed in order to estimate the Lyapunov function value, since this is not

available for measurement in practice. Hence, additional precautions need to be undertaken when implementing the strategy. In particular, filtering effects are studied in detail for a Lyapunov-based resetting mechanism applied on an adaptive backstepping controller for parametric-strict-feedback systems. Tuning guidelines are also provided in order to prevent erroneous resets due to the filtering effects. Simulations of a car braking on a road, partly covered with ice or water, is given as the first example application presented in this thesis. Improved transient performance is shown in these cases of sudden changes in the road/tyre friction parameter.

Another challenge in using this resetting strategy is how to ensure parameter convergence of the fast observer described above. In addition to assume that the exciting signal is sufficiently rich during the transient period where typically a reset takes place, some monitoring of the richness of this signal is proposed followed by a suitable action to be taken.

This first example system is tested using simulations, hence being able to compare estimated and real values of the plant parameters. The other two examples presented in this thesis are not having this quality, due to plant parameters being unknown, but they illustrate other aspects being important when performing experimental testings.

Transient conditions, may also happen for ships operating in rough seas. There is a considerable loss in propeller thrust in case of ventilation and in-and-out-of-water effects. The today's industrial standard for electrically driven thrusters are shaft speed proportional-integral (PI) controllers, optimized for dynamic positioning (DP) and low speed manoeuvering in normal sea conditions. In extreme sea conditions, however, the propeller may start to spin when severe thrust losses occur. Hence, a Lyapunov-based controller state resetting strategy for the integrator state in the PI-controller is proposed. Increased transient performance in propeller speed is shown by experimental tests, carried out in a test basin, being the second example application presented in this thesis.

The reset strategy is also augmented to a thruster controller for transit operations. Additional losses due to operation in transit need to be handled. This is managed by modifying the plant model and upgrading the PI-controller used in the DP case. Experimental tests in a towing tank are carried out in order to show the increased transient performance in the propeller speed, constituting this thesis' third example application. In this case, also the power fluctuations are reduced, leading to reduced risk of blackout in the vessel power distribution system, in extreme sea conditions.

Preface

This thesis is the main result of my doctoral studies, undertaken in the period November 2003 through October 2007 at the Norwegian University of Science and Technology (NTNU), only interrupted by being assistant lecturer and when on parental leave. My funding has been provided by a scholarship from the Research Council of Norway (NFR).

Even though this thesis should summarize what I have been doing in my period as doctoral student, looking at the Contents, I realize that many of the things I spent time on, working towards my dissertation, ended up in nothing.

Anyway, most of all I would like to thank my supervisor, Tor Arne Johansen at the Department of Engineering Cybernetics. He has been a great advisor, always being available for answering my questions. The only times I have waited for more than twenty-four hours for his answer, is when he has been sitting on a plane between the continents. Despite his several ongoing projects, he has always been available for discussions and directions.

I would also like to thank my fellow PhD students for a great working environment. A special thanks to Johannes Tjønnås, my office mate, for both his scientific and philosophical discussions being invaluable in working out a PhD; Ivar Ihle, Morten Breivik, Frank Jakobsen, Andreas Egeberg, Jon Espen Ingvaldsen and Roger Skjetne for being travelling companions, discussion partners and coffee brake participators; Gullik Jensen for his advises in combining a family life with working on a PhD; Øyvind Smogeli, Luca Pivano and Asgeir J. Sørensen for their collaboration and joint publications.

I would like to thank my parents for their love and support. I would also like to thank my kids; Andrea for keeping my head in activity during my spare time, with her nonstop talking and her hunger after getting answers on questions, spanning from insects living in the mud to people walking on the moon; Sofia for making me happy in difficult times during the work on my PhD study, from birth to taking her first unstable steps. Finally, thank you, Lene, my dear wife for your love and support. You have always been kind and supportive, cheerful and encouraging, and you have shown patience at my late arrivals during experimental tests in the lab. I dearly love and respect you deeply!

Drammen, Norway
October 2007 Jostein Bakkeheim

Abbreviations

ABS	Anti-lock brake system
AS	Asymptotically stable
CLF	Control Lyapunov function
DP	Dynamic positioning
ES	Exponentially stable
FPP	Fixed pitch propeller
GAS	Globally asymptotically stable
GES	Globally exponentially stable
GP	Gaussian process prior
LTC	Local thruster controls
LTI	Linear time invariant
MMAC	Multiple model adaptive control
MPC	Model predictive control
MRAC	Model reference adaptive control
PE	Persistently exciting
PI	Proportional-integral
PID	Proportional-integral-derivative
PMS	Power management system
RHC	Receding horizon control
UC	Uniformly continuous
UGS	Uniformly globally stable
UUB	Uniform ultimately bounded

Contents

Chapter 1

Introduction

This thesis addresses the idea of improving transient behavior by controller state resetting of dynamic controllers. Controllers with integrate action or controllers with adaptation are example of such dynamic controllers. The idea is to improve the performance of an already existing controller by adding a controller state reset mechanism. In this way, the performance in steady-state or close to steady-state is not affected with this extension. Only performance in transient regimes is affected, reducing the time for the system to settle.

This first chapter starts with a short explanation of the concept of transient performance, followed by a brief history of the developments leading to the work presented in this thesis. The next part motivates for the selected strategy by presenting some industrial applications that may benefit from using the control strategy discussed in this thesis. Finally, the contributions of this thesis are summarized, before an outline of the rest of the thesis is given.

1.1 Background

1.1.1 Transient Performance

It is well known that there does not exist one particular control development procedure applicable for all nonlinear systems. There exist, however, lots of design tools that are suitable for particular *classes* of nonlinear systems. These tools are sometimes just focusing on developing a stabilizing controller, hence mostly concerned about the asymptotic stability (AS) requirement. In applications, however, the controlled system's transient performance is often important.

Feedback linearization is one example of such a nonlinear control design procedure where the main focus is on developing a stabilizing controller, rather than focusing on the system's transient performance. The idea is to first linearize the nonlinearities in the system, and then use well known linear control theory to develop a stabilizing controller. This may, however, cancel out some useful terms that would have increased the system's transient performance, for example systems that initially contain *nonlinear damping* terms. A more sophisticated choice of a stabilizing controller may leads to a closed-loop system with better transient performance, see Khalil (2002) for more details. A different approach of increasing the transient performance of

a class of feedback linearizable systems is, however, handled in Ciliz & Cezayirli (2006). The paper presents a parameter estimate reset technique, similar to the one discussed in this thesis.

Other control systems that have been subjects for transient improvements are adaptive systems. The states of traditional adaptive schemes may experience large initial transients. Hence, in Krstic, Kanellakopoulos & Kokotovic (1995), two design methods for adaptive control of a certain class of nonlinear systems are presented. The two design methods are referred to as *tuning function controller* and *modular design methods*. The strategies lead to adaptive approaches having improved transient performance compared to more traditional design methods. Also see the references in Krstic et al. (1995) for results on transient improvements in adaptive control designs.

The above transient improvement strategies are based on continuous control methods. The next section discusses *switching in control*, a different approach that may be utilized in order to improve a system's transient performance.

1.1.2 Switching in Control

Switching in control is an old idea, but most of the work in the literature has been carried out in recent years. There are situations where continuous stabilizing controllers do not exist, which makes switching control techniques especially suitable (e.g. nonholonomic systems), see Liberzon & Morse (1999). Although switching in control is necessary in some situations, its main motivation is to increase system performance or to simplify design and implementation. There are however lots of issues to be considered when introducing switching in control. In Liberzon & Morse (1999) three basic problems in stability analysis and design are presented in a conceptual way. The first problem is: *Find conditions that guarantee that the switched system is AS for any switching signal.* When all subsystems are stable, there may be situations where the total switched system is rendered unstable, see e.g. Utkin (1977). AS is however proven if there exist a common Lyapunov function for the set of systems, the problem is to find conditions under which there exists such a common Lyapunov function. The next problem is: *Identify those classes of switching signals for which the switched system is AS.* Under the assumption that all individual subsystems are stable, stability will be ensured if the switching is sufficiently slow. Dwell time switching and hysteresis switching are important issues in identifying such switching signals, see Morse (1996) for dwell time switching and Middleton, Goodwin, Hill & Mayne (1988) and Hespanha (1998) for hysteresis switching. In dwell time switching, after each switch for a certain period of time switching is prohibited. In hysteresis switching, a performance measurement is used in order to decide when to perform a switch, where the increase in performance needs to overcome a predefined hysteresis index. Some general techniques using Lyapunov functions, also suitable for nonlinear systems, are reported in Hespanha & Morse (1999), using average dwell time property of switching signal. The last problem is: *Construct a switching signal that makes the switched system AS.* In situations where none of the subsystems are stable, a switching signal needs to be constructed in order to render the total system stable. Some theory exists for linear time invariant (LTI) systems, but especially for nonlinear systems there are lots of open questions to be answered in the future. For an introduction to hybrid systems, i.e. systems combining discrete and continuous dynamics, see e.g. Decarlo, Branicky, Pettersson & Lennartson (2000) or Goebel, Hespanha, Teel, Cai & Sanfelice (2004). An introduction to switched systems can be found in Liberzon (2003) or Liberzon & Morse (1999).

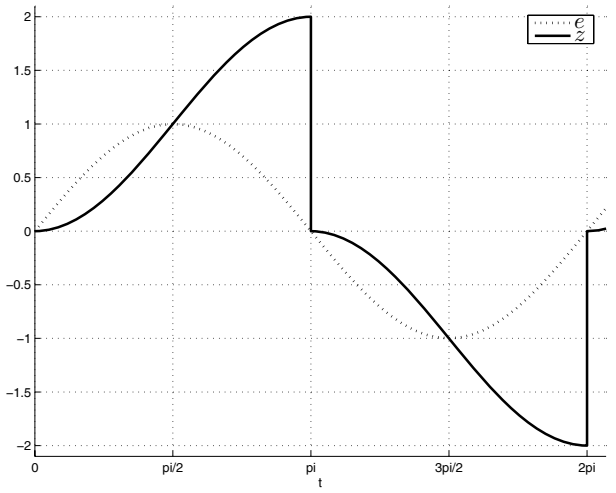

Figure 1.1: Sinusoidal response of Clegg Integrator. e is input to the integrator and z is the integrator state, reset to zero when the input is zero.

As pointed out above, switching in control may be performed in order to increase the system's performance, which is also the topic in this thesis. For instance, in situations where the environmental conditions are changing rapidly, selecting a controller that also performs switching may best handle these incidents. Gain scheduling is a well known example of a controller that performs switching between different gains in order to adapt to different environmental conditions. In this way, well known linear control methodology can in some cases be used to control nonlinear systems. Gain scheduling is conceptually simple, and, indeed, practically successful for a number of applications. The main problem with this strategy is that only limited theoretical guarantees of stability in nonlinear operation exists, hence relying just on loose practical guidelines in controller development procedures. An analytical framework for gain scheduling is however presented in Rugh (1991). See also Johansen, Hunt, Gawthrop & Fritz (1998) for an alternative way of performing gain scheduling. The referred paper suggests linearization and local controller design, not only at the equilibrium points, but also in transient operation regimes. Transient improvements may be achieved by increasing the number of linear time-invariant controllers.

A different approach of switching in control is taken when performing *controller state reset*. Some or all of the controller states are reset to different values in order to gain improved performance for the closed-loop system. The idea of resetting controller states where first proposed by Clegg (1958), and resumed in 1970's by Krishnan & Morowitz (1974) and Horowitz & Rosenbaum (1975). Figure 1.1 shows the response of a Clegg Integrator for a sinusoidal input signal. A renewed interest of this systems came up in late 1990's, see Beker, Hollot & Chait (2004) and the reference therein. A common strategy for these controllers are that they are resetting the output of the controller to zero when the input, i.e. the control error, is zero. This turns out to improve phase lag properties in control of linear systems.

A more sophisticated switching strategy is found in so-called multiple model adaptive control

(MMAC) frameworks. The idea is not new, in Athans, Castañon, Dunn, Greene, Lee, Sandell Jr. & Willsky (1977) multiple Kalman filter-based models was used in order to improve the accuracy of the state estimation in estimation control problems. The MMAC idea was however not performed using switching, but rather a convex combination of the control determined by different models was used. Further, no stability results were reported for this MMAC strategy.

Switching in context of adaptive control was first introduced in Mårtensson (1986). He presented the concept of *direct switching*, i.e. the choice of when to switch to the next controller, in a predetermined sequence, is based directly on the output of the plant. The method has shown little practical utility. *Indirect switching* in MMAC is more attractive for applications, first proposed by Middleton et al. (1988). In indirect switching, multiple models are used to determine both when and to which controller one should switch. Later, Morse, Mayne & Goodwin (1992) adapted the idea of Middleton et al. (1988) in order to use switching techniques for model reference adaptive control (MRAC) when the relative degree of the plant is unknown.

In the MMAC references above, switching was used in order to solve global stability problems in adaptive control. In Narendra & Balakrishnan (1994), however, the system was by itself stable without switching. Switching between multiple models was instead used in order to improve performance of certainty equivalence adaptive control for linear systems in an MRAC framework. The switching algorithm was selecting the model yielding the minimum of a performance cost index. Further, an architecture suitable both for linear and nonlinear systems was reported in Narendra & Balakrishnan (1997). Details were however just presented for LTI systems. In Narendra & Balakrishnan (1997) the MRAC approach in Narendra & Balakrishnan (1994) was left and replaced with a set of identification models of the plant. A performance cost index was used in order to select the best model of the plant. See Narendra, Balakrishnan & Ciliz (1995) for a qualitative description of the approaches presented in Narendra & Balakrishnan (1994) and Narendra & Balakrishnan (1997). See also Zhivoglyadov, Middleton & Fu (2000), Anderson, Brinsmead, Liberzon & Morse (2001) and Cezayirli & Ciliz (2004) for other references on MMAC for linear systems.

The extension of MMAC to also covering nonlinear systems can be found in Chen & Narendra (2001), Narendra & George (2002), Dougherty, Arbogast & Cooper (2003), Chaudhuri, Majumder & Pal (2004) and Cezayirli & Ciliz (2006). The different approaches reported above are typically distinguished either by type of adaptive controller under consideration, or the resetting strategy and criterion applied.

An MMAC approach where the reset criterion was using a Lyapunov function was initially presented in Kalkkuhl, Johansen, Lüdemann & Queda (2001). The reset criterion was resetting some or all of the controller states to a different value based on a decision involving use of the Lyapunov function. Unlike the approaches based on the Clegg Integrator, the reset was not necessarily to zero, but rather to a value that ensured a negative drop in the Lyapunov function value. The plant considered in Kalkkuhl et al. (2001) was of so-called parametric-strict-feedback form, where adaptive backstepping was used in order to control the system. The MMAC approach reported in Kalkkuhl et al. (2001) was deviating from the one in the references above in terms of using a performance index, not only for the estimator error, but for all states involved in the system through the control Lyapunov function. In Kalkkuhl, Johansen & Lüdemann (2002), the strategy of Kalkkuhl et al. (2001) was applied on a wheel slip application. Bakkeheim & Johansen (2006) is an extension of Kalkkuhl et al. (2002), discussing the effect of estimating the steady-state position, and giving tuning guidelines for the controller. In Ciliz & Cezayirli (2006), MMAC was

developed for adaptive control of feedback linearizable systems. The control Lyapunov function for the linearized feedback controller was used in the reset criterion.

Switching logic in the above references was based on the use of *multiple Lypaunov functions*. In Branicky (1998), multiple Lyapunov functions are introduced as a tool for analyzing stability. In the above references and in this thesis, the Lyapunov function is used in order to both guarantee stability and as a tool for increasing systems transient performance.

Lyapunov-based reset may also be applied in systems resetting the integrator state of proportional-integral (PI) controllers. In Bakkeheim, Smogeli, Johansen & Sørensen (2006), this was shown for a propeller operating in rough seas. Since the Lyapunov function value in Bakkeheim et al. (2006) was not available for measurement, an estimate of this was used in the implementation of the reset procedure. The effect of estimating the Lyapunov function value was in Bakkeheim et al. (2006) only discussed, but experimental results were included for verifying the benefits of using this strategy.

1.2 Motivation

Proportional-integral-derivative (PID) controllers are still in domination when selecting controller strategy in industrial control applications. The industry is, however, adapting slowly the more sophisticating controller approaches. Model predictive control (MPC) and adaptive control are examples of more sophisticated control strategies that have become standard in particular control problems.

Despite the established controller strategies are well tested and found to be extremely useful in industrial applications, they may fall short when operating in special situations. Continuous feedback controllers are the dominating group of these controllers. This may be the best choice in normal conditions, but extreme conditions may occur every now and then. In these conditions, the continuous feedback controller may lead to unacceptable performance, or even fail performing their tasks. One needs to balance tradeoffs between robustness and sensitivity to noise and disturbances. To be sure the controller has an acceptable behavior also in extreme conditions, one may pay the price of reducing the performance in normal conditions.

In order to emphasize the above problem statement, among many, five simple application examples are given below.

Controlling the shaft speed of power generators connected to a common power distributional network is crucial in order to maintain a constant frequency on the power network. In normal conditions the controllers need to counteract slow varying disturbances caused by, for instance, small variations in total load on the power grid. But extreme situations may occur. For instance a sub-network may be disconnected from the network due to some fault, so-called *unintentional islanding*. Then the load is lower than before and this may cause the generators to over-speed. This, in turn, may be dangerous for gas turbines and turbo-charged diesel engines due to surging that may break the compressor blades, etc. These situations may not be handled in an optimal way due to the controller being tuned for operating in normal conditions. The necessity for better speed control is further increasing with a *distributed power generation*, where small power plants will have less rotational inertia and total inertia on the network compared to a *centralized power generation*. See Radan, Sørensen, Ådnanes & Johansen (2007) for more details on challenges regarding power generation and distribution on ships.

During well drilling in the petroleum industry, the annular downhole pressure in the mud (drilling fluid) along the well bore must be kept above a minimum collapse/pore pressure to prevent reservoir fluid flow into the well, and below a fracture pressure. In conventional drilling, a choke valve and a backpressure pump is used to control the wellbore pressure, typically by applying a PI-controller on the choke. In so-called *direct bottomhole control*, the bottomhole pressure at the critical depth is stabilized at a desired set-point directly, based on a bottomhole pressure measurement. However, an estimate of the pressure is needed between samples because the transfer rate of the measurement is usually slow, or for additional safety because the sensor itself may be unreliable. Hence, the PI-controller relies heavily on integral action to balance the pressure drop caused by friction, which is significant, and the proportional feedback gain must be low to prevent generating pressure pulses by fast changes in the control input. As a result, the control system will react slow to fast pressure changes. The drill bit may, however, reach an unexpected overpressured gas pocket, such an incident is commonly called a *kick*. A fast reaction to this incident needs, however, to be taken in order to prevent the kick to escalate into a blowout when the formation fluids reach the surface. Blowouts can cause significant damage to drilling rigs, and injuries or fatalities to rig personnel.

Robots have to manipulate loads of various sizes, weights, and mass distributions. If controllers with constant gains are used and the load parameters, of the objects to be handled by the manipulator, are not accurately known, robot motion can be either inaccurate or unstable, see Sciavicco & Siciliano (2000). Adaptive control may be utilized in order to adapt the controller to handle the unknown parameters. Compared to robust control, adaptive control is superior in dealing with uncertainties in constant or slowly varying parameters, see e.g. Slotine & Li (1991). If, however, a change in a load parameter suddenly occurs, e.g. the manipulator loses the load during operation, unwanted behavior may occur due to the slow varying parameter estimation of the adaptive controller.

Another example where a controller needs to handle both slow varying phenomena in combination with sudden changes in environmental conditions is anti-lock brake systems (ABS) in cars. Totally different controller performance is needed when the car is braking on a road with homogeneous road conditions compared to heterogeneous road conditions, e.g. one that is partly covered with ice or water. See Petersen (2003) for general details regarding wheel slip control.

In electrically driven thruster control for ship propulsion and dynamic positioning, PI-controller on the shaft speed is the industrial standard. The controller is tuned such that it is optimized for normal weather conditions. In extreme weather conditions, however, the propeller will start to spin in case of ventilation and in-and-out-of-water effects. See Smogeli (2006) for more details regarding vessel operation in extreme sea conditions.

As seen in the examples above, there is need for controllers being able to handle both normal working conditions and situations where sudden changes in environmental conditions occur.

One way to approach this problem is to decouple the controller performance specification into two regimes; one for normal operations and another for extreme situations. This must be done in such a way that the mechanism triggering the extreme case part of the controller needs to distinguish between measurement noise and extreme conditions. Switching in control may be a solution to this problem. This will however force upon additional precautions needed to be addressed during controller developments and stability analysis. A Lyapunov-based controller state reset procedure will lead to a controller having these decoupled properties. The mentioned controller strategy will be presented and employed on selected applications, constituting the main

subject of this thesis.

Sliding mode control is another control strategy having two distinct behaviors for transient and close-to-steady-state control. The strategy is not new, theoretical background of the analysis and design of sliding mode control may be found in publications of the early 1930s. A finite-time reaching phase is the transient part of the behavior, while an exponential convergent sliding phase is the close-to-steady-state behavior part of the controller. The sliding mode controller is not considered in this thesis, see Utkin, Guldner & Shi (1999) for more details.

1.3 Contribution

The overall motivation for this thesis has been to point out the problem of handling extreme situations in prevailing controllers in industrial applications. Further, establish a common framework for solving these problems using Lyapunov-based reset strategy. And finally try out this in practical applications, in order to justify the framework. The applications presented in this thesis are only tested using simulation and small scale testing, but provides a start for justifying the method in full-scale applications. The following are believed to be the main contributions of this thesis, organized by chapters:

Chapter 2: A framework for the Lyapunov-based controller state resetting is given for general nonlinear systems. The effects of estimating the Lyapunov function, rather than having perfect knowledge to this, are discussed. The idea of separating the performance specification and design of the reset controller, into one part that handles normal conditions and one that handles extreme conditions, is described. An illustrative example is also given in order to motivate the strategy. This chapter is based on the first part of Bakkeheim, Johansen, Smogeli & Sørensen (2008).

Chapter 3: An already proposed Lyapunov-based reset mechanism for parametric-strict-feedback system is studied in detail. Particular attention is paid on the effects of data filtering, due to estimation of the Lyapunov function value. Tuning guidelines for these data filtering processes are also given. Finally, an application to wheel slip control is extended. The main material of this work has been reported in Bakkeheim & Johansen (2006).

Chapter 4: The use of the Lyapunov-based reset strategy on marine propulsion and thruster control systems operating in dynamic positioning (DP) or low speed maneuvering is introduced. The reset strategy handles losses in propeller torque that are introduced when operating in rough seas. Increasing performance, compared to a prevailing propeller speed PI-controller, is shown by experimental results carried out in a basin. This work is reported in the second part of Bakkeheim et al. (2008).

Chapter 5: The marine anti-spin strategy above is augmented to be valid for systems in transit operations. The dynamic PI-controller used in the dynamic position or low speed maneuvering situation is changed in order to handle additional losses introduced when ship is in transit operation. Experiments in a towing tank setup is carried out in order to show the performance improvements. This work is reported in Bakkeheim, Pivano, Johansen & Smogeli (2007).

Appendix A: A procedure of tuning a linear controller applied on a nonlinear plant model, is proposed. The nonlinear plant model is presented by a nonparametric model, also providing uncertainty of both the model mean and its derivatives. The direct estimate of the locally linearized model with its corresponding parameter variance is mapped into the closed-loop systems location of poles in the complex plane. The resulting location of the poles are given as a mean value with corresponding uncertainty boundaries, guiding the selection of plant parameters in order to achieve a stable closed-loop system. This chapter is reported in Bakkeheim, Murray-Smith & Johansen (2005).

Appendix B: A combined power/torque controller for marine propulsion systems is combined with an anti-spin strategy, in order to operate in rough seas. In normal conditions with moderate seas, the combined power/torque controller has earlier been shown to have better performance compared to the shaft speed controller, but fails during operation in extreme sea conditions. The proposed controller with the anti-spin procedure is shown to be preferable for ships operating in DP or low speed maneuvering, during all sea states. Simulations are provided to validate the performance of the control scheme. This work is reported in Smogeli, Hansen, Sørensen & Johansen (2004).

Appendix C: An already proposed nonlinear thrust controller for a fixed pitch marine propeller designed for transit operations is combined with an anti-spin strategy in order to operate in all sea states. A common torque loss estimator is used both in order to estimate loss due to nonzero advance speed and loss due to operation in extreme seas. Experimental tests performed in a towing tank is used in order to validate the controller performance. This work is presented in Pivano, Bakkeheim, Johansen & Smogeli (2008).

1.4 Publications

The following is a complete list of the author's accepted publications written during the work of the PhD study. Note that the author's surname has changed from *Hansen* to *Bakkeheim* during the period of the given publications.

Conference Papers

- Hansen, J. & Johansen, T. A. (2004), 'Transient Performance, Resetting and Filtering in Nonlinear Multiple Model Adaptive Control', *in* 'Proceedings of IEEE American Control Conference (ACC'04)', Boston, Massachusetts.

- Smogeli, Ø. N., Hansen, J., Sørensen, A. J. & Johansen, T. A. (2004), 'Anti-spin control for marine propulsion systems', *in* 'Proceedings of IEEE Conference on Decision and Control (CDC'04)' Paradise Island, Bahamas.

- Bakkeheim, J., Murray-Smith, R. & Johansen, T. A. (2005), 'Nonparametric Identification of Linearizations and Uncertainty using Gaussian Process Models - Application to Ro-

bust Wheel Slip Control', *in* 'Proceedings of IEEE Conference on Decision and Control (CDC'05)', Seville, Spain.

- Bakkeheim, J., Smogeli, Ø. N., Johansen, T. A. & Sørensen, A. J. (2006), 'Improved Transient Performance by Lyapunov-based Integrator Reset of PI Thruster Control in Extreme Seas', *in* 'Proceedings of IEEE Conference on Decision and Control (DCD'05)', San Diego, USA.

- Bakkeheim, J., Pivano, L., Johansen, T. A. & Smogeli, Ø. N. (2007), 'Integrator Reset Antispin for Marine Thrusters Operating in Four-Quadrants and Extreme Sea Conditions', *in* 'Proceeding of IFAC Conference on Control Applications in Marine Systems (CAMS'07)', Bol, Croatia.

- Pivano, L., Bakkeheim, J., Johansen, T. A. & Smogeli, Ø. N. (2008), 'A Four-Quadrant Thrust Controller for Marine Propellers with Loss Estimation and Anti-Spin', *in* 'Proceedings of IFAC World Congress', Seoul, Korea. Accepted.

Journal Papers

- Bakkeheim, J. & Johansen, T. A. (2006), 'Transient Performance, Estimator Resetting and Filtering in Nonlinear Multiple Model Adaptive Backstepping Control', *IEE Proceedings - Control Theory & Applications* **153**(5), 536–545.

- Bakkeheim, J., Johansen, T. A. , Smogeli, Ø. N. & Sørensen, A. J. (2008), 'Lyapunov-based Integrator Resetting with Application to Marine Thruster Control', *IEEE Transactions on Control Systems Technology*. Accepted.

1.5 Outline of the Thesis

This thesis is divided into three parts: Theory, Applications and Other Publications. The first part presents the framework for the controller strategy. The second part gives three example applications in order to illustrate and evaluate the method presented in the framework. The examples are presenting the strategy both in a theoretical and practical way. The last part presents some other publications carried out during the work on the PhD study. The work of these papers are not directly related to the framework, but included because they are solving the application problems, discussed in part two, in slightly different ways.

Part I

Theory

Chapter 2

Framework

The goal of this chapter is to assemble different strategies into a common framework, i.e. utilize Lyapunov functions in order to decide when a controller state reset is appropriate. The Lyapunov function is in this way used as a design tool, and in combination with existing stability theory for switched systems, the stability analysis of the closed-loop system with controller state reset follows directly. The idea in the framework presented here is basically such that for a given closed-loop system with a dynamic controller, improved transient performance is achieved when reset of the controller states gives negative jumps in the Lyapunov function value. The proposed framework assumes that a Lyapunov function is given, and that full state measurement is available for feedback. A dedicated fast responding estimator is required for the Lyapunov function value.

A simple example is presented in order to clarify the idea behind Lyapunov-based controller state resetting. A Lyapunov function is developed for the example system which also performs a suitable measurement of the system transient energy. Simulation results with measurement noise and changes in unknown parameter values are given in order to justify the strategy.

The work in this chapter is based on the first part of Bakkeheim et al. (2008).

2.1 System Components and Functions

This first section presents the different components and functions that constitutes the Lyapunov-based reset controller framework, depicted in the block-diagram in Figure 2.1.

2.1.1 Plant

Consider the following plant model:

$$\dot{\xi} = f(\xi, u, \theta) \tag{2.1}$$

$$y = h(\xi), \tag{2.2}$$

where $\xi \in \mathbb{R}^n$ is the plant state vector, $u \in \mathbb{R}^m$ is the control input and $\theta \in \mathbb{R}^p$ is some unknown but constant disturbance or plant parameter. The vector field $f(\cdot, \cdot, \cdot)$ may be nonlinear. $y \in \mathbb{R}^v$ is the plant output, where $h(\cdot)$ may be nonlinear. It is assumed that state ξ is available for feedback.

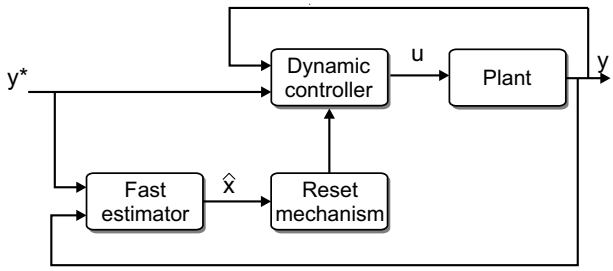

Figure 2.1: Controller setup with state reset of dynamic controller.

2.1.2 Dynamic Controller

Let y^* denote some desired control reference. The task of the controller is to control the error $y^* - y$ to zero, hence control the state ξ to some desired steady-state $\xi^*(\theta, y^*)$. This steady-state depends on the known desired control reference, but it may also depends of the unknown parameter vector θ.

Since the plant model contains some unknown parameters in θ, it is common to augment the system with a set of controller states

$$\dot{z} = g(\xi, z, y^*), \tag{2.3}$$

where the controller state vector $z \in \mathbb{R}^q$ may represent an estimate of the unknown constants in θ, leading to (2.3) being a part of an adaptive controller. On the other hand, z may represent integrator states in an integral action control algorithm, where θ represents a disturbance to be rejected.

In addition to the dynamics (2.3) the controller is assumed to take the form

$$u = \gamma(\xi, z, y^*) \tag{2.4}$$

leading to the closed-loop system

$$\dot{\xi} = f(\xi, \gamma(\xi, z, y^*), \theta) \tag{2.5}$$

$$\dot{z} = g(\xi, z, y^*). \tag{2.6}$$

The design of the controller (2.3)-(2.4) may not be a trivial task because the closed-loop system (2.5)-(2.6) depends on the unknown parameters in θ in addition to being nonlinear. However, the design of an asymptotically stabilizing controller (2.3)-(2.4) is outside the scope of this chapter and is simply assumed to be available. A straightforward solution to this task, however, may be via linearization, but it will only guarantee local regulation. Nonlocal regulation may be achieved by using nonlinear design tools, such as sliding mode control, adaptive backstepping control, nonlinear receding horizon control (RHC) etc. see Khalil (2002) for more examples of nonlinear design tools.

The main idea in this thesis is to improve transient performance of the existing closed-loop control system (2.5)-(2.6) by utilizing the fact that the states z may be instantaneously reset to a different value taken from a finite set of candidates $z_i \in \mathcal{H}$ at any time instants, described in the section that follows.

2.1.3 Reset Mechanism

The main task for the reset mechanism is to provide reset commands to the dynamic controller. The reset mechanism includes two main components; a Lyapunov function that measures the system's transient energy, and a reset algorithm that includes logic for calculating reset commands.

Lyapunov Function

The main focus is on improving the transient performance of already existing closed-loop dynamic control systems, hence only autonomous systems are considered. Techniques of finding a Lyapunov function for stable autonomous linear time invariant systems are well established, but unfortunately not so in the nonlinear case. There are however some techniques, like Krasovskii's method, the variable gradient method, physical motivated Lyapunov functions for robot manipulators etc., but they are limited to small classes of systems, often of low order. On the other hand, there are some techniques where a Lyapunov function is initially selected in order to design a stabilizing controller. Such a Lyapunov function is called a control Lyapunov function (CLF), introduced by Artstein (1983) and Sontag (1983). Some more details regarding CLFs are given later in this section. See also Parks (1966) for early results on Lyapunov-based adaptive design methods. The generated Lyapunov function may actively be used in the process of measuring the system's transient energy.

In order to have a reference point for the system's transient energy, the system's error state needs to be defined:

$$x = \begin{bmatrix} \xi^*(\theta, y^*) - \xi \\ z^*(\theta, y^*) - z \end{bmatrix} \tag{2.7}$$

where $x \in \mathbb{R}^{n+q}$, leading to the following closed-loop system

$$\dot{x} = F(x, u) \tag{2.8}$$

$$u = \alpha(x). \tag{2.9}$$

The dynamic part (2.8) includes both the plant dynamics (2.5) and the controller dynamics (2.6).

Remark 2.1 *$z^*(\theta, y^*) = \theta$ in an adaptive control algorithm, and $z^*(\theta, y^*)$ is the integrator steady-state value in an integral control strategy.*

Remark 2.2 *For any system represented by (2.5)-(2.6), we may map it into its error state representation by using the mapping in (2.7). Assume a system is settled in steady-state. When a jump in set-point value y^* or the unknown parameter value θ occurs, this leads to a jump in the steady-state system states ξ^* and z^*. This same situation will turn out as a jump made out of the equilibrium position $x = 0$ for the system error state. Both ways of describing this same event may be used in the thesis, depending on the particular states being studied at the moment.*

Assume $x = 0$ is an equilibrium of the closed-loop system, and $D \subset \mathbb{R}^{n+q}$ is a domain containing $x = 0$. Let $V : D \to \mathbb{R}$ be a continuously differentiable Lyapunov function for the closed-loop system such that

$$V(0) = 0 \text{ and } V(x) > 0 \text{ in } D - \{0\} \tag{2.10}$$

$$\dot{V}(x) < 0 \text{ in } D - \{0\} \tag{2.11}$$

such that $x = 0$ is an AS equilibrium point inside the domain D.

It is well known that for a controller (2.3)-(2.4) rendering the equilibrium $x = 0$ AS, there exists a Lyapunov function V. Such a function may be hard to find. While convergence properties can be proven for classes of adaptive systems, AS properties may be hard to establish. In some controller design procedures, for example optimal control and design techniques using CLFs, the Lyapunov function is obtained for free during the controller design process. In receding horizon control, the Lyapunov function value can be obtained by solving an optimization problem online at each sample, see Maciejowski (2002).

For the system (2.8), a CLF is a function $V(x)$ selected such that $\dot{V}(x) \leq -W(x)$ where $W(x)$ is a positive definite function and $u = \alpha(x)$ is guaranteeing that for all $x \in \mathbb{R}^{n+q}$ the following holds

$$\frac{\partial V}{\partial x} F(x, \alpha(x)) \leq -W(x). \tag{2.12}$$

A precise notion of a CLF is given in the following definition.

Definition 2.1 *A smooth positive definite and radially unbounded function $V : \mathbb{R}^{n+q} \rightarrow \mathbb{R}$ is called a control Lyapunov function (CLF) for (2.8) if*

$$\inf_{u \in \mathbb{R}^m} \left\{ \frac{\partial V}{\partial x}(x) F(x, u) \right\} < 0, \ \forall x \neq 0. \tag{2.13}$$

It is in Artstein (1983) shown that (2.13) is not only necessary, but also sufficient for the existence of a control law satisfying (2.12), that is, the existence of a CLF is equivalent to global asymptotic stabilizability. The problem is, however, to initially pick functions $V(x)$ and $W(x)$, leading to a controller $\alpha(x)$ satisfying the condition in (2.12). No general method exists of finding a CLF for the system in (2.8), but methods do exist for classes of nonlinear systems. For systems affine in control, and satisfying some additional properties, a particular stabilizing control law $\alpha(x)$ is given by Sontag's formula, see Sontag (1989) for more details. See also Xiushan, Xiaodong & Haoran (2007) and the references therein for later results on constructing CLFs. CLFs are also obtained by stepping through the adaptive backstepping design procedure being used in the next chapter of this thesis, see Krstic et al. (1995) for more details on backstepping procedures.

Despite these disadvantages, controller design using Lyapunov function techniques is seen as a fairly general and useful tool for designing nonlinear control systems. In the rest of this chapter, we assume that V is known.

Reset Algorithm

A reset procedure may reset the controller state $z(t)$ to a different value $z_i \in \mathcal{H}$ taken from a set of candidates $\mathcal{H}$. A reset at time t is done by resetting the state $z(t^+) = z_i$, where t^+ denotes an infinitesimal small time increment of t. AS is preserved if this is performed only when it leads to a negative jump in the Lyapunov function, $V(x(t^+)) < V(x(t))$, $\forall x(t) \in D$. This is formally stated in the following theorem.

Theorem 2.1 *Given a closed-loop system with dynamic controller as in (2.5)-(2.6). Assume that V is a Lyapunov function that proves the equilibrium point of the closed-loop system (2.5)-(2.6) to be AS in D. Further assume that $\Delta V_i(t)$ denotes a jump in the Lyapunov function value when the controller state is reset to a different value $z_i \in \mathcal{H}$. Further, if z is reset to the value z_i only if $\Delta V_i(t) < 0$ and $x(t) \in D$, the equilibrium point of the nonlinear system in (2.5)-(2.6) remains AS in D.*

Proof. The reader is referred to Branicky (1998), where the switching system is proved to be AS in sense of Lyapunov if $\Delta V_i(t) < 0$. Next, the condition $\Delta V_i(t) < 0$ leads to a negative jump in the Lyapunov function, which also leads to $\dot{V}(x) < 0$ in $D - 0$, hence AS follows. ■

Remark 2.3 *In Theorem 2.1 the closed-loop system (2.5)-(2.6) is assumed to be AS, but also other stability properties may be considered such as exponentially stable (ES). The resulting closed-loop system with controller state reset is in this case ES. Other types of asymptotically stability properties may also apply. However, it is less interesting to talk about transient performance of marginally stable systems, hence of limited interest in this thesis.*

Remark 2.4 *The power of using Lyapunov functions in control design and analysis comes from its generality; it is applicable to all kinds of control systems, be they linear or nonlinear, time-varying or time-invariant, finite dimensional or infinite dimensional. The way of strive for increased transient performance by reset only when leading to drop in Lyapunov function value, inherits this generality. The limitations of using this methodology lies however in the fact that it is often difficult to find a Lyapunov function for a given system.*

Assume a reset to a lower Lyapunov function value gives a more favorable transient response, then a reset according to the description above, will lead to a closed-loop system (2.5)-(2.6) with improved transient performance. Appropriate selection of the Lyapunov function will increase the system transient performance when the controller state is reset, this issue is emphasized by an example in Section 2.3.

Remark 2.5 *In situations where several reset candidates give a negative drop in the Lyapunov function value, the one corresponding to the most negative drop is selected.*

Both range and sparseness of controller state reset candidates need to be addressed when selecting a suitable set $\mathcal{H}$. The set $\mathcal{H}$ needs to cover the feasible region of controller state z, while sparseness is given as a tradeoff between noise performance and speed of convergence. The span of the set $\mathcal{H}$ is typically given by the feasible set-point region y^* and the feasible parameter region θ.

2.1.4 Fast Estimator

This section motivates the need for an estimator as depicted in Figure 2.1.

Estimate $V(\hat{x})$

Since θ may be unknown, x is not available in general, see (2.7). Hence, the reset mechanism may use $V(\hat{x})$, where $\hat{x}$ is an estimate of x. The estimate $\hat{x}$ may be estimated directly, or indirectly by

first estimating the unknown plant parameter θ, i.e. $\hat{\theta}$. Note that in an adaptive control scheme where the controller state z acts as an estimate of the unknown parameter θ, the estimate $\hat{\theta}$ will be different from the estimate within the dynamic controller, with different properties. The speed of convergence of $\hat{\theta}$ is required to be faster than z, even though they are estimating the same parameter. This is guaranteed by appropriately tuning the estimator for $\hat{\theta}$. The more slowly varying state z may be reset to a different value in order to increase the transient response of x. The fast and hence maybe noisy signal $\hat{\theta}$ is giving a rough guideline for the value of the steady-state. It must be fast in order to make the reset respond quickly after some abrupt change in disturbance or set-point, otherwise there would be no improvements in transient performance. See e.g. Ioannou & Sun (1996) for more general details on design of on-line parameter estimators. Also see the estimator parts of the example applications given in Chapters 3 - 5 in addition to Section 2.3.5 of this chapter, for more specific details.

Limitations and Assumptions

There is, however, one assumption that needs to be stated in order to ensure satisfactory performance. In the theoretical outlines given in this thesis, it is assumed that the unknown parameter value θ is a time-invariant constant. The assumption is initially given in order to make sure the fast estimator is providing a correct estimate of the state x. However, the assumption may be relaxed to instead assuming that after a jump in θ, the fast estimator needs to be settled at this new value of θ before yet another jump in θ takes place. In practice, the assumption of θ being constant between each jump incidents may further be relaxed to allowing slow varying changes in its value. These slow varying changes in θ are taken care of by the closed-loop system itself, but assumed to be slow enough in order to not triggering a controller state reset. The resulting assumption is ensured to be satisfied by appropriately tuning the controller parameters.

2.2 Performance Specifications

Compared to a dynamic controller without state reset, there may be some drawbacks. In what follows, we discuss both advantages and disadvantages when including the controller state reset mechanism described in Section 2.1.3.

2.2.1 Separating Performance

The performance specification and tuning of the controller may be separated into two regimes. The separation divides the tuning of the overall controller into two separate steps. First, the closed-loop controller without resetting is tuned. In this step, particular attention is made on the noise sensitivity and robustness, leading to satisfactory performance when the system is subjected to small perturbations. In step two, the transient performance is addressed. This is mainly done by appropriate choice of Lyapunov function and sparseness of reset candidates. The two regimes are described as follows:

Small-perturbation Regime

A dynamic system is said to be settled when it is operating in this regime. The system states are then in equilibrium or close to equilibrium, and the Lyapunov function value is generally small (close to zero) in this regime. Measurement noise, small perturbations in parameter value or set-point value may lead the system out of the equilibrium for a while, but the AS closed-loop controller brings the system back towards the equilibrium. The reset algorithm should be tuned such that the reset mechanism does not act while in this regime. The performance is solely given by the closed-loop system without reset (2.5)-(2.6).

Transient Regime

A dynamic system is said to be in a transient regime when the system is far away from the equilibrium. This may be due to a considerable change in the set-point value or in plant parameter value. In this regime, the controller state reset mechanism takes action, trying to decrease the time to reach the system's new equilibrium point. The controller state reset mechanism rapidly detects the out-of-equilibrium condition by a positive jump in the Lyapunov function value through the fast estimate $\hat{x}$. The reset algorithm will take action by demanding an appropriate reset of controller state z, reducing the Lyapunov function value.

2.2.2 Transient Performance

Both analysis and design in the literature are mostly concerned about the asymptotic performance requirement or the small perturbation regime. In applications, however, the system's transient performance is often more important. Especially, analytical quantification and systematic improvement of transient performance have been challenging problems in adaptive control. The adaptive backstepping design in Krstic et al. (1995), however, addresses the problem of transient performance in an analytical way. It is well known that during the initial period, while the parameter estimates are poor, the states of most adaptive schemes may exhibit large initial transients, see e.g. Ioannou & Sun (1996). In Krstic et al. (1995), transient improvement is achieved following two different strategies; *tuning function design* and *modular design*. In tuning function design, rapid exchange of information is utilized between the controller and identifier. This is done by incorporating the parameter update law in the adaptive controller. In this way the controller takes into account the effect of the parameter estimation transients. In the modular design, a stronger controller is selected in order to suppress the destabilizing effects of poor parameter estimates, hence improved transient performance is achieved.

Chapter 3 in this thesis gives an example of an adaptive control application using tuning function design from Krstic et al. (1995), where the transient performance is further increased by the controller state reset strategy.

2.2.3 Robustness

In the reset procedure, there are certain issues to be taken into account. The estimation $V(\hat{x})$ will be subject to a time lag compared to the actual value $V(x)$. The time lag is minimized by appropriate tuning of the estimator. A fast estimator may lead to increased sensitivity to noise and modelling uncertainties. However, a simple methodology given in Kalkkuhl et al. (2002)

suggests to introduce a threshold δ in order to reduce undesirable switching due to noise and modelling uncertainties, i.e. reset to $x(t^+)$ only if $V(x(t^+)) < V(x(t)) - \delta$. Appropriate choice in sparseness of reset candidates $z_i \in \mathcal{H}$ may also give reduction of undesirable switching, see Chapter 3. Also note that the reset strategy above may leads to chattering effects, due to not exactly knowing the steady-state value. Introduction of a short dwell time τ between each reset action will reduce this problem, see Hespanha (2003).

2.2.4 Persistence of Excitation

When (2.5)-(2.6) constitutes an adaptive control, the regulation $y^* - y \to 0$ may be achieved without necessary achieving the parameter convergence $z \to z^*$ where $z^* = \theta$. The phenomenon is well known from adaptive control theory, see e.g. Ioannou & Sun (1996). Another interesting question is whether the fast estimator leads to convergence $\hat{x} \to x$ or not. This may be crucial in preventing erroneous reset of the dynamic controller. Flawless convergence of the fast estimator may in some situations demanding the exciting signal to be rich enough. In order to make this initially vague notion a bit more precise, the concept of persistently exciting (PE) signals needs to be defined.

Definition 2.2 *A piecewise continuous signal vector $\phi : \mathbb{R}^+ \to \mathbb{R}^n$ is persistently exciting (PE) in $\mathbb{R}^n$ with a level of excitation $\alpha_0 > 0$ if there exist constants α_1, $T_0 > 0$ such that*

$$\alpha_1 I \geq \frac{1}{T_0} \int_t^{t+T_0} \phi(\tau)\phi^T(\tau)d\tau \geq \alpha_0 I, \quad \forall t \geq 0. \tag{2.14}$$

Intuitively, the persistent excitation of $\phi(t)$ implies that the vectors $\phi(t)$ corresponding to different times t cannot always be linearly dependent. In estimation schemes, the vector $\phi(t)$ contains signals available for measurement, but since they are not known a priori the PE condition is hard to verify a priori.

In order to guarantee the fast estimator described in Section 2.1.4 not to provide an erroneous estimate of the unknown parameter leading to an erroneous reset, some actions needs to be taken. One way of guaranteeing the estimate $\hat{\theta}$ to be of some level of trust, is to monitor if the PE condition is too weak before reset is allowed. Another way would be to introduce some perturbation signals in the input of the plant, in order to increase the PE condition. It is also important to mention that in some estimation schemes, the PE condition does not need to be satisfied in order to achieve correct estimator convergence.

In this thesis we monitor PE and do not reset if the PE condition is week, see Chapter 3 for an example of monitoring the PE condition. A general way of monitoring PE is hard to establish, since this is depending on the estimator structure, plant model etc. However, since PE is only needed while in transient regime, the condition is typically satisfied when necessary.

2.3 Illustrative Example

A simple but illustrative example is given in order to show how to address all the needs in the above framework.

2.3.1 Plant

Consider the following linear plant example:

$$\begin{aligned}\dot{\xi} &= -\frac{1}{T}\xi + \frac{1}{T}u + \theta \\ y &= \xi + n\end{aligned} \tag{2.15}$$

where θ is some unknown scalar plant parameter, T is a positive time constant for the plant and n is measurement noise.

2.3.2 Dynamic Controller

A suitable controller for the plant (2.15) is a conventional PI-controller:

$$\begin{aligned}u &= K_p\left(y^* - y\right) + K_I z \\ \dot{z} &= y^* - y\end{aligned} \tag{2.16}$$

where $K_p > 0$ is the proportional gain and $K_I > 0$ is the integrator gain. The controller is dynamic due to $z \in \mathbb{R}$ being the integrator state. The state z may be reset to a different value z_i at any time instant.

2.3.3 Lyapunov Function

Assume the reference input y^* is constant, and the error states are defined as $x_1 = y^* - y$ and $x_2 = \frac{1}{K_I}y^* - \frac{T}{K_I}\theta - z$, the closed-loop error system is

$$\dot{x}_1 = -\frac{1}{T}\left(1 + K_p\right)x_1 + \frac{1}{T}K_I x_2 \tag{2.17}$$

$$\dot{x}_2 = -x_1, \tag{2.18}$$

and in compact form it constitutes a LTI system

$$\dot{x} = Ax \tag{2.19}$$

where

$$A = \begin{bmatrix} -\frac{1}{T}\left(1 + K_p\right) & \frac{1}{T}K_I \\ -1 & 0 \end{bmatrix}.$$

If A is Hurwitz, then there exists a solution $P^T = P > 0$ of the Lyapunov equation

$$A^T P + PA = -Q \tag{2.20}$$

where $Q^T = Q > 0$. From this, the Lyapunov candidate

$$V(x) = x^T P x \tag{2.21}$$

will prove stability of the closed-loop system (2.19). For the purpose of resetting the controller state z, the problem is however to pick a suitable Q in (2.20) such that (2.21) will be an appropriate measure of transient energy of (2.19). The existence of $Q^T = Q > 0$ rendering $P^T = P > 0$, the solution of (2.20), is however a necessary and sufficient condition for (2.19) to be strictly stable. On the other hand, picking a positive definite P and solving Q from (2.20), may not lead to a positive definite solution Q, even if A is Hurwitz, see e.g. Slotine & Li (1991) for more details.

A convenient way to find a suitable Lyapunov function is to use a LQ-controller, see Anderson & Moore (1989). For the system $\dot{x} = \bar{A}x + \bar{B}u$ where

$$\begin{aligned} \bar{A} &= \begin{bmatrix} -\frac{1}{T} & 0 \\ -1 & 0 \end{bmatrix} \\ \bar{B} &= \begin{bmatrix} \frac{1}{T} \\ 0 \end{bmatrix} \end{aligned} \tag{2.22}$$

and the state feedback vector $\bar{K} = [K_p \quad -K_I]$ of the controller $u = -\bar{K}x$ is given by

$$\bar{K} = \bar{R}^{-1}\bar{B}^T P \tag{2.23}$$

where P is the solution of the algebraic Riccati equation:

$$0 = -P\bar{A} - \bar{A}^T P + P\bar{B}\bar{R}^{-1}\bar{B}^T P - \bar{Q}, \quad P \geq 0. \tag{2.24}$$

$\bar{R}$ and $\bar{Q}$ are forming the cost function

$$\bar{J} = \int_{\tau=t}^{\infty} \left(\bar{R}u^2 + x^T\bar{Q}x\right) d\tau \tag{2.25}$$

where $\bar{R} > 0$, $\bar{Q} \geq 0$. Using P from (2.24), the Lyapunov function in (2.21) will in addition to prove stability of (2.19) also act as a meaningful measure of the transient energy of the same system (2.19).

2.3.4 Motivating Controller State Resetting

Assume $T = 0.5$, and selecting $\bar{R} = 0.1$ and $\bar{Q} = \text{diag}(0.1, 0.1)$, the controller parameters turns out to be $K_p = 0.73$ and $K_I = 1$, hence $A = [-3.46, 2; -1, 0]$. Figure 2.2(a) shows the phase portrait of the closed-loop error system with state propagations for four different initial conditions. $x_2(t)$ is the integrator error state of the system, and may be reset instantaneously to a different value x_{2i} at time t^+, where t^+ denotes an infinitely small time increment of t.

Assume the closed-loop system error state is located off the equilibrium point at t_0, say $x(t_0) = [2; -1]$, perhaps due to a set-point change or a large disturbance. Figure 2.2(a) shows this situation, where no reset, reset to $x_2(t_0^+) = 0$, reset to $x_2(t_0^+) = 1$ and reset to $x_2(t_0^+) = 2$, takes place at $t_0 = 1$ before the system continues to flow towards the desired equilibrium. Figure 2.2(b) shows the resulting transient for the plant error state x_1 as a result of the given reset of the state x_2. Assume the best transient behavior is when the plant error state x_1 reaches a small neighborhood of the origin as fast as possible, and without any significant overshoot. Compared to the lowest plot, showing the situation of not taking any reset actions, a better performance is

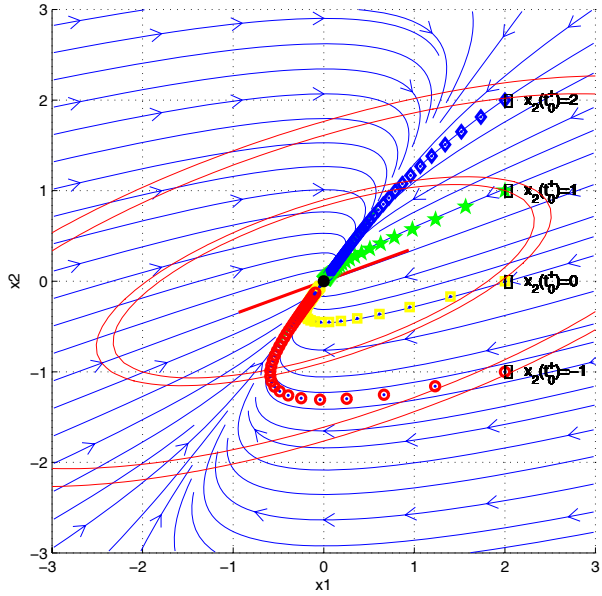

(a) Phase portrait of system (2.19), illustrating flow from different initial conditions, manipulated by resetting the integrator state x_2.

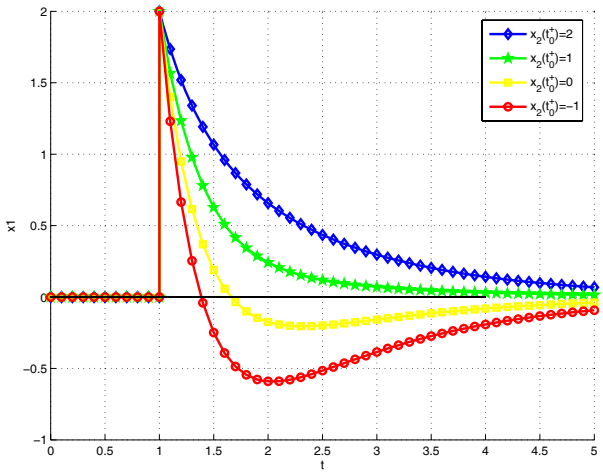

(b) Resulting transients for plant error state x_1 for different initial conditions in integrator state x_2.

Figure 2.2: Phase portrait and state transient for system (2.19) where $T = 0.5$, $K_I = 1$ and $K_p = 0.73$, hence $A = [-3.46,\ 2;\ -1,\ 0]$. The reset mechanism may only change the initial state $x_2(t_0^+)$ through z, hence $x_1(t_0^+)$ is equal in all four situations.

achieved by resetting the controller state to its steady-state value $x_2(t_0^+) = x_2^* = 0$. Even better performance is however achieved if controller state is reset to a value not equal to the steady-state, but instead to $x_2(t_0^+) = 1$. Note that the performance is not further improved if the integrator error state x_2 is reset to a higher value, e.g $x_2(t_0^+) = 2$.

A Lyapunov function may be used to decide when to perform a reset, and to what value of the controller state the reset gives the best system transient performance. By only executing a reset when this leads to a negative jump in the Lyapunov function value, the system stability properties will remain to be satisfied, see Theorem 2.1. By selecting a Lyapunov function that also gives a good indication of the system transient performance, both transient reduction and maintenance of stability will be achieved. The quadratic Lyapunov function (2.21) where $P = [0.0366, -0.05; -0.05, 0.1732]$ being the solution of the Riccati equation (2.24) proves stability of the overall system in addition to give measure of the system transient. Level curves of this particular Lyapunov function is included in Figure 2.2(a). Note from Figure 2.2 that reset from $x_2(t) = -1$ to $x_2(t^+) = 1$ gives the greatest drop in the Lyapunov function value, and also the best transient performance of the example system.

2.3.5 Parameter Estimate

Since x in $V(x)$ is not known due to $x_2 = \frac{1}{K_I}y^* - \frac{T}{K_I}\theta - z$ with θ unknown, an estimate $\hat{x}$ is needed in order to utilize a Lyapunov-based reset procedure. Estimation of x_2 may be directly estimated or indirectly estimated by first estimating the plant parameter θ. A simple way of estimating θ is given by first defining an observer for the state ξ:

$$\dot{\hat{\xi}} = a\left(\xi - \hat{\xi}\right) - \frac{1}{T}\xi + \frac{1}{T}u + \hat{\theta} \tag{2.26}$$

where $a > 0$. Further defining the state error $e = \xi - \hat{\xi}$ and the parameter error $\tilde{\theta} = \theta - \hat{\theta}$ yields the error dynamics

$$\dot{e} = -ae + \tilde{\theta}. \tag{2.27}$$

Selecting the Lyapunov function candidate for the estimator to be

$$V_{est}(e, \tilde{\theta}) = \frac{1}{2}e^2 + \frac{1}{2}\frac{1}{\gamma}\tilde{\theta}^2. \tag{2.28}$$

Further assume the adaptive law is given by

$$\dot{\hat{\theta}} = \gamma e \tag{2.29}$$

where $\gamma > 0$. The time derivative of (2.28) along the trajectories of (2.27) and (2.29) is $\dot{V}_{est} = -ae^2$, hence negative semidefinite. Note, however, that $\dot{V}_{est}$ is negative everywhere, except on the line $e = 0$, where $\dot{V}_{est} = 0$. In order to maintain $\dot{V}_{est} = 0$, the trajectory of the system must be confined to the line $e = 0$. Unless $\tilde{\theta} = 0$, this is impossible because $e \equiv 0 \Rightarrow \dot{e} \equiv 0 \Rightarrow \tilde{\theta} = ea \equiv 0$ from (2.27). Hence parameter convergence of observer is maintained, see the theorem of Barbashin and Krasovskii, e.g. Khalil (2002) for more details.

Remark 2.6 *In this simple example, we are able to prove convergence of the adaptive law. However, in some situations this may not be the case if PE is not satisfied. See Section 2.2.4 for more details on PE and what action to be taken in situations where PE is not satisfied.*

Remark 2.7 *The estimate $\hat{\theta}$ will in fact be corrupted by some measurement noise n. This is however left out in the development of the estimator above, and instead taken care of by appropriate choice of threshold value δ and sparseness of $z_i \in \mathcal{H}$, as noted earlier in this chapter. This is further discussed in the simulation example.*

2.3.6 Reset Algorithm

The reset algorithm is performing reset to candidate z_i when $\Delta V_i(\hat{x}) + \delta < 0$, where

$$\Delta V_i(x) = V(x_i) - V(x) = p_{11}\left(x_{1i}^2 - x_1^2\right) + 2p_{12}\left(x_{1i}x_{2i} - x_1x_2\right) + p_{22}\left(x_{2i}^2 - x_2^2\right). \quad (2.30)$$

Due to x not known because θ is unknown, an estimate $\hat{x}$ is used:

$$\hat{x} = \begin{bmatrix} y^* - y \\ z^*(\hat{\theta}) - z \end{bmatrix} \quad (2.31)$$

and

$$x_i = \begin{bmatrix} y^* - y \\ z^*(\hat{\theta}) - z_i \end{bmatrix} \quad (2.32)$$

hence the change in Lypaunov function value (2.30) becomes

$$\Delta V_i(\hat{x}) = 2p_{12}\left(\left(y^* - y\right)\left(z - z_i\right)\right) + p_{22}\left(2z^*(\hat{\theta})\left(z - z_i\right) + z_i^2 - z^2\right). \quad (2.33)$$

2.3.7 Simulation Example

Figure 2.3 shows simulation plots of the plant (2.15) with the controller (2.16). The controller parameters are $K_I = 1$ and $K_P = 0.73$ and the plant parameter $T = 0.5$ as in Figure 2.2. Changes in equilibrium are however in Figure 2.3 triggered by jump in the unknown parameter θ and set-point y^*. Initially $\theta = 1$ but at $t = 15$, the parameter makes a jump to $\theta = 2$ and stays there for 5 seconds before it jumps back again. The set-point is initially $y^* = 0$, but at $t = 2$ it jumps to $y^* = 3$, stays there for 8 seconds before it jumps down to $y^* = 1$. These scenarios are shown as solid lines in the upper plot and the next below in Figure 2.3, respectively. The resulting controller state z, i.e. the integrator state of the PI-controller, is seen as a dotted line in the plot below. The resulting controller output u can be seen in the plot next down.

In Figure 2.4, however, the same system and scenario as in Figure 2.3 is given, but in this case the controller state reset is made active. The reset mechanism is using the parameter estimator presented in Section 2.3.5 where the parameters $a = 4$ and $\gamma = 50$ are selected such that $\hat{\theta} \to \theta$ is faster than $z \to z^*$, see Section 2.1.4. This estimate enters into the reset algorithm (2.33) together with the Lyapunov function parameters $p_{12} = -0.05$ and $p_{22} = 0.1732$, obtained by solving the Riccati equation (2.24). The estimated Lyapunov function is depicted in the second plot from below for both cases. In order to complete the reset mechanism, the finite set of reset candidates

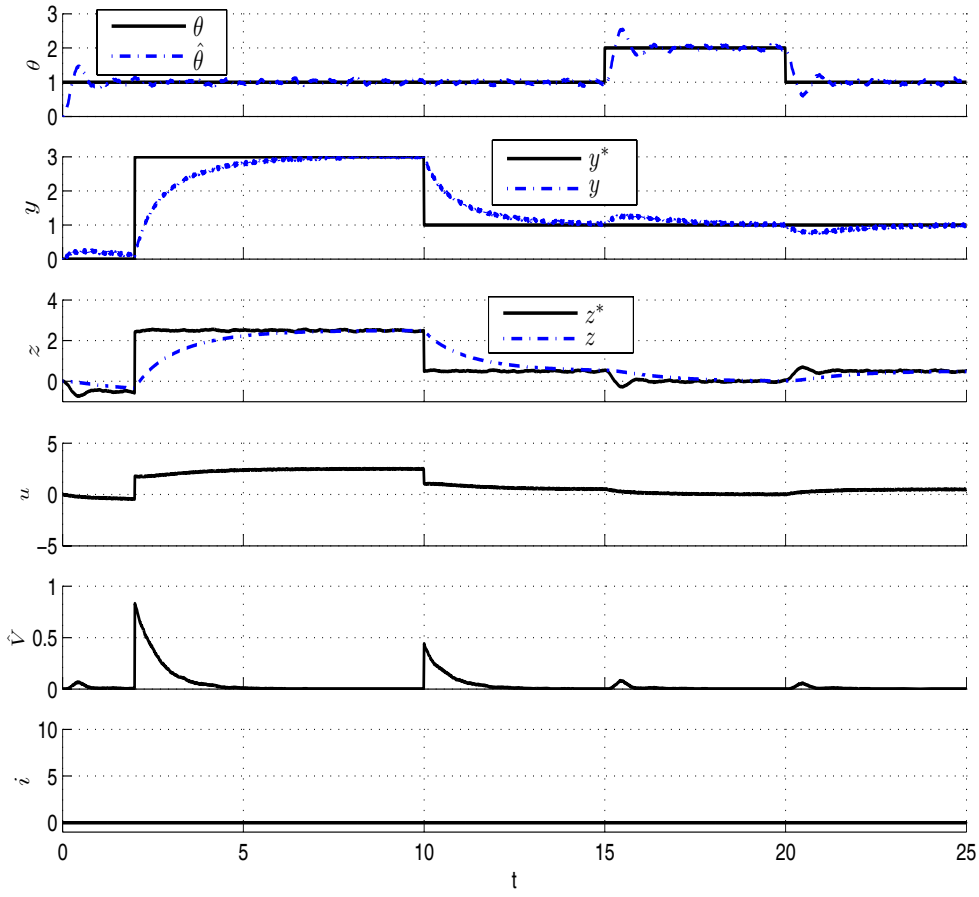

Figure 2.3: Simulation plot of system given a scenario of set-point change y^* at $t = 2$ and $t = 10$, and parameter change θ at $t = 15$ and $t = 20$ for the PI-controller without reset.

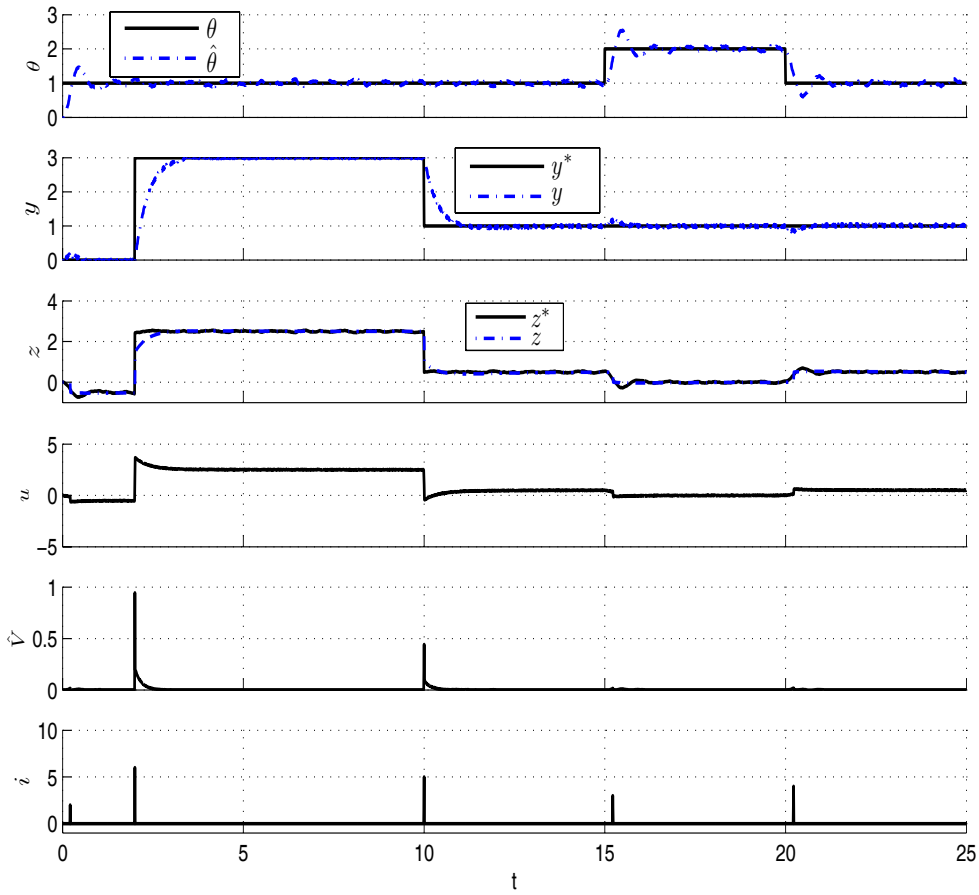

Figure 2.4: Same simulation scenario as in Figure 2.3, but for the PI-controller with reset.

$\mathcal{H}$ needs to be determined. Assume the set-point y^* is in the region $[y^*_{min},\, y^*_{max}] = [0,\, 3]$, and the unknown parameter θ is in the region $[\theta_{min},\, \theta_{max}] = [1,\, 2]$. From Section 2.3.3 we have $z^* = y^*/K_I - T\theta/K_I$, hence the set $\mathcal{H}$ needs to span the region $[z^*_{min},\, z^*_{max}] = [-1,\, 2.5]$. By using trial and error, the finite set of reset candidates is $\mathcal{H} = \{-1,\, -0.5,\, 0,\, 0.5,\, 1.0,\, 1.5,\, 2.0,\, 2.5\}$ and the reset threshold parameter $\delta = 0.01$.

In case of reset, the controller state z is reset to a value that corresponds to the index number i in $\mathcal{H}$. Note the reduction in transients of $\hat{V}$ when the controller state is reset. This is also seen as improved transient performance for the plant variable y. In addition to performing faster transient response in case of reset, the overall steady-state noise properties are not being changed. This is so even though the reset mechanism is making use of the noisy signal $\hat{\theta}$.

Part II

Applications

Chapter 3

Application to Adaptive Backstepping Control

This chapter considers an MMAC method based on adaptive nonlinear backstepping control where the parameter estimate may be instantaneously reset based on a criterion that requires a negative jump in the associated control Lyapunov function, initially reported in Kalkkuhl et al. (2002). Particular attention is paid to transient effects of data filtering, which must be introduced in any practical implementation of the MMAC algorithm in order to reduce the sensitivity to noise, disturbances and model uncertainty. The main contribution of this chapter is insight into the robust behavior of the adaptive system resulting from the filtering, and an investigation into the trade-offs between high transient performance and robustness to uncertainty. Data filter tuning guidelines are also presented, illustrated using a simulation example. The main material of this chapter has been presented in Bakkeheim & Johansen (2006) which is based on the work reported in Hansen & Johansen (2004).

3.1 Introduction

The main motivation for introducing reset of the parameter estimator in adaptive systems is to increase the transient performance without increasing the steady-state noise sensitivity. The transient performance has a strong relationship to the choice of the adaptation gain matrix. The higher the values of the diagonal elements of the adaptation gain matrix, the better the transient performance of the system. However, the sensitivity of the system to noise and other uncertainty increases with higher values. Introducing parameter resetting to rapidly counteract large parameter estimator errors may lead to a system having both fast transient response and a low steady-state noise sensitivity, see Figure 3.1. Such systems are called MMAC, being a well established approach for implementing adaptive systems with fast transient response.

A fairly general class of continuous time systems that allow backstepping adaptive design are considered in Kalkkuhl et al. (2002). A unique feature of the approach in Kalkkuhl et al. (2002) is that proving globally asymptotic stability (GAS) is combined with the development of the reset algorithm. This is done by using the control Lyapunov function from the adaptive

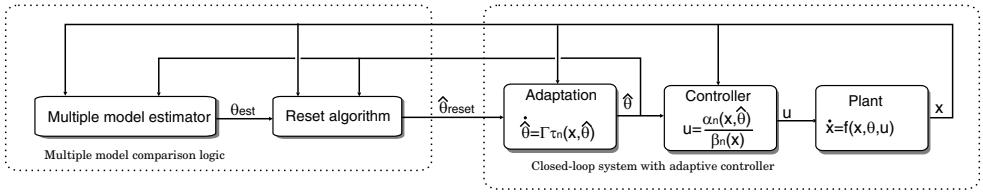

Figure 3.1: Illustration of MMAC approach. The parameter estimate of the adaptation law is reset when the multiple model comparison logic predicts a potential reduction in the Lyapunov function. This approach inherits both the robustness property of adaptive controller and the transient reduction property of parameter resetting.

backstepping design as a criterion for performing reset. In particular, as a negative jump in the control Lyapunov function is required, it is also proven that a reset will lead to improved transient performance, in the sense that the Lyapunov function measure of transient "energy" is minimized as a consequence of the parameter estimator reset. However, the analysis in Kalkkuhl et al. (2002) is based on some simplifications, in particular neglecting the effect of some filters that must be introduced in a practical implementation of the resetting algorithm in order to reduce the effect of noise, disturbances and model uncertainty.

3.2 Multiple Model Adaptive Controller with Resetting

3.2.1 Adaptive Controller

The systems to be studied in this chapter are so-called parametric-strict-feedback systems

$$\begin{aligned} \dot{x}_1 &= x_2 + \varphi_1(x_1)^T\theta \\ &\vdots \\ \dot{x}_{n-1} &= x_n + \varphi_{n-1}(x_1, x_2, \ldots, x_{n-1})^T\theta \\ \dot{x}_n &= \beta(x)u + \varphi_n(x)^T\theta \end{aligned} \tag{3.1}$$

where $\theta \in \mathbb{R}^k$ represents an unknown parameter vector and the φ_i's represent known smooth nonlinearities. In this chapter the so-called *tuning function design* procedure is preferred, see Krstic et al. (1995) for more details.

The backstepping adaptive controller and its corresponding adaptation law for the system (3.1) are given by

$$u = \frac{\alpha_n(x, \hat{\theta})}{\beta(x)} \tag{3.2}$$

$$\dot{\hat{\theta}} = \Gamma\tau_n(x, \hat{\theta}) \tag{3.3}$$

where the adaptation gain matrix $\Gamma = \Gamma^T > 0$. The control law α_n and the tuning function τ_n are given by the following recursive equations

$$\begin{aligned} z_i &= x_i - \alpha_{i-1} \\ \alpha_i(x_1, \ldots, x_i, \hat{\theta}) &= -z_{i-1} - c_i z_i - w_i^T \hat{\theta} + \sum_{k=1}^{i-1} \frac{\partial \alpha_{i-1}}{\partial x_k} x_{k+1} + \frac{\partial \alpha_{i-1}}{\partial \hat{\theta}} \Gamma \tau_i + \sum_{k=2}^{i-1} \frac{\partial \alpha_{k-1}}{\partial \hat{\theta}} \Gamma w_i z_k \\ \tau_i(x_1, \ldots, x_i, \hat{\theta}) &= \tau_{i-1} + w_i z_i \\ w_i(x_1, \ldots, x_i, \hat{\theta}) &= \varphi_i - \sum_{k=1}^{i-1} \frac{\partial \alpha_{i-1}}{\partial x_k} \varphi_k \end{aligned} \tag{3.4}$$

and $z_0 = 0$, $\alpha_0 = 0$, $\tau_0 = 0$, $c_i > 0$. The state z represents the error state. c_i are positive constants, rendering the system stable. The overall closed-loop error system is given by

$$\dot{z} = A_z(z, \hat{\theta}) z + W(z, \hat{\theta})^T \tilde{\theta} \tag{3.5}$$

$$\dot{\hat{\theta}} = \Gamma W(z, \hat{\theta}) z \tag{3.6}$$

where

$$A_z = \begin{bmatrix} -c_1 & 1 & 0 & \cdots & 0 \\ -1 & -c_2 & 1 + \sigma_{23} & \cdots & \sigma_{2n} \\ 0 & -1 - \sigma_{23} & \ddots & \ddots & \vdots \\ \vdots & \vdots & \ddots & \ddots & 1 + \sigma_{n-1,n} \\ 0 & -\sigma_{2n} & \cdots & -1 - \sigma_{n-1,n} & -c_n \end{bmatrix} \tag{3.7}$$

where

$$\sigma_{jk}(x, \hat{\theta}) = -\frac{\partial \alpha_{j-1}}{\partial \hat{\theta}} \Gamma w_k \tag{3.8}$$

and

$$W(z, \hat{\theta})^T = \begin{bmatrix} 1 & 0 & \cdots & 0 \\ -\frac{\partial \alpha_1}{\partial x_1} & 1 & \ddots & \vdots \\ \vdots & \ddots & \ddots & 0 \\ -\frac{\partial \alpha_{n-1}}{\partial x_1} & \cdots & -\frac{\partial \alpha_{n-1}}{\partial x_{n-1}} & 1 \end{bmatrix} F(x)^T \tag{3.9}$$

where

$$F(x) = [\varphi_1(x_1), \ldots, \varphi_n(x)]. \tag{3.10}$$

Along the trajectories of the closed-loop system, the control Lyapunov function

$$V(x, \hat{\theta}) = \frac{1}{2} z^T z + \frac{1}{2} (\hat{\theta} - \theta)^T \Gamma^{-1} (\hat{\theta} - \theta) \tag{3.11}$$

proves GAS, because its time-derivative is negative:

$$\dot{V} = -z^T C z \tag{3.12}$$

where $C = \text{diag}(c_1, \ldots, c_n) > 0$, hence satisfying the nominal stability condition. See Krstic et al. (1995) for more details.

3.2.2 Ideal Estimator Reset Criterion

In Kalkkuhl et al. (2002) an extension of this design is introduced by allowing the parameter estimate to be reset instantaneously from $\hat{\theta}(t)$ to $\hat{\theta}(t^+)$, where t^+ denotes an infinitely small time increment of t. Note that at these instants in time the parameter update law (3.3) does not apply, leading to the control Lyapunov function $V(t)$ being discontinuous as a function of time. Suppose the parameter estimate is reset at time t to a value $\hat{\theta}(t^+) = \hat{\theta}_i$. The corresponding jump in the Lyapunov function is given by

$$\Delta V_i(t) = V(x(t), \hat{\theta}_i) - V(x(t), \hat{\theta}(t)) = \Delta V_{z_i}(t) - \frac{1}{2}\left(\hat{\theta}_i - \hat{\theta}(t)\right)^T \Gamma^{-1}\left(2\theta - \hat{\theta}(t) - \hat{\theta}_i\right) \tag{3.13}$$

where

$$\Delta V_{z_i}(t) = \frac{1}{2}\left(z(t^+, \hat{\theta}_i)^T z(t^+, \hat{\theta}_i) - z(t)^T z(t)\right) \tag{3.14}$$

A stability-preserving and performance-improving reset condition is now $\Delta V_i(t) < 0$, as summarized in the following lemma, being a special case of Theorem 2.1.

Lemma 3.1 *Suppose the parameter estimate is reset at time t to $\hat{\theta}(t^+) = \hat{\theta}_i$ only if $\Delta V_i(t) < 0$. Then the adaptive control system with estimator resetting satisfies*

$$\dot{V}(t) \leq -z^T C z \tag{3.15}$$

where $\dot{V}(t)$ is interpreted in the usual distributional sense when $V(t)$ is discontinuous.

Remark 3.1 *Without any reset, the time-derivative of the Lyapunov function is given by (3.12), such that reset makes $V(t)$ decay faster.*

Direct application of this lemma assumes that θ used in the expression (3.13) can be estimated perfectly from measurement data, and in Kalkkuhl et al. (2002) a method of estimating the unknown θ is given. However, they neglect the effect of data filters that must be incorporated in a practical algorithm in order to achieve robustness with respect to noise and uncertainty. Below, the method is reviewed and the filter transients are studied in detail.

3.2.3 Parameter Estimator

Assume a finite number of fixed parameter hypotheses $\hat{\theta}_1, \ldots, \hat{\theta}_h$ that are compared at each time instant to see which one gives the largest decrease in $\Delta V_i(t)$. As soon as a negative value of one or more of $\Delta V_i(t)$s is detected, the parameter estimate of the adaptation law is reset by the parameter hypothesis $\hat{\theta}_i$ corresponding to the $\Delta V_i(t)$ with the most negative value. The multiple parameter hypothesis leads to the name MMAC.

The first step in the development of the parameter estimator is done by filtering both sides of the parametric-strict-feedback equations (3.1)

$$\begin{aligned} sH_1(s)x_1 &= H_1(s)x_2 + H_1(s)\left[\varphi_1(x_1)^T\theta\right] \\ &\vdots \\ sH_{n-1}(s)x_{n-1} &= H_{n-1}(s)x_n + H_{n-1}(s)\left[\varphi_{n-1}(x_1,x_2,\ldots,x_{n-1})^T\theta\right] \\ sH_n(s)x_n &= H_n(s)\left[\beta(x)u\right] + H_n(s)\left[\varphi_n(x)^T\theta\right] \end{aligned} \tag{3.16}$$

where $H_i(s)$ is typically a low-pass or band-pass filter. The main purpose of these filters is to replace non-realizable differentiation operations by appropriate high-pass filters, in addition to reducing the effect of high-frequency noise, low-frequency disturbances and other model uncertainty in the estimation model. The following scalar definitions are introduced

$$\begin{aligned} y_1(t) &= sH_1(s)x_1 - H_1(s)x_2 \\ &\vdots \\ y_{n-1}(t) &= sH_{n-1}(s)x_{n-1} - H_{n-1}(s)x_n \\ y_n(t) &= sH_n(s)x_n - H_n(s)\left[\beta(x)u\right] \end{aligned} \tag{3.17}$$

in order to define the vector $y(t) = \left[\ y_1(t), \quad \ldots, \quad y_n(t)\ \right]^T$. From (3.16), we have the following relationship

$$\begin{aligned} y(t) &= \left[\ H_1(s)\left[\varphi_1(x_1)^T\theta\right], \quad \ldots, \quad H_n(s)\left[\varphi_n(x)^T\theta\right]\ \right]^T \\ &= H(s)\left[F(x)^T\theta\right] \end{aligned} \tag{3.18}$$

where the vector $F^T(x) = [\varphi_1(x_1), \varphi_2(x_1,x_2), ..., \varphi_n(x)]^T$ and the $n \times n$-matrix $H(s) = \text{diag}\,(H_1(s),\ldots,H_n(s))$.

In order to study transients arising from the filter's initial state, which have been neglected so far, we consider a state-space realization of (3.18). The parameter θ is assumed constant after time 0. This is possible by transforming any sudden changes of the parameter value into corresponding jumps in the filter state's initial conditions. Consequently, the issue of nonzero initial conditions is not limited to filter initialization, but also to system parameter changes beyond our control, see Section 2.1.4 for more details.

Lemma 3.2 *The filter (3.18) may be written in the regressor form*

$$y(t) = \zeta^T(t)\theta + \breve{y}(t) \tag{3.19}$$

where the $n \times 1$-vector $y(t)$ and the $n \times k$-matrix $\zeta^T(t) = \left[\ \zeta_1(t), \quad \zeta_2(t), \quad \ldots, \quad \zeta_n(t)\ \right]^T$ are given by the following two state-space realizations

$$\begin{aligned} \dot{x}_y &= Ax_y + BF(x)^T\theta \\ y &= Cx_y + DF(x)^T\theta \end{aligned} \tag{3.20}$$

$$\begin{aligned}\dot{x}_\zeta &= Ax_\zeta + BF(x)^T \\ \zeta^T &= Cx_\zeta + DF(x)^T\end{aligned} \tag{3.21}$$

where A, B, C and D are given by $A = diag(A_1, \ldots, A_n)$, $B = diag(B_1, \ldots, B_n)$, $C = diag(C_1, \ldots, C_n)$ and $D = diag(D_1, \ldots, D_n)$, and (A_i, B_i, C_i, D_i) are realizations of the filter transfer function $H_i(s)$. Further, the transient term $\breve{y}(t)$ is given as

$$\breve{y}(t) = Ce^{At}\left(x_y(0) - x_\zeta(0)\theta\right) \tag{3.22}$$

Proof. Note that the dimensions of the corresponding system matrices in (3.20) and (3.21) are equal, whereas the dimensions of the filter states are not. This is because in the first case an $n \times 1$-vector $F(x)^T\theta$ is filtered, whereas in the latter case an $n \times k$-matrix $F(x)^T$ is filtered.

Further, rewrite (3.20) and (3.21) as

$$y(t) = C^T e^{At}x_y(0) + C^T \int_0^t e^{A(t-\tau)}BF(x(\tau))^T\theta d\tau + DF(x(t))^T\theta \tag{3.23}$$

$$\zeta^T(t) = C^T e^{At}x_\zeta(0) + C^T \int_0^t e^{A(t-\tau)}BF(x(\tau))^T d\tau + DF(x(t))^T \tag{3.24}$$

and (3.24) may again be rewritten into

$$C^T \int_0^t e^{A(t-\tau)}BF(x(\tau))^T d\tau + DF(x(t))^T = \zeta^T(t) - C^T e^{At}x_\zeta(0) \tag{3.25}$$

Further, (3.23) may be expressed as

$$\begin{aligned}y(t) &= C^T e^{At}x_y(0) + \left(C^T \int_0^t e^{A(t-\tau)}BF(x(\tau))^T d\tau + DF(x(t))^T\right)\theta && (3.26)\\ &= C^T e^{At}x_y(0) + \left(\zeta^T(t) - C^T e^{At}x_\zeta(0)\right)\theta && (3.27)\\ &= \zeta^T(t)\theta + C^T e^{At}x_y(0) - C^T e^{At}x_\zeta(0)\theta && (3.28)\end{aligned}$$

which gives (3.19) and (3.22). ■

Defining the predictor

$$\hat{y}_i(t) = \zeta^T(t)\hat{\theta}_i, \tag{3.29}$$

we obtain an expression for the prediction error

$$e_i(t) = y(t) - \hat{y}_i(t) = \zeta^T(t)\left(\theta - \hat{\theta}_i\right) + \breve{y}(t). \tag{3.30}$$

Multiplying both sides of (3.30) by $\zeta(t)$ gives

$$\zeta(t)e_i(t) = \zeta(t)\zeta^T(t)\left(\theta - \hat{\theta}_i\right) + \zeta(t)\breve{y}(t). \tag{3.31}$$

Because the term $\zeta(t)\zeta^T(t)$ may be singular, equation (3.31) cannot in general be solved for θ. One approach may be to filter both sides of (3.31). For simplicity, we consider a first order filter, $G(s) = 1/(1+\tau_g s)$, hence

$$G(s)\left[\zeta(t)e_i(t)\right] = \left\{G(s)\left[\zeta(t)\zeta^T(t)\right]\right\}\left(\theta - \hat{\theta}_i\right) + G(s)\left[\zeta(t)\breve{y}(t)\right]. \tag{3.32}$$

The idea is now to solve (3.32) with respect to the constant θ. In order to analyze the effect of the unknown transient term in (3.32) and the unknown transient arising from the initial state of the filter $G(s)$, we consider a state-space realization of the $G(s)$ filter. For convenience, first define two zero-state terms in (3.32) as

$$g_i(t) = \frac{1}{\tau_g}\int_0^t e^{-\frac{t-\tau}{\tau_g}}\zeta(\tau)e_i(\tau)d\tau \tag{3.33a}$$

$$S(t) = \frac{1}{\tau_g}\int_0^t e^{-\frac{t-\tau}{\tau_g}}\zeta(\tau)\zeta^T(\tau)d\tau. \tag{3.33b}$$

The following lemma shows how θ can be decomposed into one computable part and an unknown transient part. In the next section, we will consider the effect of neglecting the unknown transient term.

Lemma 3.3 *Assuming persistence of excitation of $\zeta(t)$, that is, there exists an $\varepsilon > 0$ such that for all $t \geq 0$, $S(t) \geq \varepsilon I$, then the unknown parameter θ may be represented as follows*

$$\theta = \theta_{est}(t) + \theta_{trans}(t) \tag{3.34}$$

where the computable part is

$$\theta_{est}(t) = S^{-1}(t)g_i(t) + \hat{\theta}_i \tag{3.35}$$

and the transient term is

$$\theta_{trans}(t) = -e^{-\frac{t}{\tau_g}}S^{-1}(t)S(0)\Delta\theta - S^{-1}(t)\frac{1}{\tau_g}\int_0^t e^{-\frac{t-\tau}{\tau_g}}\zeta(\tau)\breve{y}(\tau)d\tau \tag{3.36}$$

and $\Delta\theta$ models the transient effect of a jump in θ at time 0.

Proof. In order to consider the transient effect of a jump in θ at time 0, we also consider the time interval from t_0 to 0, where $t_0 < 0$ is a time when the system was at steady-state. Hence, $\theta(\tau)$ is viewed as time varying, having the constant value θ_0 before time 0 and the constant value θ from time 0, see Figure 3.2.

First, note that the term $\zeta(t)\zeta^T(t)\left(\theta - \hat{\theta}_i\right)$ of (3.31) when located inside an integral may be

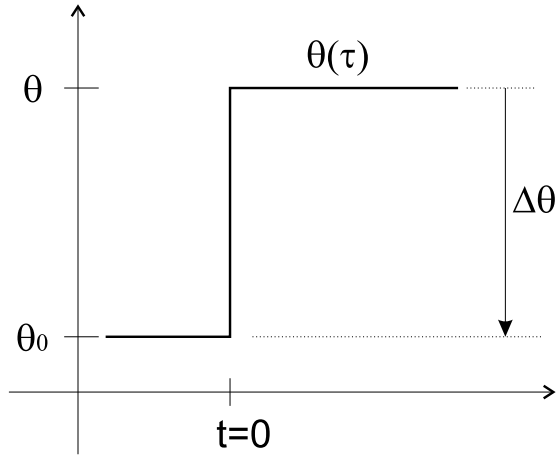

Figure 3.2: Illustration of how to interpret the time-varying parameter $\theta(\tau)$ as two constant values, θ_0 and θ. θ_0 represents the parameter value just before a jump takes place at time 0, and θ represents the value just after. Also the constant $\Delta\theta = \theta_0 - \theta$ is included in the figure.

rewritten as follows

$$
\begin{aligned}
&\frac{1}{\tau_g}\int_{t_0}^{t} e^{-\frac{t-\tau}{\tau_g}}\zeta(\tau)\zeta^T(\tau)\left(\theta(\tau)-\hat{\theta}_i\right)d\tau \\
&\quad= \frac{1}{\tau_g}\int_{t_0}^{t} e^{-\frac{t-\tau}{\tau_g}}\zeta(\tau)\zeta^T(\tau)\theta(\tau)d\tau - \frac{1}{\tau_g}\int_{t_0}^{t} e^{-\frac{t-\tau}{\tau_g}}\zeta(\tau)\zeta^T(\tau)\hat{\theta}_i d\tau \\
&\quad= e^{-\frac{t}{\tau_g}}\frac{1}{\tau_g}\left(\int_{t_0}^{0} e^{\frac{\tau}{\tau_g}}\zeta(\tau)\zeta^T(\tau)\theta_0 d\tau + \int_{0}^{t} e^{\frac{\tau}{\tau_g}}\zeta(\tau)\zeta^T(\tau)\theta d\tau\right. \\
&\qquad\left. - \int_{t_0}^{t} e^{\frac{\tau}{\tau_g}}\zeta(\tau)\zeta^T(\tau)\hat{\theta}_i d\tau + \int_{t_0}^{0} e^{\frac{\tau}{\tau_g}}\zeta(\tau)\zeta^T(\tau)\theta d\tau - \int_{t_0}^{0} e^{\frac{\tau}{\tau_g}}\zeta(\tau)\zeta^T(\tau)\theta d\tau\right) \\
&\quad= e^{-\frac{t}{\tau_g}}\frac{1}{\tau_g}\left(\int_{t_0}^{0} e^{\frac{\tau}{\tau_g}}\zeta(\tau)\zeta^T(\tau)\theta_0 d\tau + \int_{t_0}^{t} e^{\frac{\tau}{\tau_g}}\zeta(\tau)\zeta^T(\tau)\theta d\tau\right. \\
&\qquad\left. - \int_{t_0}^{t} e^{\frac{\tau}{\tau_g}}\zeta(\tau)\zeta^T(\tau)\hat{\theta}_i d\tau - \int_{t_0}^{0} e^{\frac{\tau}{\tau_g}}\zeta(\tau)\zeta^T(\tau)\theta d\tau\right) \\
&\quad= \frac{1}{\tau_g}\int_{t_0}^{t} e^{-\frac{t-\tau}{\tau_g}}\zeta(\tau)\zeta^T(\tau)\left(\theta-\hat{\theta}_i\right)d\tau + e^{-\frac{t}{\tau_g}}\frac{1}{\tau_g}\int_{t_0}^{0} e^{\frac{\tau}{\tau_g}}\zeta(\tau)\zeta^T(\tau)\left(\theta_0-\theta\right)d\tau \\
&\quad= S(t)\left(\theta-\hat{\theta}_i\right) + e^{-\frac{t}{\tau_g}}S(0)\Delta\theta. \qquad (3.37)
\end{aligned}
$$

Further, we may rewrite (3.32) in the time domain as

$$\frac{1}{\tau_g}\int_0^t e^{-\frac{t-\tau}{\tau_g}}\zeta(\tau)e_i(\tau)d\tau = \frac{1}{\tau_g}\int_{t_0}^t e^{-\frac{t-\tau}{\tau_g}}\zeta(\tau)\zeta^T(\tau)\left(\theta(\tau)-\hat{\theta}_i\right)d\tau + \frac{1}{\tau_g}\int_0^t e^{-\frac{t-\tau}{\tau_g}}\zeta(\tau)\breve{y}(\tau)d\tau. \tag{3.38}$$

Using the definitions in (3.33a) and (3.33b) together with the result of the calculation in (3.37), (3.38) may be rewritten as

$$g_i(t) = S(t)\left(\theta-\hat{\theta}_i\right) + e^{-\frac{t}{\tau_g}}S(0)\Delta\theta + \frac{1}{\tau_g}\int_0^t e^{-\frac{t-\tau}{\tau_g}}\zeta(\tau)\breve{y}(\tau)d\tau. \tag{3.39}$$

Solving for θ

$$\theta = S^{-1}(t)g_i(t) + \hat{\theta}_i - e^{-\frac{t}{\tau_g}}S^{-1}(t)S(0)\Delta\theta - \frac{1}{\tau_g}S^{-1}(t)\int_0^t e^{-\frac{t-\tau}{\tau_g}}\zeta(\tau)\breve{y}(\tau)d\tau \tag{3.40}$$

which may be written as in (3.34), where the computational and transient term is given in (3.35) and (3.36). ■

Assuming $S(t) \geq \varepsilon I$, we consider the direct estimate of θ, that is, $\theta_{est}(t)$ in (3.35). The overall idea of using the estimate $\theta_{est}(t)$ of the unknown parameter θ in (3.13) for the reset criterion is based on the fact that $\theta_{trans}(t)$ may settle much faster than the parameter estimate $\hat{\theta}(t)$ in the update law (3.3), such that $\theta_{est}(t)$ will be a better estimate than $\hat{\theta}(t)$ during a transient phase. On the other hand, the accuracy of the estimate $\theta_{est}(t)$ will indeed be much more sensitive to noise than $\hat{\theta}(t)$, since the dynamics of the filters $G(s)$ and $H_i(s)$ are usually much faster than the dynamics of $\hat{\theta}(t)$ in (3.3). This may be considered to be of less importance, as $\theta_{est}(t)$ is intended to be used as an estimate only during a transient phase. We remark that the estimate (3.35) is similar to the estimate proposed in Kalkkuhl et al. (2002), the main difference being here that we consider in detail the effect of $\theta_{trans}(t)$.

As stated above, a form of persistence of excitation must be assumed for (3.33b). It can be seen from (3.35) that poor conditioning of $S(t)$ generally means that the estimate $\theta_{est}(t)$ is inaccurate. The persistence of excitation condition will typically hold during transients, where a reset may be profitable. On the other hand, when close to steady-state, the persistence of excitation condition may not hold, but in such an instance there is no need for reset anyway. Hence, reset is not permitted when $S(t)$ is found to be too poorly conditioned. This is done by on-line monitoring the singularity condition of $S(t)$. A reset is not allowed if $S(t)$ becomes too close to singular.

3.3 Transient Analysis of the Effect of Filtering and Uncertainty

3.3.1 Main Result

First we define an estimate of the Lyapunov function (3.11) based on the estimate $\theta_{est}(t)$ from the previous section

$$V_{est}(z,\hat{\theta}) = \frac{1}{2}z^T z + \frac{1}{2}\left(\hat{\theta}-\theta_{est}\right)^T \Gamma^{-1}\left(\hat{\theta}-\theta_{est}\right). \tag{3.41}$$

An instantaneous jump $\hat{\theta}(t^+) = \hat{\theta}_i$ leads to an instantaneous change in $V_{est}(t)$

$$\Delta V_{i,est}(t) = \frac{1}{2}\left(z(t^+,\hat{\theta}_i)^T z(t^+,\hat{\theta}_i) - z(t)^T z(t)\right) - \frac{1}{2}\left(\hat{\theta}_i-\hat{\theta}(t)\right)^T \Gamma^{-1}\left(2\theta_{est}(t)-\hat{\theta}(t)-\hat{\theta}_i\right). \tag{3.42}$$

The point of interest is located in the difference between the jump in the adaptive control Lyapunov function (3.13) and its estimated value (3.42) being used in the reset criterion $\Delta V_{i,est}(t) < 0$.

It is assumed that a negative jump in the exact adaptive control Lyapunov function (3.11) is desirable whenever this is possible (recall Lemma 3.1).

Criterion 3.1 *To ensure avoiding erroneous reset using $\Delta V_{i,est}(t) < 0$ instead of $\Delta V_i(t) < 0$ as the reset criterion, a negative value of $\Delta V_{i,est}(t)$ must lead to a negative value of $\Delta V_i(t)$. The converse is not necessary.*

Using $\theta = \theta_{est}(t) + \theta_{trans}(t)$, from Lemma 3.3, (3.42) can be written

$$\Delta V_{i,est}(t) = \Delta V_i(t) + \frac{1}{2}\left(\hat{\theta}_i-\hat{\theta}(t)\right)^T \Gamma^{-1}\left(2\theta_{trans}(t)\right). \tag{3.43}$$

It is easily seen that the estimate $\Delta V_{i,est}(t)$ tends to the correct value $\Delta V_i(t)$, since $\theta_{trans}(t) \to 0$ as $t \to \infty$. The following theorem gives sufficient conditions for Criterion 3.1.

Theorem 3.1 *Suppose*

$$\Delta V_{i,est}(t) < 0. \tag{3.44}$$

Then, no erroneous reset, according to Criterion 3.1, will occur if the following inequality also holds

$$\frac{1}{2}\left(\hat{\theta}_i-\hat{\theta}(t)\right)^T \Gamma^{-1}\left(2\theta_{trans}(t)\right) \geq 0. \tag{3.45}$$

Notice that $\theta_{trans}(t)$ cannot be assumed to be known, so this theorem cannot be used in a direct way to formulate a better reset criterion. Instead, we pursue addition insight from this result in the following sections.

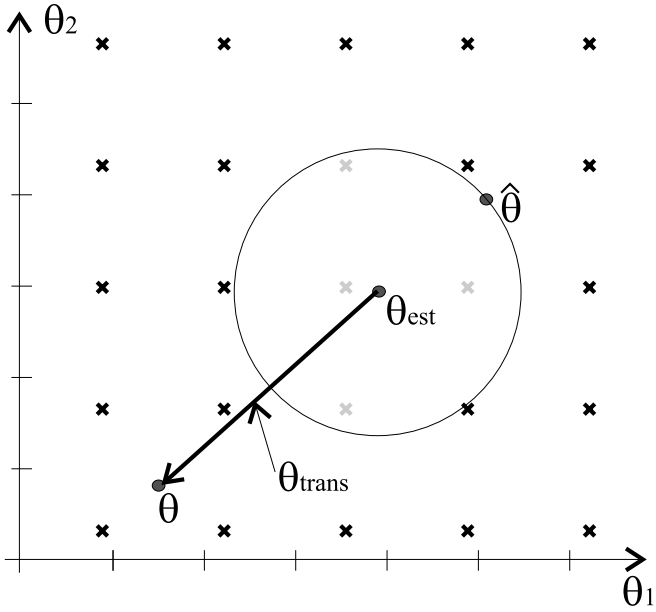

Figure 3.3: Visualization of inequality (3.44) of Theorem 3.1. The black and gray crosses are reset candidates. The gray ones satisfy condition (3.44), whereas the black ones do not.

3.3.2 Geometric Interpretation for First Order Systems

First assume for simplicity that z is of dimension one, which leads to $\Delta V_{z_i}(t) = 0$, such that (3.44) may be written

$$\frac{1}{2}\left(\hat{\theta}_i - \theta_{est}(t)\right)^T \Gamma^{-1}\left(\hat{\theta}_i - \theta_{est}(t)\right) - \frac{1}{2}\left(\hat{\theta}(t) - \theta_{est}(t)\right)^T \Gamma^{-1}\left(\hat{\theta}(t) - \theta_{est}(t)\right) < 0 \tag{3.46}$$

which is the same as claiming $||A\left(\hat{\theta}_i - \theta_{est}(t)\right)||^2 < ||A\left(\hat{\theta}(t) - \theta_{est}(t)\right)||^2$, with the Cholesky factorization $\Gamma^{-1} = A^T A$. For simplicity, assume equal diagonal elements in Γ, leading to the fact that the inequality can be rewritten as $||\hat{\theta}_i - \theta_{est}(t)|| < ||\hat{\theta}(t) - \theta_{est}(t)||$. This can be done without loss of generality because Γ may be transformed to cI by linear transformation of the coordinate axis in the θ-system. The given inequality, and indeed (3.44), is satisfied if the estimator reset candidate $\hat{\theta}_i$ is located inside the circle centered in $\theta_{est}(t)$, with radius $||\hat{\theta}(t) - \theta_{est}(t)||$. This is depicted in Figure 3.3, where the estimator reset candidates satisfying (3.44) are made gray, in contrast to the black ones not satisfying (3.44).

Further, for Theorem 3.1 to hold, the inequality (3.45) must hold as well. This inequality may be seen as the *forbidden region* inside the circle, and is visualized as the shaded area in Figure 3.4.

According to (3.45), the angle between the two vectors $\theta_{trans}(t)$ and $\hat{\theta}_i - \hat{\theta}(t)$ must be between

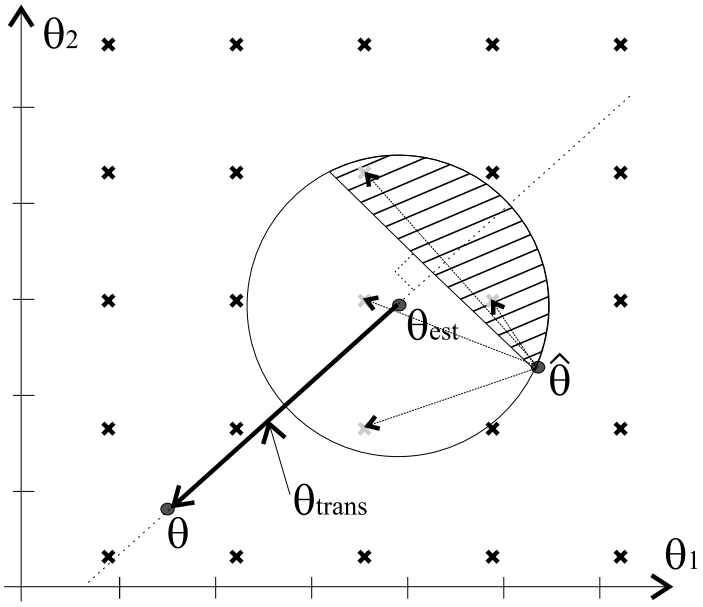

Figure 3.4: Visualization of inequality (3.45) of Theorem 3.1 in terms of a forbidden region. As in Figure 3.3, the black and gray crosses are reset candidates. The gray ones satisfy condition (3.44), whereas the black ones do not. In addition, only the gray ones outside the forbidden region (shaded area) satisfy condition (3.45).

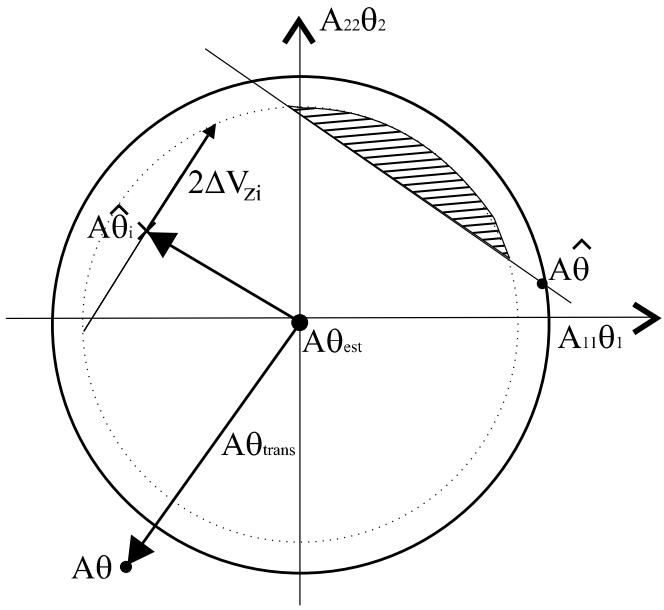

Figure 3.5: Visualization of inequality (3.45) of Theorem 3.1 with positive jump $\Delta V_{z_i}(t) > 0$ as a forbidden region.

$\pm 90^\circ$ for any reset candidate $\hat{\theta}_i$, if an erroneous reset is to be avoided.

3.3.3 Geometric Interpretation for Systems of Higher Order

Next assume that Γ may not have equal diagonal elements and z may not be scalar. The latter means that $\Delta V_{z_i}(t)$ may be different from zero. The inequality in (3.44) may be written as

$$||A\left(\hat{\theta}_i - \theta_{est}(t)\right)||^2 + ||z(t^+)||^2 - ||z(t)||^2 < ||A\left(\hat{\theta}(t) - \theta_{est}(t)\right)||^2 \tag{3.47}$$

and (3.45) becomes

$$\frac{1}{2}\left(A(\hat{\theta}_i - \hat{\theta}(t))\right)^T (2A\theta_{trans}(t)) \geq 0. \tag{3.48}$$

This leads to two different situations: one in which $\Delta V_{z_i}(t)$ is negative and another in which it is positive. Consider first the positive case

$$||A\left(\hat{\theta}_i - \theta_{est}\,(t)\right)||^2 + 2\Delta V_{z_i}(t) < ||A\left(\hat{\theta}\,(t) - \theta_{est}\,(t)\right)||^2. \tag{3.49}$$

Hence, a similar geometric interpretation can be given in a space that is similar to the θ-space in terms of the transformation matrix A; see Figure 3.5 for the case when $\Delta V_{z_i}(t) > 0$.

The other case where $\Delta V_{z_i}(t) < 0$ is interpreted in a similar way, but by expanding the circular region, is not discussed for reasons of brevity. If θ has dimension higher than 2, the

geometric interpretations may be generalized in a straightforward manner using hyper-spheres and hyper-planes.

3.3.4 Resetting Criterion Revisited

In the context of the above geometric interpretation, avoiding erroneous resets due to filter transients essentially amounts to avoiding reset candidates within the forbidden region that may violate (3.45) in Theorem 3.1, shown as the hatched half-moon shaped area in Figure 3.5. We first remark that exact knowledge of this area requires knowledge of the direction of the vector $\theta_{trans}(t)$, which links the points θ and $\theta_{est}(t)$. This information is not generally available.

However, from the discussion in section 3.3.2, it is clear that if the point $\theta_{est}(t)$ is located on a straight line between θ and $\hat{\theta}(t)$ and initially $\hat{\theta}(0) = \theta_{est}(0)$, the forbidden region degenerates to a point, which means that no erroneous reset will ever occur. $\hat{\theta}(0) = \theta_{est}(0)$ essentially means that $\hat{\theta}(t)$ has reached its steady-state value θ before a new, sudden change of θ takes place (this is assumed without loss of generality to occur at time 0). Note that the necessity of letting $\hat{\theta}(t)$ reach its steady-state may be fulfilled without having to wait for its slow dynamics. This is so because resets may have taken place during its settlement, hence speeding up its dynamic behavior.

At first glance, it may seem unlikely that $\theta_{est}(t)$ will be confined to such a straight line, but it turns out that this may in fact be a close to typical situation, as pointed out in the following theorem.

Theorem 3.2 *Assume the dynamics of the closed-loop system (3.1)-(3.3) without reset is viewed to be infinitely slow compared to the system's data filter dynamics. Further assume the filters, $H_1(s), H_2(s), ..., H_n(s)$ are of order one and equal. If $S(t) \geq \varepsilon I$ where $\varepsilon > 0$ for all $t \geq 0$, then the trajectory of $\theta_{est}(t)$ is a straight line between $\theta_{est}(0)$ and θ.*

Proof. Since $\theta = \theta_{trans}(t) + \theta_{est}(t)$ is constant, we have to prove that $\theta_{trans}(t)$ evolves in straight lines. $\theta_{trans}(t)$ may be written as

$$\theta_{trans}(t) = -e^{-\frac{t}{\tau_g}} S^{-1}(t)S(0)\Delta\theta - \frac{1}{\tau_g}S^{-1}(t)\int_0^t e^{-\frac{t-\tau}{\tau_g}}\zeta(\tau)Ce^{A\tau}BF^T(x)\Delta\theta d\tau \qquad (3.50)$$

where the relation $x_y(0) - x_\zeta(0)\theta = BF^T(x)\theta_0 - BF^T(x)\theta = BF^T(x)\Delta\theta$ has been used in combination with (3.22).

Further, using the filter assumption, $C = I$, $A = -\frac{1}{\tau_h}I$ and $B = \frac{1}{\tau_h}I$, where τ_h is the time constant of filters $H_i(s)$, we obtain

$$\theta_{trans}(t) = -e^{-\frac{t}{\tau_g}} S^{-1}(t)S(0)\Delta\theta - \frac{1}{\tau_g}S^{-1}(t)\frac{1}{\tau_h}\int_0^t e^{-\frac{t-\tau}{\tau_g}}\zeta(\tau)e^{-\frac{\tau}{\tau_h}I}F^T(x)\Delta\theta d\tau. \qquad (3.51)$$

Further, assuming the dynamics of the closed-loop system without reset is infinite slow compared to the filter dynamics, we may view $S(t) = S(0) = \acute{S}$ and $\zeta(t) = \acute{\zeta}$ as constants

$$\theta_{trans}(t) = -e^{-\frac{t}{\tau_g}}\Delta\theta - \frac{1}{\tau_g\tau_h}\int_0^t e^{-\frac{t-\tau}{\tau_g}}\acute{S}^{-1}\acute{\zeta}e^{-\frac{\tau}{\tau_h}I}\acute{F}^T\Delta\theta d\tau. \qquad (3.52)$$

Note that the assumption of infinitely slow dynamics, hence $F^T(x) = \acute{F}^T$, has also been used. (3.52) may be seen as a first order low pass filtering of straight line behavior input signal, whose transient terms because of initial conditions are moving in parallel with this input. This leads to an output result $\theta_{trans}(t)$ also with straight line behavior; hence, $\theta_{est}(t)$ moves in straight lines. ■

It follows that the straight line assumption is not severely unrealistic with fast filters such that the forbidden region is typically a small subset of the circle in the geometric interpretation in Figure 3.4. This will be further discussed and justified in the context of the example in section 3.4.

3.3.5 Noise and Model Uncertainty

Low-frequency noise, that is, model uncertainties are suppressed by the adaptation, whereas high-frequency noise is suppressed by low-pass filtering techniques.

Given the filter as stated in Theorem 3.2, the behavior of $\theta_{est}(t)$ will evolve in a straight line between $\theta_{est}(0)$ and θ. If the system is subjected to noise, the behavior of $\theta_{est}(t)$ will not be fully straight. Instead, the straight line behavior is degenerated to nearly straight, superimposed by noise. But this may be further suppressed by means of the grid coarseness of reset candidates. Increasing the distance between reset candidates will reduce the risk of erroneous resetting because of noise. This is illustrated in the example in the next section.

3.4 Case Study - Automotive Wheel Slip Control

3.4.1 Augmented Quarter Car Model

A case study that illustrates the concepts given in this chapter is an extension of the wheel slip control system presented in Kalkkuhl et al. (2002). The simple model in Kalkkuhl et al. (2002) is a quarter car model. With reference to Figure 3.6, the state of interest is the wheel slip λ, defined as

$$\lambda = \frac{v - \omega r}{v} \tag{3.53}$$

which is the normalized difference between the horizontal quarter car speed v and the speed of the wheel perimeter ωr. Because of the shape of the friction curve, Figure 3.7, a slip value of 0.15 is chosen as the set-point value, which gives close to maximum friction, see Lüdemann (2002) for more details.

In addition to the simple quarter car model in Kalkkuhl et al. (2002), the dynamics of the actuator is also included. The system may be presented as follows

$$\dot{x}_1 = k\check{x}_2 + \varphi_{1,1}(x_1)\theta_1 \tag{3.54}$$

$$\tau_a\dddot{\check{x}}_2 = u - \check{x}_2 \tag{3.55}$$

where x_1 represents the wheel slip error, $x_1 = \lambda - 0.15$, $k\check{x}_2$ represents the brake force and u is the clamping force commanded to the actuator. The parameter k is an unknown factor that represents the conversion of clamping force from the actuator output to the actual brake force in the quarter car system. k can then be seen as a gain that connects the two sub-systems (3.54) and

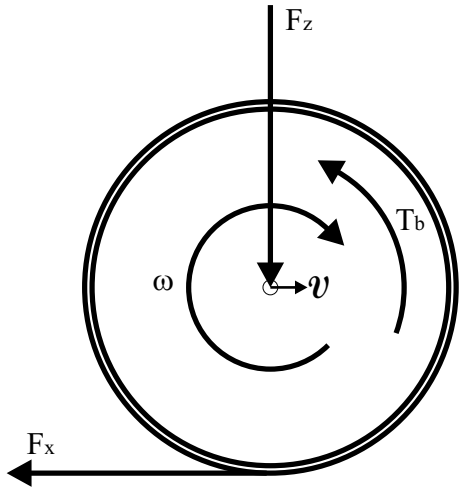

Figure 3.6: Quarter car forces and torques. v is the longitudinal speed at which the car travels, ω is the angular speed of the wheel, F_z is the vertical force, F_x is tyre friction force and T_b is brake torque.

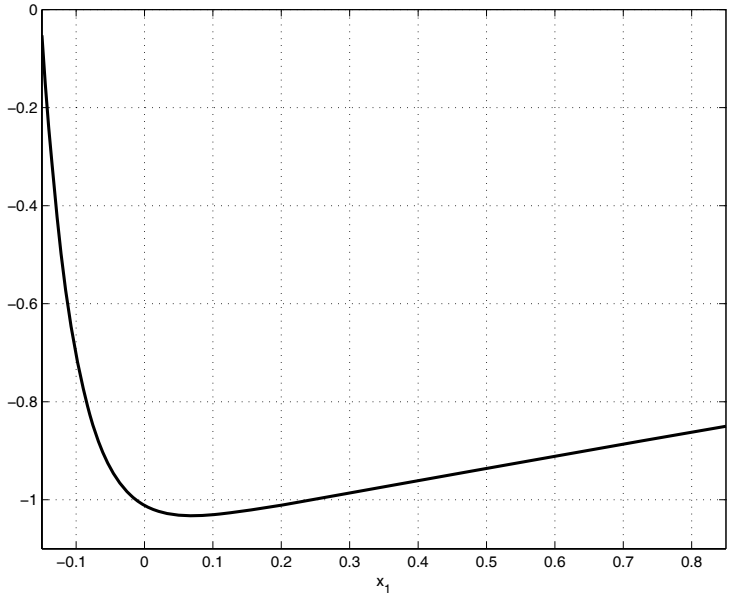

Figure 3.7: Nonlinearity $\phi_{1,1}$.

(3.55), whose domain is assumed to be $k \in [0.8, 1.2]$. A realistic choice of the actuator dynamics time constant τ_a is 0.08 sec. The nonlinear function $\varphi_{1,1}(x_1)$ represents the friction curve as in Kalkkuhl et al. (2002)

$$\varphi_{1,1}(x_1) = -(1 + 0.05(0.85 - x_1))\left(1.02 - e^{(-20x_1-3)} - 0.2x_1\right). \tag{3.56}$$

The domain of the road/tyre friction coefficient θ_1 is from $\theta_1 = 0$, indicating no tyre/road surface friction to $\theta_1 = 1$ corresponding to maximum friction (dry asphalt surface).

The model (3.54) - (3.55) is not in standard parametric-strict-feedback form (3.1), and has to be transformed to this form to be controlled by the strategy described in Section 3.2. By defining $x_2 = k\ddot{x}_2$, and assuming $\frac{\tau_a}{k} \approx \tau_a$ due to the relatively little uncertainty in $k \approx 1$, (3.54) and (3.55) may be written as

$$\dot{x}_1 = x_2 + \varphi_{1,1}(x_1)\theta_1 \tag{3.57}$$

$$\dot{x}_2 = \frac{1}{\tau_a}u - \theta_2\frac{1}{\tau_a}x_2 \tag{3.58}$$

which in turn can be written in parametric-strict-feedback form (3.1) using $\beta(x) = \frac{1}{\tau_a}$, $\varphi_1^T(x_1) = [\varphi_{1,1}(x_1), 0]$, $\varphi_2^T(x_2) = [0, \varphi_{2,2}(x_2)]$ and $\theta^T = [\theta_1, \theta_2]$, where $\theta_2 = \frac{1}{k}$ and $\varphi_{2,2}(x_2) = -\frac{1}{\tau_a}x_2$.

3.4.2 Simulation Scenario

The simulation is based on a situation of a car braking on a heterogeneous road surface: for example, asphalt that is partly covered with ice or water. This leads to rapidly changing road/tyre friction coefficient θ_1. In addition to this, the amount of force transferred from the actuator to the wheel is given by the force gain coefficient θ_2. The force transmission may change almost instantaneously because of failure in the hydraulics or the brake pads becoming wet. A worst case scenario is when both θ_1 and θ_2 change their values at the same time. The scenario to be simulated is represented by the step changes in θ, as shown by the solid line in Figure 3.8.

3.4.3 Reset Algorithm and Tuning

The adaptive controller may be tuned by first disabling the reset algorithm. The parameters of the adaptive controller are chosen as $c_1 = 1$, $c_2 = 30$ and $\Gamma = 0.5I$, leading to satisfactory adaptive system performance. The filters $G(s), H_1(s), ..., H_n(s)$ of the estimator are all chosen to be low-pass filters of order one, all with time constants equal to 85 ms. This is slow enough to reduce noise sensitivity of the estimate $\theta_{est}(t)$, while also being fast enough for the transient performance to not slow down significantly.

In this example $\theta \in \mathbb{R}^2$, which means that the choice of parameter reset candidates is made as a grid pattern in the plane. The "density" of the pattern must be selected to address the trade-off between noise sensitivity and transient performance. As the density of the grid pattern increases, the parameter estimate approaches the behavior of using $\theta_{est}(t)$ directly, as an estimator in the adaptive system. As the grid pattern becomes more coarse, only large transients will benefit from the resetting strategy. The grid pattern used in this example is in Figure 3.9, indicated with small crosses in a 3×5 pattern.

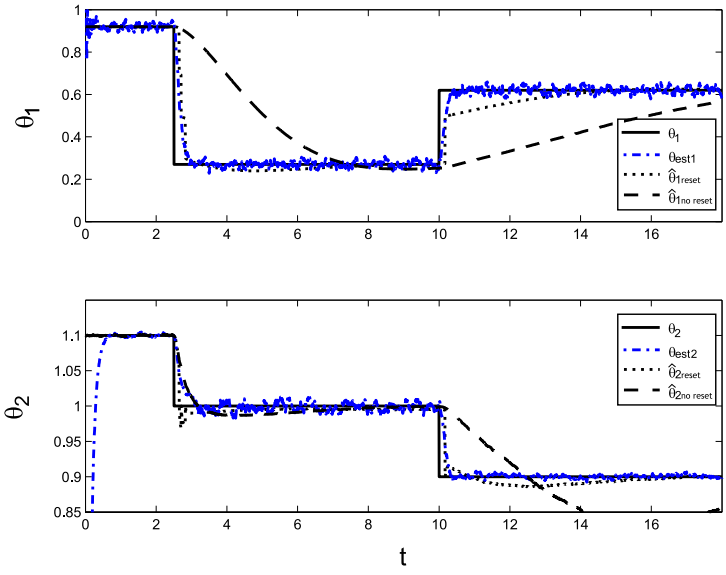

Figure 3.8: Parameter adaptation with and without reset.

3.4.4 Simulation Results

Figure 3.10 shows the value of the Lyapunov function as a function of time for a simulation of the adaptive system with and without reset. Even though no safeguard regarding avoidance of erroneous reset is used, the resulting Lyapunov function response in Figure 3.10 shows no signs that such an occurrence has taken place.

By comparing the two situations for a system with and without reset in Figure 3.8, the fast filter dynamics greatly improve the transient performance without increasing the noise sensitivity (see also Figure 3.9). The effect of filtering leads to the parameter estimate making several small jumps in the right direction rather than one big jump directly to the right estimate (or possibly the wrong estimate because of noise and other uncertainty).

It can be verified that $S(t)$ and $\zeta(t)$ do not vary much during the transients, justifying the assumptions of Theorem 3.2. In the example, $\theta_{est}(t)$ does indeed seem to move roughly on a straight line during each period when θ is constant, cf. Figure 3.9, due to the tuning of the data filters being made in accordance with the guidelines derived above. Since the grid pattern is fairly coarse, $\hat{\theta}(t)$ is somewhat off the line between θ and $\theta_{est}(t)$ most of the time. Still, no erroneous resets were made in the simulation example, which is the typical situation with the present tuning. Immediately after a reset has taken place, there may be a short time interval when the forbidden region is quite large. However, the likelihood of an erroneous reset during this phase is still fairly small as the circle containing all reset candidates becomes smaller, typically containing only the one to which a reset has already been made.

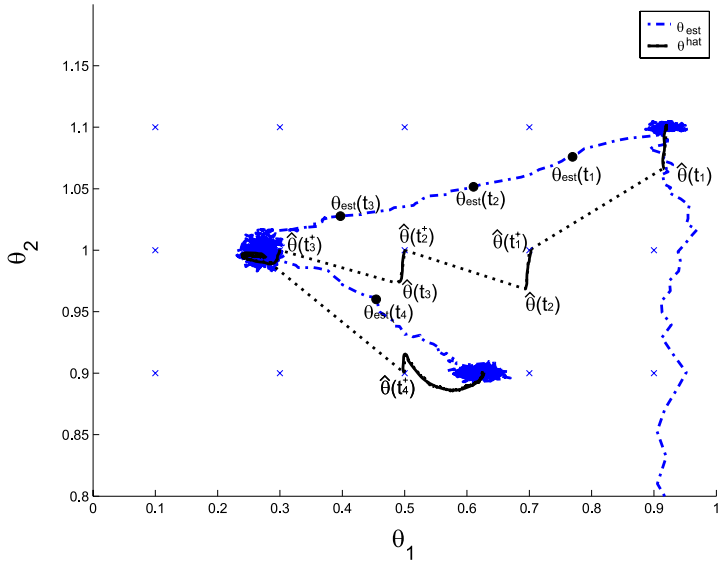

Figure 3.9: Parameter adaptation evolving in the two-dimensional θ-space. Reset is performed at $t_1 = 2.2s$, $t_2 = 2.3s$, $t_3 = 2.4s$ and $t_4 = 10.1s$.

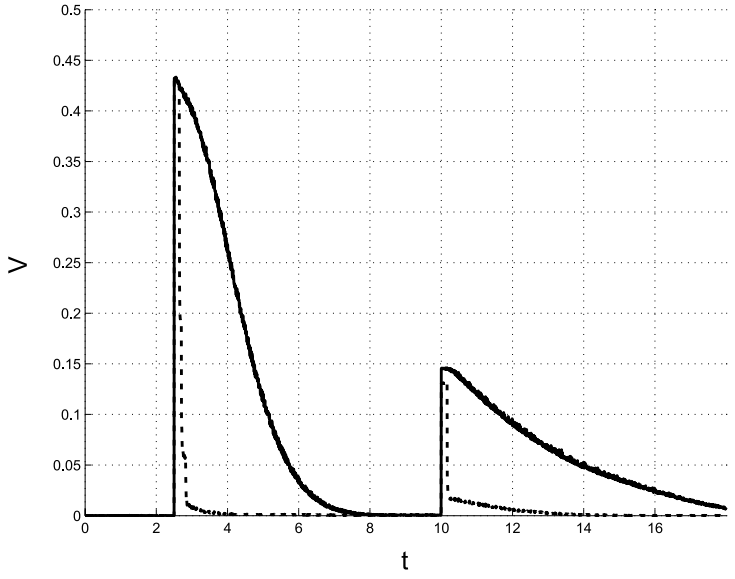

Figure 3.10: Lyapunov function with (dotted) and without (solid) reset.

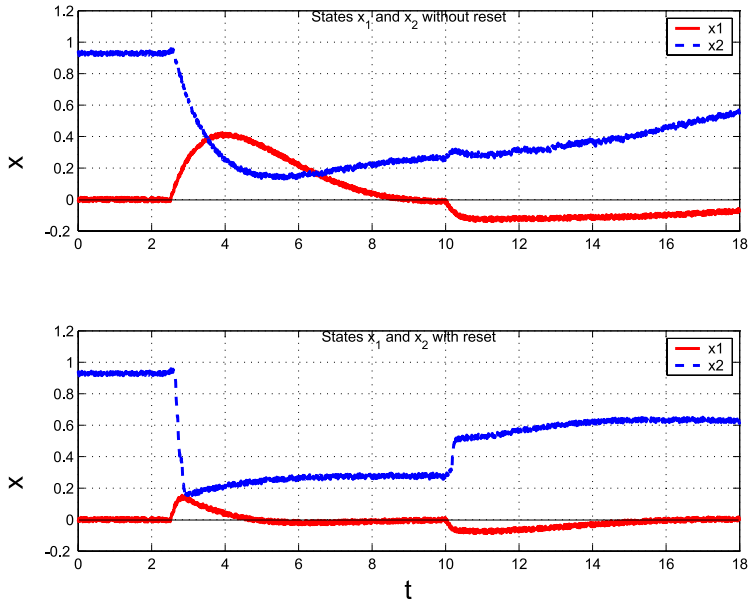

Figure 3.11: State trajectories, with and without reset. Note that $x_1 = 0$ is the reference for x_1.

3.5 Concluding Remarks

Introducing parameter resetting in nonlinear adaptive control may greatly improve the transient performance without increasing the systems noise sensitivity significantly. This chapter has studied the effect of data filters in MMAC. Such filters introduce transients that complicates the estimation of jumps in the control Lyapunov function that results from parameter estimate resets. We provide insight into causes for erroneous resets due to such filter transients, addressing the inherent tradeoff between rapid transient response, and model and data uncertainty. Data filter tuning guidelines have been proposed and shown to work well in simulations.

Chapter 4

Application to Thruster Anti-spin in DP

The following two chapters present a controller state reset strategy for marine vessels. The motivation for using this strategy is to improve transient behavior in extreme sea conditions. Transients arise when the ship operates in these conditions, where disturbances such as ventilation and in-and-out-of-water effects may give rise to loss in propeller thrust. Propeller shaft speed PI-controllers, being the today's industrial standard for fixed pitch propellers (FPP), are working as the backbone in both cases. This first chapter presents the idea utilized on a regular PI-controller, restricted to DP vessels where the advance speed u_a is low. u_a is the speed of the inlet water to the propeller disc. The method is illustrated with experimental results. The work in this chapter is reported in the second part of Bakkeheim et al. (2008).

4.1 Introduction

The control hierarchy of a marine thruster control system consists of a high-level controller giving commands to a thrust allocation algorithm, which in turn gives commanded thrust set-points to the different local thruster controls (LTC), see Sørensen (2005). Examples of high-level controllers are DP systems, joysticks and autopilots. The introductional section of this chapter gives a short overview of the today's standard in propulsion systems for marine vessels as well as presenting some of the drawbacks of these systems.

4.1.1 Electrically Driven Thrusters

Figure 4.1 shows a typical overview of an electrically driven marine DP system. The thrusters draw power from power buses where the power is supplied by generators driven by diesel engines or gas turbines. This way of generating and transferring power to thrusters is becoming the standard in advanced ship propulsion for offshore vessels, cruise vessels, navy ships and some advanced tankers. The power generation will consists of multiple engines. The advantage of such an arrangement is that the number of running aggregates can be selected to have an optimum

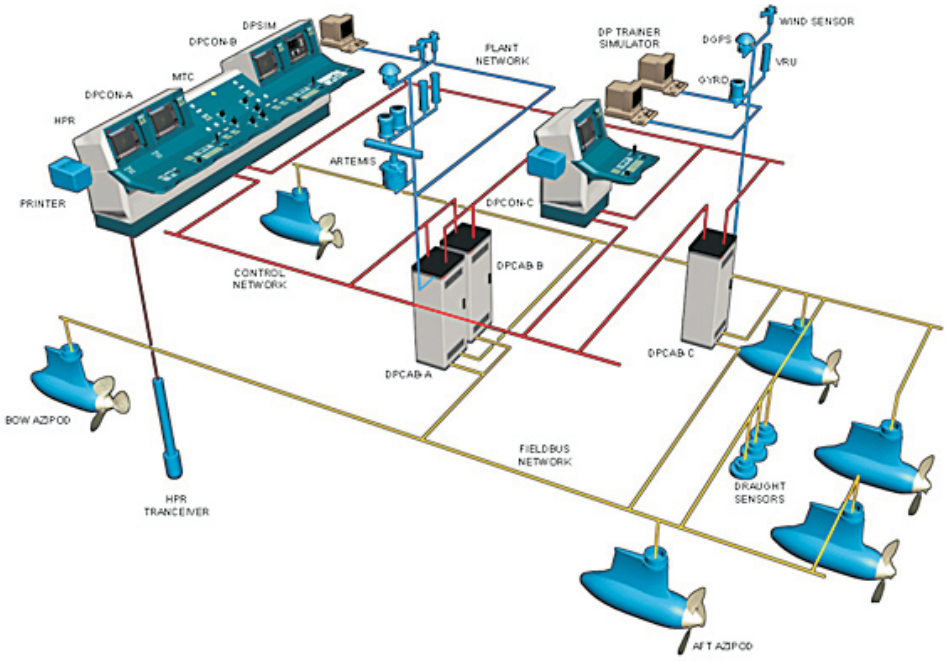

Figure 4.1: Overview of an electrically driven marine DP system. Courtesy of ABB, www.abb.com.

loading of each engine, see Lauvdal & Ådnanes (2000). When the available power on the bus becomes low, the power management system (PMS) will start the next unit. There is always need for having some reserves at the power bus, in order to prevent blackout when sudden changes in need for power is demanded, see Radan, Smogeli, Sørensen & Ådnanes (2006).

4.1.2 Thrust Losses

For a FPP operating in DP, the thrust production is quadratically dependent on the propeller speed. This is however valid only when the propeller is deeply submerged. If the propeller is above, or even close to the water surface, the thrust production may be constant or even decrease when increasing the propeller speed. Two situations that lead to thrust loss is depicted in Figure 4.2. These losses are referred to as loss due to ventilation and loss due to in-and-out-of-water effects. In Figure 4.2(a), the propeller disk is submerged, but due to the pressure difference in front and back of the propeller disk, a vortex is building up on the low-pressure side. Air may be sucked in to the propelled disk area through the vortex, leaving the propeller disk to spin inside an air bubble, hence reducing propeller thrust. In Figure 4.2(b), however, the reduction of thrust is a result of the propeller disk partly being above the water surface. Both these cases typically occur during operation in extreme seas, see Figure 4.3.

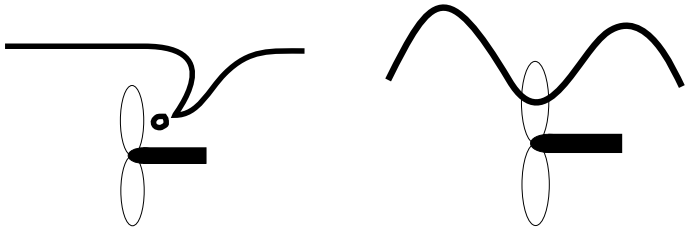

(a) Ventilation (b) In-and-out-of-water effects

Figure 4.2: Thrust losses.

Figure 4.3: A ship in extreme sea conditions. An anti-spin protection is needed in order to prevent the propeller from spinning when experiencing ventilation and in-and-out-of-water effects.

The knowledge of the propeller thrust and torque, together with the thrust induced pressure force on the hull, is fundamental in order to achieve high vessel control performance.

4.1.3 Today's Industrial Standard of LTC

High-level control structures are widely covered in the literature. In the last years also LTC has gained growing interest in the literature see Smogeli (2006), Whitcomb & Yoerger (1999*a*), Pivano, Johansen, Smogeli & Fossen (2007), Bakkeheim et al. (2006) and the references therein.

The industrial standard in marine LTC are conventional PI-controllers, controlling the propeller shaft speed. The PI-controller may be tuned such that the performance is acceptable in both steady-state and transient regimes. The tighter the PI-controller is tuned, the better the controller will perform in transient regimes. This will in turn increase the sensitivity to noise and increase variations in torque, power and mechanical load, which is not beneficial while in steady-state operation in waves. In normal operation, there may be no need for high transient performance. When the ship is in extreme seas, however, the propeller may start to spin due to ventilation (air suction from the free surface) and in-and-out-of-water effects, see Figure 4.2. This, in turn, may lead to wear-and-tear of the ship's propulsion equipment and undesired transients on the power bus that may increase the risk of blackouts due to overloading of the generator sets as pointed out in Section 4.1.1.

The reason for using feedback from the propeller shaft speed in the industrial standard PI-controller, is due to its availability. Better performance would be achieved by using propeller thrust as feedback. Unfortunately a propeller system is not usually equipped with thrust sensors, while propeller speed is easily measured relatively accurate. Precise thruster models are then needed in order to get as accurate estimate of the propeller thrust as possible. In conventional LTC, these models are not including effects like in-and-out-of-water effects and ventilation, hence the controller performance in extreme sea conditions is reduced.

4.2 Anti-spin in Marine Thruster Control for DP Operation

In order to increase the LTC performance in extreme sea conditions, the thrust losses phenomena mentioned in Section 4.1.2 may be handeled with an anti-spin controller, see Smogeli, Hansen, Sørensen & Johansen (2004), Smogeli, Sørensen & Minsaas (2006), Smogeli & Sørensen (2006) and Smogeli (2006). The anti-spin controller in these references is based on a combination of power and torque thruster controller. A similar approach is considered here, but instead the anti-spin controller is based on a standard shaft speed PI-controller, where the integrator value may be reset if appropriate, following the framework presented in Chapter 2. The advantage of such a reset approach is that only minor software updates are needed to upgrade prevailing installations. Experimental test results are included in order to justify the method, see also Bakkeheim et al. (2006) for preliminary results.

An illustration of the LTC presented in this chapter is seen in Figure 4.4. From the high-level control module, the desired propeller thrust T_{pd} is given as an input to the controller. Further, a direct mapping transforms this into the desired shaft speed ω_d. This is in turn fed into a set-point mapping, which may limit the value of the desired shaft speed to cope with possible events of ventilation, see Smogeli, Hansen, Sørensen & Johansen (2004), Smogeli et al. (2006), Smogeli &

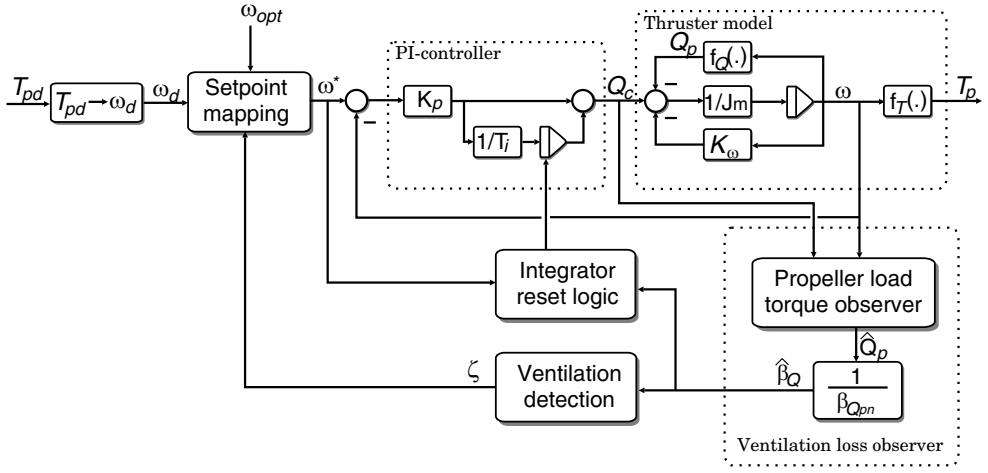

Figure 4.4: Local thruster control system with controller state reset mechanism for DP operation. A PI-controller works as a backbone for the strategy, letting the integrator state be reset to a different value decided by a reset algorithm. Improved transient performance is achieved in extreme sea conditions.

Sørensen (2006) and Smogeli (2006) for more details about ventilation. The main idea pursued in this chapter is that the dynamic part of the LTC, i.e. the integrator state in the PI-controller, may be reset to a different value only when large control errors are measured. The control error is a result of a sudden change in set-point or a ventilation incident, leading to a change in system steady-state value. The control error is measured with the aid of the estimated Lyapunov function value, measuring a positive jump in its value, see Remark 2.2. The reset of the integrator state is triggered by this positive jump in the Lyapunov function, and may leads to the thruster approaching its new steady-state value faster.

With reference to Figure 4.4, the different blocks, i.e., thruster model, PI-controller, thrust to propeller speed mapping, set-point mapping, integrator resetting, ventilation loss observer, and ventilation detection, are considered in the following.

4.2.1 Thruster Model

The rotational dynamics are described as in Fossen (2002) p. 473 by a first-order dynamic model for the propeller and shaft

$$J_m\dot{\omega} = Q_c - Q_p(\frac{h}{R}, \omega) - K_\omega\omega \tag{4.1}$$

where Q_c is the commanded torque, J_m is the rotational inertia of the propeller (including hydrodynamic added mass, shaft, gears and motor), K_ω is a linear friction coefficient, ω is the angular

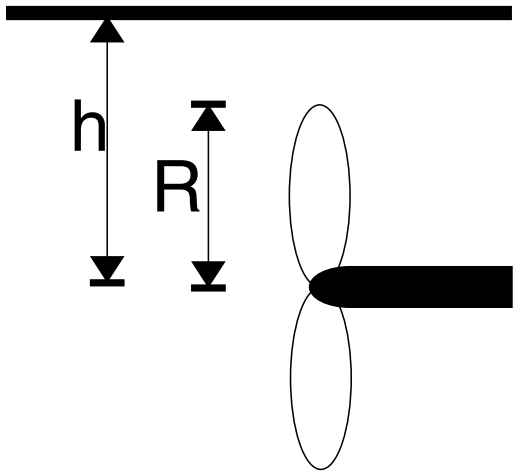

Figure 4.5: Propeller submergence h/R

speed of the propeller, and Q_p is the propeller load torque. The load torque Q_p is modelled as

$$Q_p(\frac{h}{R},\omega) = f_Q(\cdot) = Q_n(\omega)\beta_Q(\frac{h}{R},\frac{\omega}{\omega_{max}}) \tag{4.2}$$

where h/R is the relative submergence of the propeller, with R being the radius of the propeller, and h the shaft submergence, see Figure 4.5. The nominal torque is

$$Q_n(\omega) = \Phi \text{sgn}(\omega)\omega^2 \tag{4.3}$$

where $\Phi = (K_{Q0}\rho D^5)/(4\pi^2)$, D is the propeller diameter, and ρ is the density of water. K_{Q0} is the nominal torque coefficient commonly used for DP and low speed manoeuvering operations, when the advance speed u_a is low. Different nominal coefficients K_{Q0} for positive and negative speed may be used. For notational simplicity, we consider only one nominal coefficient. For transit operations with higher u_a, other models for K_Q can be established, this is further handled in Chapter 5. β_Q in (4.2) expresses the torque loss, which is the ratio of actual to nominal torque, where ω_{max} is a chosen maximum speed of the propeller. Figure 4.6(a) shows a typical shape of this torque loss coefficient. With reference to the figure, $\beta_Q = 1$ indicates no loss in propeller thrust while $\beta_Q = 0$ indicates that the propeller does not produce any thrust at all. When the propeller is fully submerged, i.e. $h/R > 1$, there will be no thrust losses for low propeller speed. For these low speeds, the thrust loss factor β_Q will decrease linearly with decreasing propeller submergence, ending up being zero for propeller spinning in free air, i.e. $h/R < 1$. This situation is due to the phenomenon called in-and-out-of-water effects, see Figure 4.2(b). For higher propeller speed, however, the situation is a bit different. When the propeller speed is above a certain limit there is no such linear dependence. Later in the thesis, this limit is referred to as ω_{opt}, hence from Figure 4.6, $\omega_{opt}/\omega_{max} = 0.45$. For propeller speed above this limit, there is an almost discrete transition in β_Q when moving form deeply submerged propeller to a

propeller being located close to the water surface. This transition is due to the vortex building up at the low pressure side of the propeller, and referred to as ventilation effects, see Figure 4.2(a). Figure 4.6(b) shows the same information, but instead presenting the losses as non-dimensional propeller load torque Q/Q_{max}. Note from Figure 4.6 that in the case of ventilation, there is no use of increasing the propeller speed in order to increase the propeller thrust. It actually turns out to decrease the thrust rather than increase it, see Smogeli (2006) for more details.

The propeller thrust is modelled as

$$T_p = f_T(\cdot) = \frac{K_{T0}\rho D^4}{4\pi^2}\text{sgn}(\omega)\omega^2\beta_T(\frac{h}{R}, \frac{\omega}{\omega_{max}}) \tag{4.4}$$

where β_T is a thrust loss coefficient related to β_Q. K_{T0} is the nominal thrust coefficient, i.e. for $u_a = 0$. In transit where $u_a \neq 0$, an alternative thrust coefficient $K_T(u_a)$ could be used, see Chapter 5.

4.2.2 PI-controller

The shaft speed is given by a PI-controller

$$Q_c = K_p\left(\omega^* - \omega\right) + z \tag{4.5}$$

where $K_p > 0$ is the proportional gain and the integrator state is

$$\dot{z} = K_I\left(\omega^* - \omega\right) \tag{4.6}$$

with $K_I = K_p/T_i$ and $T_i > 0$ the integral time constant. The complete closed-loop system becomes

$$\begin{aligned}\dot{\omega} &= \frac{1}{J_m}\left(-K_p\omega + K_p\omega^* - K_\omega\omega - Q_p(\frac{h}{R},\omega) + z\right) \\ \dot{z} &= -K_I\omega + K_I\omega^*.\end{aligned} \tag{4.7}$$

Assuming h/R and the set-point for the PI-controller ω^* are constant, we obtain steady-state values for z, i.e.

$$z^* = K_\omega\omega^* + Q_p(\frac{h}{R},\omega^*). \tag{4.8}$$

Based on the definition of the error variables $\tilde{\omega} = \omega^* - \omega$ and $\tilde{z} = z^* - z$, we have the following error dynamics

$$\begin{aligned}\dot{\tilde{\omega}} &= \frac{1}{J_m}\left(\tilde{z} - \left(K_p + K_\omega\right)\tilde{\omega} + \left(Q_p(\frac{h}{R},\omega) - Q_p(\frac{h}{R},\omega^*)\right)\right) \\ \dot{\tilde{z}} &= -K_I\tilde{\omega}.\end{aligned} \tag{4.9}$$

Further defining $\tilde{x} = [\tilde{\omega},\ \tilde{z}]^T$, the control error may be written in compact form

$$\dot{\tilde{x}} = A\tilde{x} + \frac{1}{J_m}F(\tilde{x}, \frac{h}{R}, \omega^*) \tag{4.10}$$

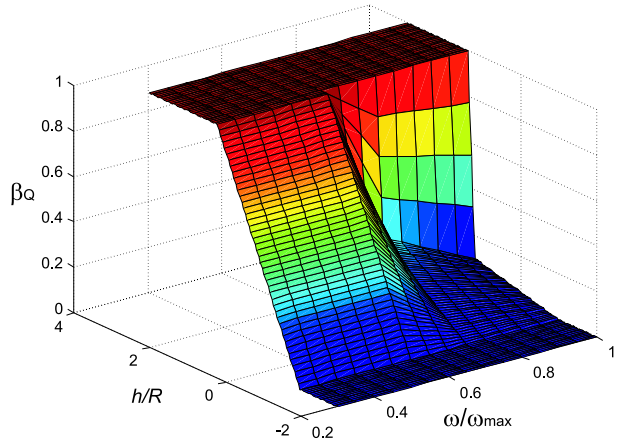

(a) Ventilation loss function β_Q.

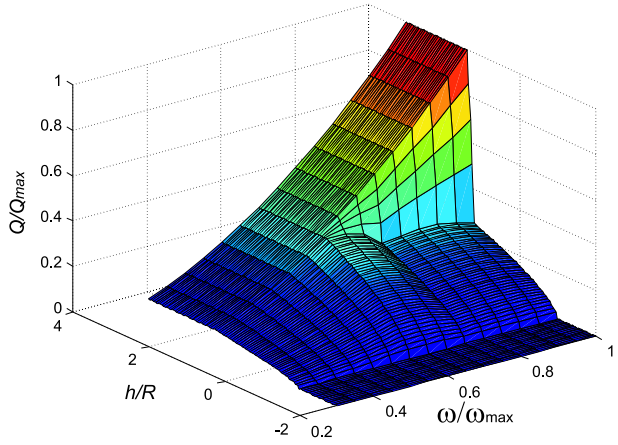

(b) Propeller load torque.

Figure 4.6: Simulation model of ventilation loss and propeller load torque as functions of relative submergence h/R and relative shaft speed ω/ω_{max}. These models are based on experimental results from a cavitation tunnel.

where

$$A = \begin{bmatrix} -\frac{1}{J_m}(K_\omega + K_p - a) & \frac{1}{J_m} \\ -K_I & 0 \end{bmatrix} \tag{4.11}$$

$$F(\tilde{x}, \frac{h}{R}, \omega^*) = \begin{bmatrix} f\left(\frac{h}{R}, \omega^*, \tilde{\omega}\right) \\ 0 \end{bmatrix} \tag{4.12}$$

$$f(\frac{h}{R}, \omega^*, \tilde{\omega}) = Q_p(\frac{h}{R}, \omega^* - \tilde{\omega}) - Q_p(\frac{h}{R}, \omega^*) - a\tilde{\omega}. \tag{4.13}$$

The linear part $a\tilde{\omega}$ is subtracted from the nonlinearity in (4.9), leaving $F(\tilde{x}, \frac{h}{R}, \omega^*)$ as the remaining nonlinear part in (4.10). This is done in order to incorporate a linear approximation of the nonlinear part of the system as accurately as possible. The nonlinear system may then be approximated by a linear system when we search for a Lyapunov function, and analyze the effects of the nonlinearity later.

4.2.3 Lyapunov Function

We know that for a LTI system where the system matrix A is Hurwitz, there exists a solution $P^T = P > 0$ of the Lyapunov equation

$$A^T P + PA = -Q \tag{4.14}$$

where $Q^T = Q > 0$ and in general

$$P = \begin{bmatrix} p_{11} & p_{12} \\ p_{12} & p_{22} \end{bmatrix}. \tag{4.15}$$

The following choice of Lyapunov candidate

$$V(\tilde{x}) = \tilde{x}^T P \tilde{x} \tag{4.16}$$

will prove stability for the LTI system.

By including some properties of the matrix Q in addition to the one stated in the LTI case, a Lyapunov function proving stability for the nonlinear system (4.10) may be generated, as pointed out in the following proposition.

Proposition 4.1 *Assume ω^* and h/R constant, and suppose K_I and K_p are chosen such that A is Hurwitz and $P^T = P > 0$ is a solution to the Lyapunov equation (4.14), where $Q = diag(q_{11}, q_{22}) > 0$. Further, if there exists an α such that the graph of $f(\frac{h}{R}, \omega^*, \tilde{\omega})$ is a function of $\tilde{\omega}$ inside sector $[-\alpha, \alpha]$, and there exist $\mu_1 > 0$ and $\mu_2 > 0$ such that*

$$q_{11} - \frac{1}{J_m}(\mu_1 + \mu_2)\alpha^2 - \frac{1}{J_m \mu_1}(p_{11})^2 > 0 \tag{4.17}$$

$$q_{22} - \frac{1}{J_m \mu_2}(p_{12})^2 > 0 \tag{4.18}$$

holds, then the origin $\tilde{x} = 0$ is a globally exponentially stable (GES) equilibrium point of (4.10).

Proof. The time derivative of (4.16) along the trajectories of the nonlinear system (4.10) is

$$\dot{V}(\tilde{x}) = -\tilde{x}^T Q\tilde{x} + \frac{2}{J_m}\tilde{x}^T PF(\tilde{x}, \frac{h}{R}, \omega^*). \tag{4.19}$$

The two terms in (4.19) are

$$-\tilde{x}^T Q\tilde{x} = -q_{11}\tilde{\omega}^2 - q_{22}\tilde{z}^2 - 2q_{12}\tilde{\omega}\tilde{z} \tag{4.20}$$

and

$$\begin{aligned}\frac{2}{J_m}\tilde{x}^T PF(\tilde{x}, \frac{h}{R}, \omega^*) = \frac{2}{J_m}p_{11}\tilde{\omega}f(\frac{h}{R}, \omega^*, \tilde{\omega}) \\ + \frac{2}{J_m}p_{12}\tilde{z}f(\frac{h}{R}, \omega^*, \tilde{\omega}).\end{aligned} \tag{4.21}$$

Using Young's inequality, $2xy \leq \frac{1}{\mu}x^2 + \mu y^2, \quad \forall \mu > 0$, on the second term in (4.21), we obtain

$$\begin{aligned}\frac{2}{J_m}\tilde{x}^T PF(\tilde{x}, \frac{h}{R}, \omega^*) \leq \frac{1}{J_m\mu_1}(p_{11}\tilde{\omega})^2 + \frac{1}{J_m}\mu_1 f^2(\frac{h}{R}, \omega^*, \tilde{\omega}) \\ + \frac{1}{J_m\mu_2}(p_{12}\tilde{z})^2 + \frac{1}{J_m}\mu_2 f^2(\frac{h}{R}, \omega^*, \tilde{\omega}).\end{aligned} \tag{4.22}$$

Since Q is diagonal and $f(\frac{h}{R}, \omega^*, \tilde{\omega})$ belongs to the sector $[-\alpha, \alpha]$, i.e. $f^2(\frac{h}{R}, \omega^*, \tilde{\omega}) \leq (\alpha\tilde{\omega})^2$, $\forall\tilde{\omega}$ for constant ω^* and h/R, we obtain

$$\begin{aligned}\dot{V}(\tilde{x}) \leq -\left(q_{11} - \frac{1}{J_m}(\mu_1 + \mu_2)\alpha^2 - \frac{1}{J_m\mu_1}(p_{11})^2\right)\tilde{\omega}^2 \\ -\left(q_{22} - \frac{1}{J_m\mu_2}(p_{12})^2\right)\tilde{z}^2 = -W(\tilde{x}).\end{aligned} \tag{4.23}$$

From (4.17)-(4.18), the function $W(\tilde{x})$ is positive definite, hence GES follows from Thm 4.1 in Khalil (2002). ■

From this, a stabilizing dynamic controller (4.5)-(4.6) is developed for the system (4.1), where (4.16) is a Lyapunov function for the closed-loop system (4.10). The resulting Lyapunov function is, as stated in Chapter 2, not just for stability analysis but also necessary for the reset strategy.

4.2.4 Ventilation Loss Observer

Since the loss factor β_Q used in calculating the Lyapunov function value is not known, a fast estimator is needed in order to estimate this factor, see Section 2.1.4.

Based on the rotational dynamics (4.1), the observer equations for the estimated propeller load torque $\hat{Q}_p$ presented in Smogeli, Sørensen & Fossen (2004), Smogeli et al. (2006), Smogeli & Sørensen (2006) and Smogeli (2006) are written

$$\begin{aligned}\dot{\hat{\omega}} &= \frac{1}{J_m}(-\hat{Q}_p - K_\omega\hat{\omega} + Q_c) + k_1(y - \hat{y}), \\ \dot{\hat{Q}}_p &= -k_2(y - \hat{y}),\end{aligned} \tag{4.24}$$

where the propeller load torque Q_p has been modelled as a random process driven by a bounded noise, and the shaft speed ω is taken as the measured output y (and hence $\hat{y} = \hat{\omega}$). The equilibrium point of the observer error dynamics is GES in the case of a constant load torque if the observer gains k_1 and k_2 are chosen according to

$$k_1 > -K_\omega / J_m, \;\; k_2 < 0, \tag{4.25}$$

see Smogeli, Sørensen & Fossen (2004) for more details.

An estimate of the torque loss factor β_Q may be calculated based on the estimated propeller load torque $\hat{Q}_p$ from (4.24) and an estimated nominal load torque $\hat{Q}_n$. $\hat{Q}_n$ is given from (4.3) by feedback from the propeller shaft speed ω as

$$\hat{Q}_n(\omega) = \Phi \text{sgn}(\omega)\omega^2. \tag{4.26}$$

The estimated torque loss with respect to the nominal torque expected from the measured shaft speed is then

$$\hat{\beta}_Q = \alpha_b(\omega) + (1 - \alpha_b(\omega))\frac{\hat{Q}_p}{\hat{Q}_n}. \tag{4.27}$$

$\alpha_b(\omega)$ is a weighting function of the type

$$\alpha_b(y) = e^{-k|py|^r} \quad \text{for} \quad y \in \mathbb{R}, \tag{4.28}$$

where k, p and r are positive tuning gains. The weighting function is needed because the estimate otherwise would be singular for zero shaft speed Smogeli, Sørensen & Fossen (2004).

4.2.5 Thrust to Propeller Speed Mapping

The industrial standard for FPPs is shaft speed control based on a static mapping from desired thrust T_{pd} to desired shaft speed ω_d, obtained by simply taking the inverse mapping of (4.4):

$$\omega_d = 2\pi \text{sgn}(T_{pd})\sqrt{\left|\frac{T_{pd}}{K_{T0}\rho D^4}\right|}. \tag{4.29}$$

4.2.6 Reset Procedure

For a sudden change in the loss factor β_Q due to change in h/R, the Lyapunov function value may make a positive jump due to its new equilibrium point. Integrator reset may improve performance in transient regimes, when the equilibrium suddenly changes due to ventilation or set-point change, without influencing performance in steady-state, see Section 2.2.1.

To maintain stability when the integrator is reset, one may perform a reset only when this leads to a negative jump in the Lyapunov function. The following lemma states the jump value in the Lyapunov function (4.16) as a result of performing a reset of the integrator state.

Lemma 4.1 *A reset of the integrator value $z(t^+)$ to z_i, where t^+ denotes an infinitely small time increment of t, of system (4.10) leads to a jump in the Lyapunov function (4.16)*

$$\Delta V_i(t) = p_{22}\left(\tilde{z}_i^2 - \tilde{z}^2(t)\right) + 2p_{12}\tilde{\omega}(t)\left(\tilde{z}_i - \tilde{z}(t)\right) \tag{4.30}$$

where $\tilde{z}_i = z^* - z_i$.

Proof. Let $\tilde{\omega}_i = \omega^* - \omega_i$ and $\tilde{x}_i = [\tilde{\omega}_i,\ \tilde{z}_i]^T$. The jump in the Lyapunov function is calculated as

$$\begin{aligned}\Delta V_i(t) &= V(\tilde{x}_i) - V(\tilde{x}(t)) = \tilde{x}_i^T P \tilde{x}_i - \tilde{x}^T(t) P \tilde{x}(t) \\ &= p_{11}\tilde{\omega}_i^2 + p_{22}\tilde{z}_i^2 \ + 2p_{12}\tilde{\omega}_i\tilde{z}_i \\ &- p_{11}\tilde{\omega}^2(t) - p_{22}\tilde{z}^2(t) \ - 2p_{12}\tilde{\omega}(t)\tilde{z}(t) \\ &= p_{22}\left(\tilde{z}_i^2 - \tilde{z}^2(t)\right) + 2p_{12}\tilde{\omega}(t)\left(\tilde{z}_i - \tilde{z}(t)\right) \end{aligned} \tag{4.31}$$

where the fact that $\tilde{\omega}_i = \tilde{\omega}(t)$, due to the continuity of solutions of ordinary differential equations, has been used. ■

We assume a finite set of integrator reset candidates, $\mathcal{H} = \{z_1, \ldots, z_n\}$. The following result states stability when the integrator is reset.

Proposition 4.2 *Given the closed-loop system with PI-controller (4.10). Assume that V in (4.16) is a Lyapunov function that proves the equilibrium point of the nonlinear system in (4.10) to be GES. Further assume that $\Delta V_i(t)$ denotes the jump in the Lyapunov function value if the integrator of the PI-controller in (4.10) is reset to a value $z_i \in \mathcal{H}$. Then if z is reset to the value z_i only if $\Delta V_i(t) < 0$, the equilibrium point of the nonlinear system in (4.10) is GES.*

Proof. The reader is referred to the proof of Theorem 2.1 in addition to Remark 2.3, being a generalization of this proposition. Note that the condition $\Delta V_i(t) < 0$ leads to a negative jump in the Lyapunov function, which also leads to $\dot{V}(\tilde{x}) \leq -W(\tilde{x})$ see (4.23), hence GES follows. ■

Remark 4.1 *Assume the choice of Q in (4.14) is made in such a way that the Lyapunov function is an appropriate measure of remaining transient energy. Then, in addition to the overall stability being preserved with resetting, there will be a transient performance improvement if the system is reset.*

Remark 4.2 *The results in Proposition 4.1 and 4.2 assume ω^* and h/R being constant. Abrupt changes in the disturbance parameter h/R or the set-point ω^* may lead to increases in the Lyapunov function value $V(x)$. The results above state that $V(x)$ will decay exponentially between each abrupt event, with improved transient behavior. In situations where periodic disturbances or changes in set-point lead to the overall performance not being GES, the overall performance is practically improved.*

4.2.7 Ventilation Detection

The estimated loss factor $\hat{\beta}_Q$ may be subject to some fluctuations during the period of ventilation. Instead of using this estimate directly as a measure of whether the propeller is ventilating or not, a translation of this value into a discrete value ζ may be appropriate, see Smogeli, Hansen, Sørensen & Johansen (2004), Smogeli et al. (2006), Smogeli & Sørensen (2006) and Smogeli (2006). For a single ventilation incident, ζ will have the following evolution:

$$\begin{aligned} &\hat{\beta}_Q \geq \beta_{v,on} \Rightarrow \zeta = 0 \quad \text{(no ventilation)} \\ &\hat{\beta}_Q < \beta_{v,on} \Rightarrow \zeta = 1 \quad \text{(ventilation)} \\ &\hat{\beta}_Q \geq \beta_{v,off} \Rightarrow \zeta = 0 \quad \text{(no ventilation).} \end{aligned} \tag{4.32}$$

$\beta_{v,on}$ and $\beta_{v,off}$ are thresholds for beginning and termination of ventilation. Note that the ventilation detection ζ includes hysteresis, hence robustness due to measurement noise in the loss value estimate $\hat{\beta}_Q$ is achieved.

4.2.8 Set-point Mapping

In normal operation, increasing the rotational speed of the propeller leads to an increase in the propeller thrust and load torque. However, in case of ventilation, this may lead to increased dynamic loads, and hence mechanical wear-and-tear and power fluctuations, without increasing the thrust. In Smogeli (2006) both stationary and dynamical tests of these effects are studied. Due to the given controller design, and since the desired thrust T_{pd} is the input of the controller, a set-point mapping may prevent the controller from demanding torque above the limit of saturation. This will also reduce wear-and-tear of the propulsion device:

$$\omega^* = \begin{cases} \omega_{opt}, & \text{if } \zeta = 1 \text{ and } \omega_d \geq \omega_{opt} \\ \omega_d, & \text{otherwise} \end{cases} \tag{4.33}$$

where ω_{opt} is some optimal propeller speed during ventilation, $\omega_{opt}/\omega_{max} = 0.45$ in Figure 4.6(b).

4.2.9 Effects of Not Knowing the Loss Factor

Because the loss factor β_Q is unknown, the steady-state value z^* in (4.8) is estimated by

$$\hat{z}^* = K_\omega \omega^* + \Phi \text{sgn}(\omega^*) \omega^{*2} \hat{\beta}_Q \tag{4.34}$$

where the estimate of the loss factor $\hat{\beta}_Q$ is given in (4.27). Hence, the Lyapunov function value used in the integrator reset algorithm is also an estimate. Erroneous resets due to measurement noise during estimation of z^* in (4.34) is reduced by decreasing the density of integrator reset candidates in $\mathcal{H}$ as discussed in Section 2.2.3.

4.3 Experimental Test Results

An experimental setup in the Marine Cybernetics Laboratory (MCLab) at NTNU was used to test the resulting control strategy, see Figure 4.7. The thruster setup had the following physical characteristics:

D	J_m	K_ω	K_{T0}	K_{Q0}
0.25 m	0.005 kgms^2	0.01 Nms	0.575	0.075

where the maximum speed of the propeller was $\omega_{max} = 125$ rad/s. The proportional gain and integral time constant of the controller were $K_p = 0.032$ and $T_i = 0.05$, respectively.

In this setup, the thruster is stationed at a fixed horizontal position, centered in the basin. Hence, the use of the nominal thrust and torque coefficients K_{T0} and K_{Q0} in (4.29) and (4.3) are appropriate.

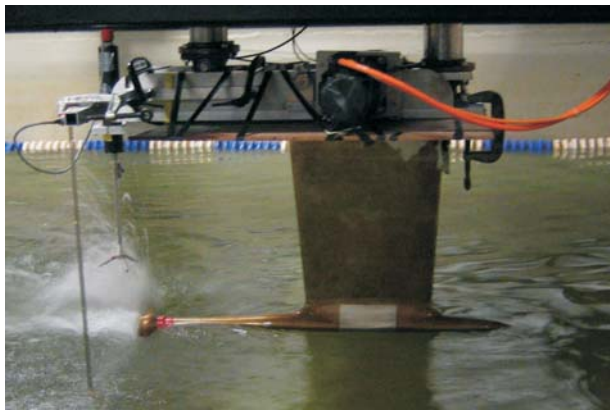

Figure 4.7: A test setup in MCLab at NTNU. The LTC for DP operation in extreme sea conditions with integrator reset was tested in a basin. The thruster vertical position was moved in order to trigger ventilation and in-and-out-of-water effects.

The nonlinear term $Q_p(\frac{h}{R},\omega) - Q_p(\frac{h}{R},\omega^*)$ in (4.13) is shown in Figure 4.8 for different values of ω^*. It is assumed, in this first stage of the controller development, that the loss factor β_Q is constant equal to 1, where the nonlinear term is most dominant.

We consider $\tilde{\omega} \in [-125, 125]$, hence $a = -0.33$ will minimize the remaining nonlinear part $f(\frac{h}{R},\omega^*,\tilde{\omega})$ enclosed inside the sector $[-\alpha,\alpha]$, see Figure 4.8. However, note that $f(\frac{h}{R},\omega^*,\tilde{\omega})$ may not be enclosed inside the sector $[-\alpha,\alpha]$ for $|\tilde{\omega}| > 125$, but due to $\tilde{\omega} \in [-125, 125]$, ES may still be ensured for all feasible initial conditions.

The resulting eigenvalues of the matrix A in (4.11) are $\lambda_1 = -73.4$ and $\lambda_2 = -1.7$. Including the sector $\alpha = 0.37$ from Figure 4.8 in Proposition 4.1, ES of the nonlinear system (4.10) is proven with $Q = \text{diag}(1,\ 0.1)$, $\mu_1 = 0.015$ and $\mu_2 = 0.00012$. The solution of (4.14) is

$$P = \begin{bmatrix} 0.006652 & -2.5 \cdot 10^{-4} \\ -2.5 \cdot 10^{-4} & 2.1081 \end{bmatrix}, \tag{4.35}$$

hence (4.16) will act as a suitable Lyapunov function.

For evaluation of the modular integrator reset strategy outlined in this example, test scenarios are given both with and without the reset module. With reference to Figure 4.6, the propeller speed region of interest is selected to be located above $\omega/\omega_{max} = 0.45$. The desired thrust was therefore chosen as $T_{pd} = 300$ N which yields $\omega_d = 73$ rad/s. Tests were performed both with and without the set-point mapping. To demonstrate LTC in extreme seas, the propeller was moved in and out of the water by raising and lowering the thruster with a period of 5 seconds and an amplitude of 15 cm. The propeller was then fully submerged at its lower position, i.e. the distance from the propeller blades to the sea surface was 5 cm. In the upper position, the shaft of the propeller was in the mean free surface.

Plots of the experimental results are shown in Figures 4.9-4.16. A wave probe was used for

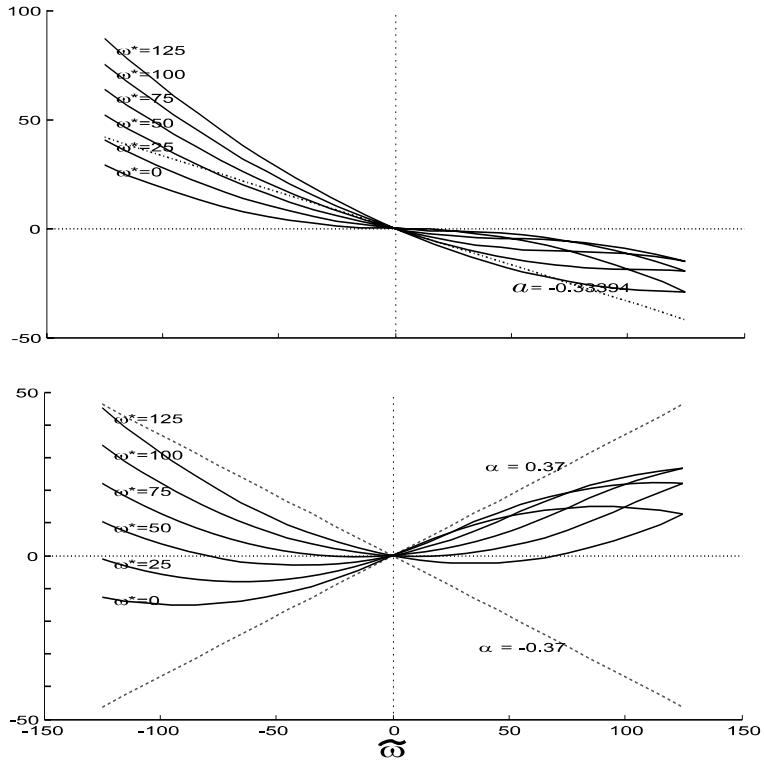

Figure 4.8: **Upper:** Load torque nonlinearities $Q_p(\frac{h}{R},\omega) - Q_p(\frac{h}{R},\omega^*)$ in (4.13) for different values of ω^* running from $\tilde{\omega} = -125$ to $\tilde{\omega} = 125$ with $\beta_Q = 1$. The dotted line represents the linear part $-a\tilde{\omega}$ in (4.13). **Lower:** The minimized nonlinear term $f(\frac{h}{R},\omega^*,\tilde{\omega})$ in (4.13) for different values ω^* for $\tilde{\omega} \in [-125, 125]$ enclosed inside sector $[-\alpha, \alpha]$ for all feasible $\tilde{\omega}$.

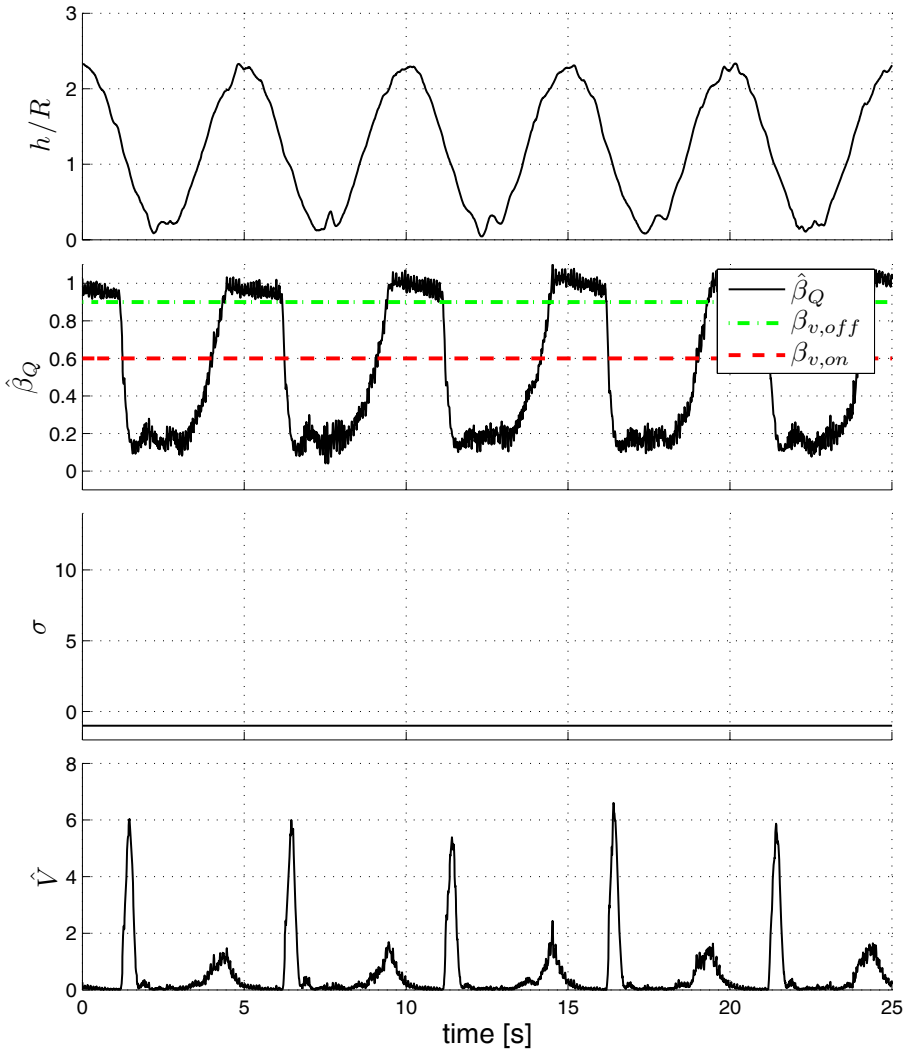

Figure 4.9: Experimental results with local thruster PI-control (no reset). Desired speed $\omega_d = 73$. The plot shows relative submergence h/R, estimated loss value $\hat{\beta}_Q$, reset index value σ and estimated Lyapunov function value $\hat{V}$. Figure 4.10 presents the rest of the plots for this situation.

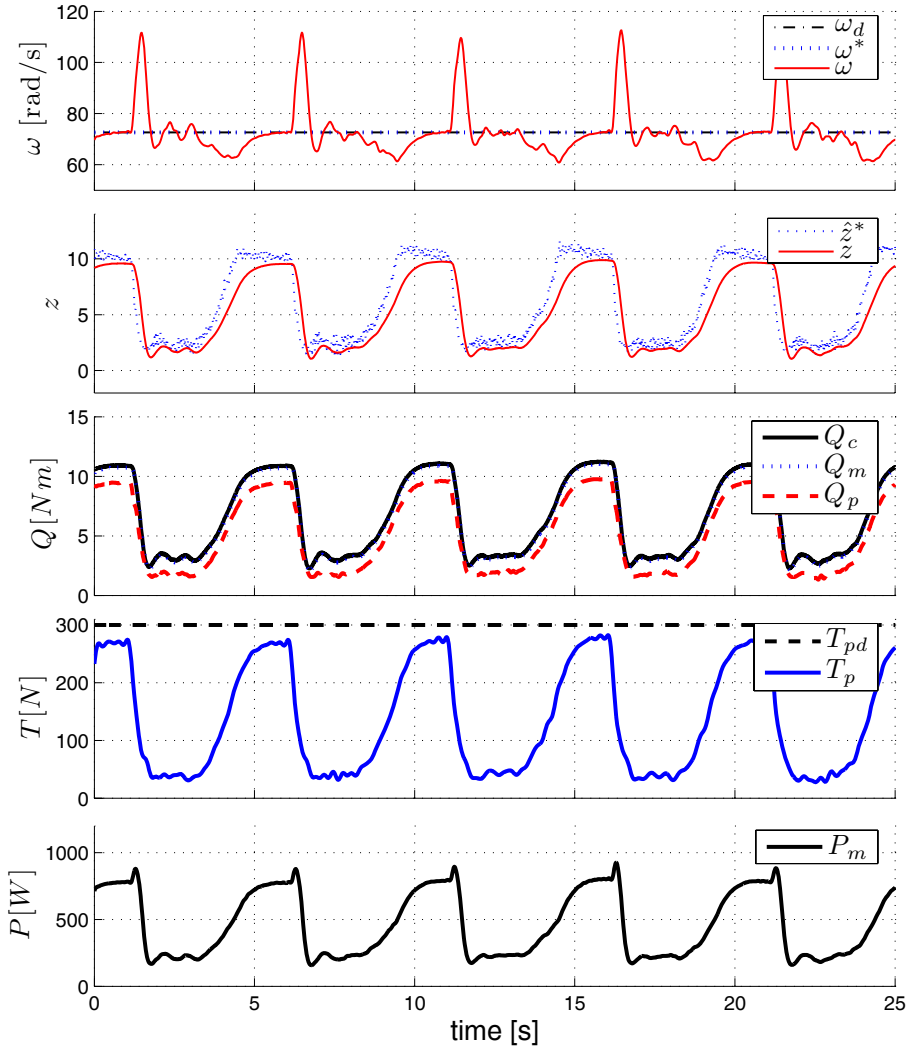

Figure 4.10: The rest of the plots of the situation presented in Figure 4.9. The figure shows the desired shaft speed ω_d, set-point for the PI-controller ω^*, actual shaft speed ω, estimated integrator value $\hat{z}^*$, actual integrator value z, commanded torque Q_c, motor torque Q_m, measured propeller torque Q_p, desired thrust T_{pd}, measured thrust T_p and motor power P_m.

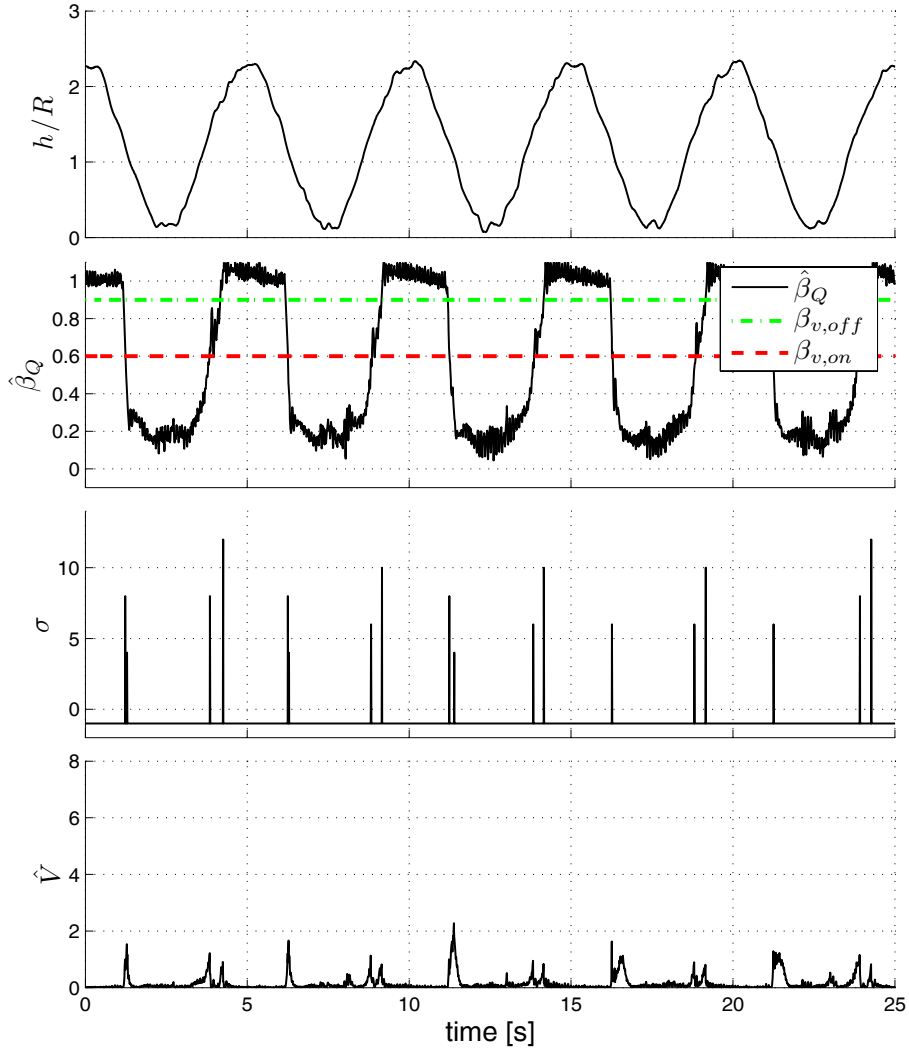

Figure 4.11: Experimental results of the same situation as in Figure 4.9-4.10, but with integrator resetting with the following candidates: $\mathcal{H} = \{0,\ 2,\ 4,\ 6,\ 8,\ 10,\ 12\}$. Figure 4.12 presents the rest of the plots for this situation.

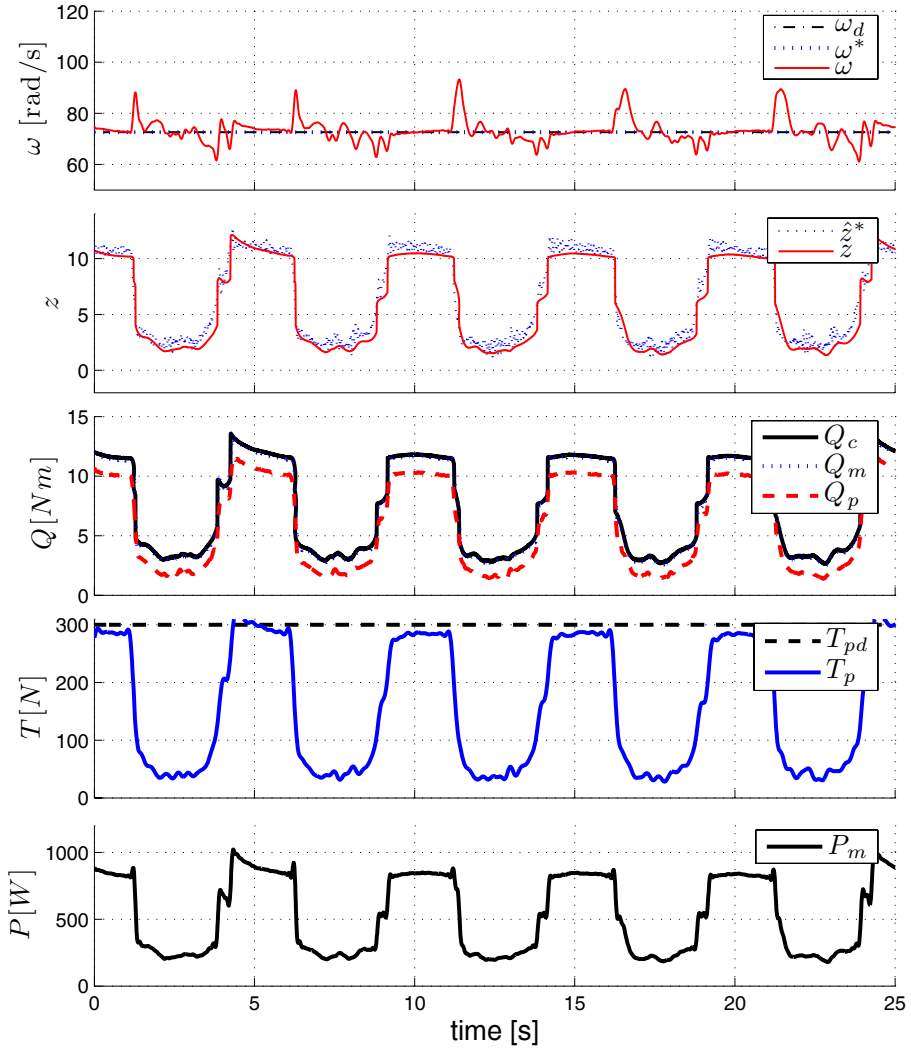

Figure 4.12: The rest of the plots of the situation presented in Figure 4.11.

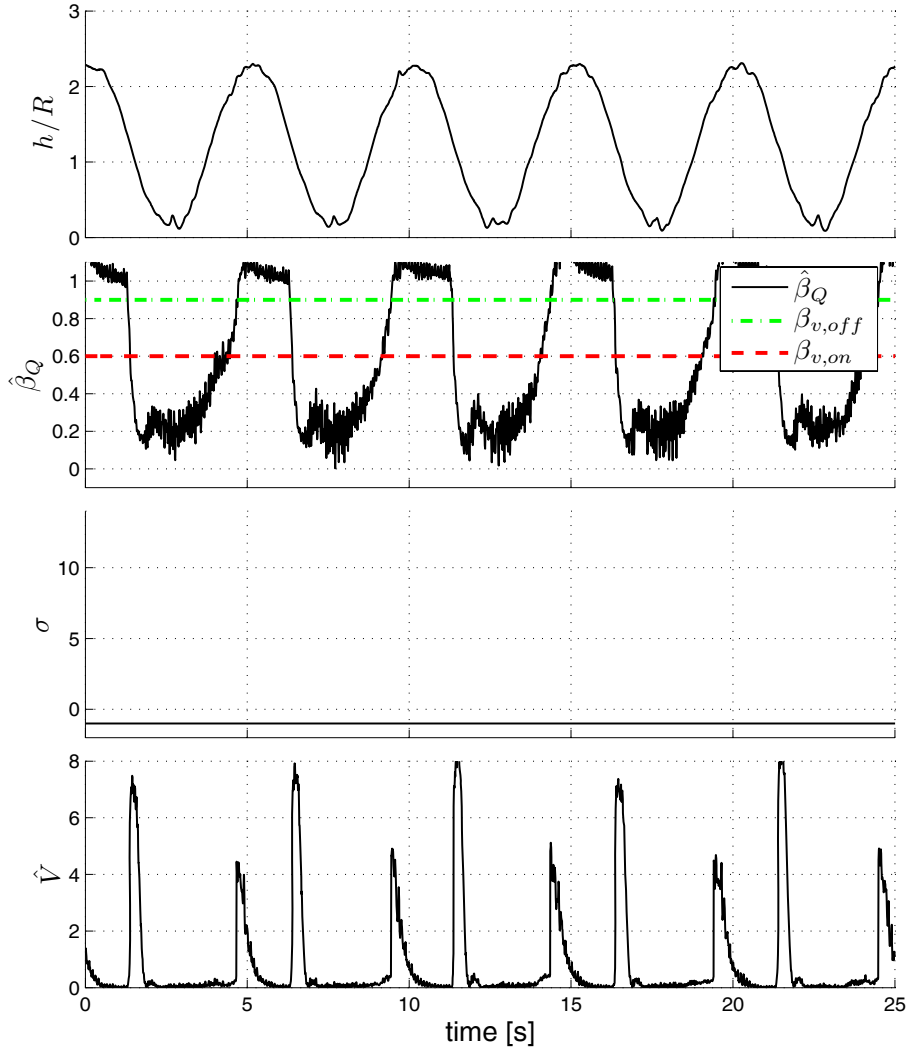

Figure 4.13: Experimental results with local thruster PI-control and set-point mapping (no reset). When ventilation is detected, the set-point of the PI-controller is changed from the initial $\omega_d = 73$, to a lower value $\omega^* = 56$. Figure 4.14 presents the rest of the plots for this situation.

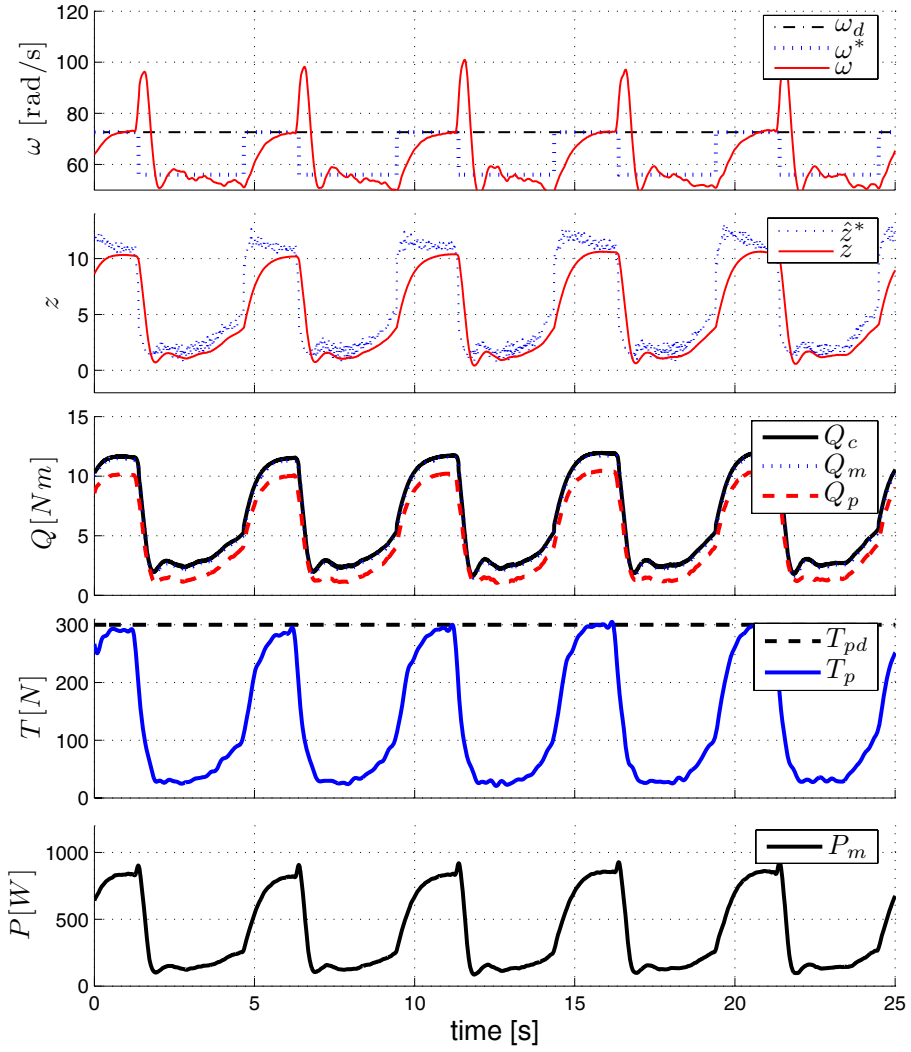

Figure 4.14: The rest of the plots of the situation presented in Figure 4.13.

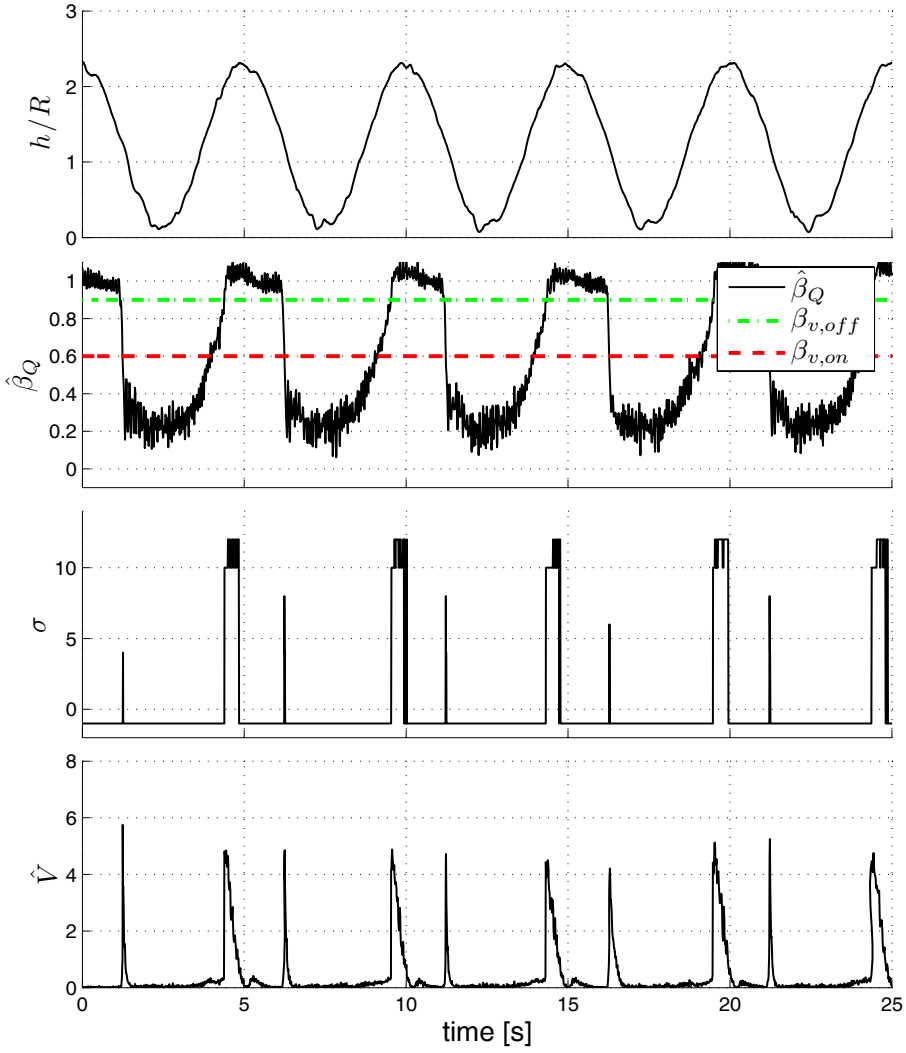

Figure 4.15: Experimental results of the same situation as in Figure 4.13-4.14, but with integrator resetting with the following candidates: $\mathcal{H} = \{0,\ 2,\ 4,\ 6,\ 8,\ 10,\ 12\}$. Figure 4.16 presents the rest of the plots for this situation.

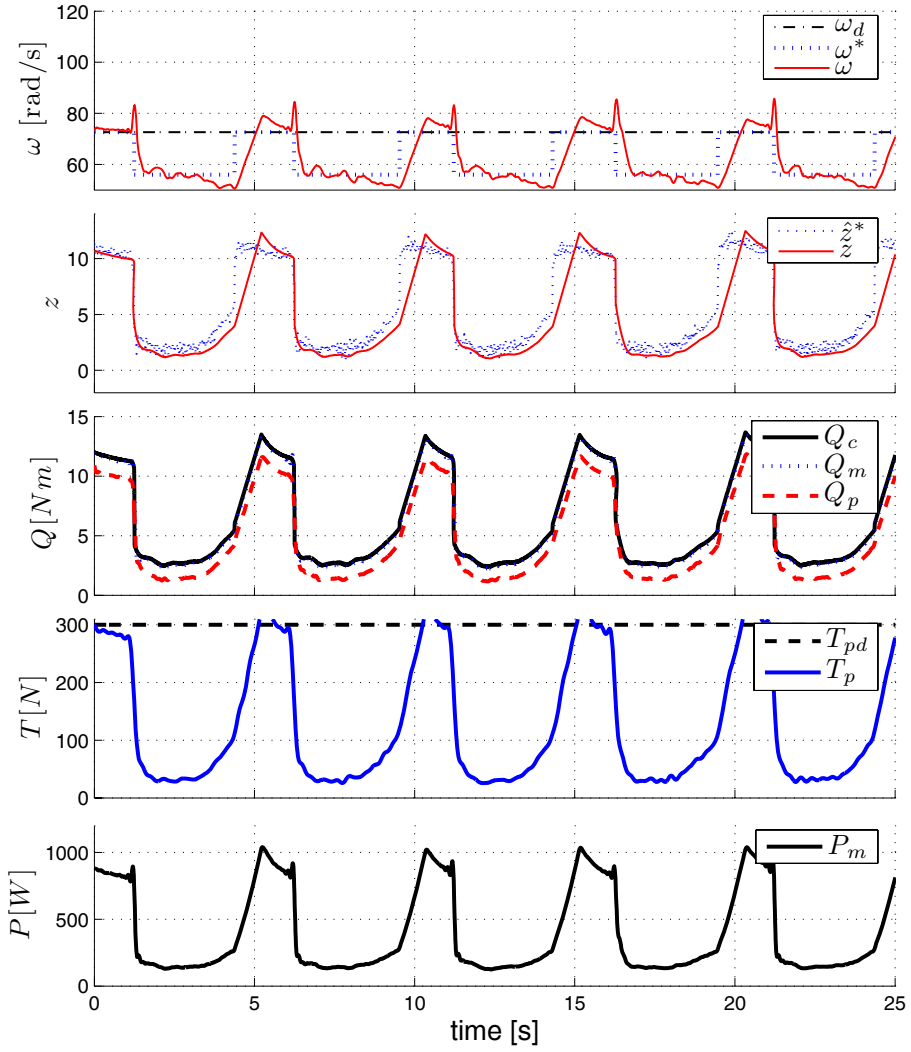

Figure 4.16: The rest of the plots of the situation presented in Figure 4.15.

measuring the relative submergence h/R. In order to plot the reset progress, $\sigma(t)$ is defined as

$$\sigma = \begin{cases} z_i, & \text{if } \Delta V_i < 0 \\ -1, & \text{otherwise} \end{cases} . \tag{4.36}$$

The exact Lyapunov function value is not available, but an estimate $\hat{V}$ is included in the plots. Thrust and torque sensors on propeller shaft were used to measure T_p and Q_p. The motor power $P_m = Q_m\omega$ is also included, for comparison reasons. The motor time constant is neglected here, supported by the agreement between commanded motor torque Q_c and measured motor torque Q_m.

The controller was implemented in Simulink, where the real-time system Opal RT-Lab QNX was used to interface the Simulink environment to the motor drive and the sensors. A sampling period of $0.008s$ was used, where a search for a new reset candidate was attempted at all samples. In situations where more than one candidate satisfied the reset criterion, the one with largest drop in Lyapunov function value was selected.

Figures 4.9-4.10 show a situation where a conventional PI-controller is used. Note the peaks in propeller speed ω when the propeller ventilates. Also note the positive jumps in the estimated Lyapunov value due to shifted equilibrium point when the propeller starts and stops ventilating. The same situation is shown in Figures 4.11-4.12, but with integrator resetting. Clearly, the reset leads to reduced peaks in ω. The plots of $\hat{V}$ show the transient reductions when the PI-controller is reset. Also note that the mean propeller thrust $\bar{T}_p$ is increased when the PI-controller is reset: the mean propeller thrust without reset is $\bar{T}_p = 136$ N while the value with reset is $\bar{T}_p = 152$ N.

Figures 4.13-4.14 and 4.15-4.16 show the same controllers as Figures 4.9-4.10 and 4.11-4.12, respectively, but with a set-point mapping to $\omega^* = 56$ when ventilation is detected. Note the peak reduction of ω in Figure 4.16, where the integrator resetting is made active. In this last situation, a positive slew rate limiter has been included at the integrator output. This reduces the noise in the estimated $\hat{\beta}_Q$, and hence reduces the risk of performing erroneous resets. A more sophisticated solution to this issue would be to implement the noise reduction in the estimator $\hat{\beta}_Q$ instead. This is not considered here. A brief discussion of this problem is included in Smogeli, Sørensen & Fossen (2004). The mean propeller thrust is in this case kept more or less constant with the introduction of integrator reset: $\bar{T}_p = 130$ N without reset, while $\bar{T}_p = 128$ N with reset. The small reduction may be due to the introduction of the slew rate limiter. A more appropriate choice of this slew rate limiter may lead to an increase rather than a decrease of the thrust.

When looking at the plots of the motor power P_m, the analysis are a bit more complex. In Figure 4.10, there are some peaks in power at the instants where the propeller starts to spin. These peaks are showing a small tendency of being reduced when the reset module is made active, see Figure 4.12. The resulting lapse in this last case is however a bit rough. This may not be a preferred behavior regarding preventing blackout in the vessel power supply. The situation is even worse in the second case, see Figures 4.14 and 4.16. The slew rate limiter is causing this behavior, hence better performance may be achieved by implement the noise reduction in the estimator $\hat{\beta}_Q$, as discussed above.

4.4 Discussion

The anti-spin strategies in Smogeli, Hansen, Sørensen & Johansen (2004), Smogeli et al. (2006), Smogeli & Sørensen (2006), Smogeli (2006) and the one presented in this chapter are all based on the same observer, set-point mapping and detection algorithm, deviating only by selection of parameter values. However, the core controllers, i.e. the controllers used in normal conditions, are not the same. In Smogeli, Hansen, Sørensen & Johansen (2004), Smogeli et al. (2006), Smogeli & Sørensen (2006) and Smogeli (2006) the core controller is a combined torque/power controller, in contrast to the one discussed here being a regular shaft speed PI-controller. In Smogeli, Hansen, Sørensen & Johansen (2004) and Smogeli & Sørensen (2006), the output of the controller is modified by a dynamic scaling factor to give a nearly constant shaft speed when ventilation is detected.

In Smogeli et al. (2006), however, a switch to a speed-controller is made when ventilation is detected. The PI-controller is in this case not equipped with integrator resetting, but the controller may be tuned tighter compared to a PI-controller for normal conditions. A comparison of the strategies presented in Smogeli, Hansen, Sørensen & Johansen (2004), Smogeli et al. (2006) and Smogeli & Sørensen (2006) is given in Smogeli (2006). By appropriately tuning the different strategies, no or little deviation in performance is experienced. This is also the case when comparing the solutions in Smogeli, Hansen, Sørensen & Johansen (2004), Smogeli et al. (2006), Smogeli & Sørensen (2006) and Smogeli (2006) with the present one. They all solve the problem of anti-spin in more or less the same way regarding performance, but separate in the way of doing this - the main performance difference lies in the choice of basic controller. The present strategy has an advantage in terms of implementation in that it only needs tuning of the reset algorithm as a separate module. The parameters of the shaft speed PI-controller module are already tuned.

4.5 Concluding Remarks

The framework presented in Chapter 2 has been applied on a PI-controller for marine thruster speed control by integrator resetting in order to improve the transient performance of the LTC.

A test of the control strategy was made in a basin, where improved performance was observed at situations where the propeller ventilates. Tests showed reduced peaks in propeller speed, hence reduction of structural loads on propeller blades, while maintaining or even increasing the mean propeller thrust. The resulting analysis of the motor power were, however, a bit more complex. Power peaks seam to be reduced in some sense when the reset module was made active, but this, in turn, led to a more rough motor power lapse. Hence, tradeoffs between fluctuations in the motor power and improved performance of the propeller speed transients need to be taken.

The experimental results are only presented for positive propeller speed $\omega > 0$. This is so because there is not provided any new information by including plots for negative propeller speed, due to the qualitative symmetry around zero. The controller presented in this chapter is however optimized for vessel operation in DP, i.e. for both positive and negative propeller speed, but for only zero or low vessel speed. This is further improved in the next chapter.

Chapter 5

Application to Thruster Anti-spin in Transit Operation

Increased performance of DP and low speed manoeuvering vessels operating in extreme seas has been presented in Chapter 4. Differently from DP and low speed manoeuvering, operating in transit introduces additional losses due to changes in the speed of the inlet water to the propeller disc. In this chapter, a new way of modelling the thruster system is used in order to cope with this limitation. By combining a reference generator with a slightly modified PI-controller and a lyapunov-based reset strategy, a marine anti-spin controller for transit operation is developed. The method is as in Chapter 4 validated by experimental tests. The work is reported in Bakkeheim et al. (2007).

5.1 Introduction

This chapter may be read independently form Chapter 4. However, reading the introductional section of Chapter 4 prior to this chapter may be preferred. Section 4.1 is discussing some important issues regarding two different phenomena leading to losses due to vessel operations in extreme sea conditions, being crucial in understanding the motivation for what follows in this chapter.

For the anti-spin controllers reported in both Smogeli, Hansen, Sørensen & Johansen (2004) and Bakkeheim et al. (2006) (see Chapter 4) only DP and low speed vessel operations are considered. Extensions of the combined power/torque approach in Smogeli, Hansen, Sørensen & Johansen (2004) to transit are given in Smogeli (2006). In this chapter, however, a similar approach as in Chapter 4 is utilized, also covering transit operation, where the vessel speed is larger than in DP and low speed manoeuvering. In transit operations, losses due to nonzero advance speed introduces control errors in the actual propeller thrust when using a static mapping from the desired thrust to the desired shaft speed. Such a static mapping was used in the controller presented in Chapter 4. In Pivano et al. (2007) a dynamic mapping from the desired thrust to the desired shaft speed is presented, compensating for losses due to nonzero advance speed. By combining the dynamic mapping in Pivano et al. (2007) with the integrator resetting strategy in Chapter 4, we get an anti-spin controller suitable also for transit operations.

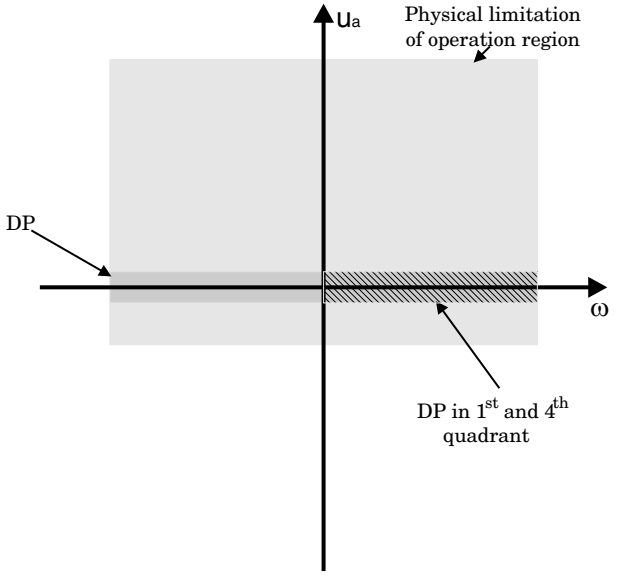

Figure 5.1: Four-quadrants operation. When operation in all four quadrants, the propeller speed ω and the vessel speed v may be both positive, both negative or of opposite magnitude. DP and low speed manoeuvering is located in the vicinity of the ω-axis, while transit operation may be located somewhere inside the physical limitation limits of the vessel.

5.1.1 Full Four-quadrants Operation

The controller given in Chapter 4 is designed for DP and low speed operations, i.e. for vessel speed close to zero. In this chapter, however, a controller designed for the full four-quadrant range is presented. Improved performance will for this controller be achieved for both maneuvering and transit operations as well as for DP operations.

Figure 5.1 shows the four-quadrant operation region. For a particular vessel, the region of operation inside the four quadrants is given by some physical limits. Typically the propeller speed may be equal in both directions, while the speed of the vessel is designed to be higher for positive vessel speed. With reference to Figure 5.1, DP and low speed manoeuvering is located in the vicinity of zero vessel speed, handled in Chapter 4. The experiments in Chapter 4 was however just presented for positive propeller speed, seen as the hatched area in Figure 5.1.

5.2 Anti-spin in Marine Thruster Control for Transit Operation

An illustration of a local thruster shaft speed controller system, considered here, is given in Figure 5.2. From the high-level control module, the desired propeller thrust T_{pd} is given as an input to the controller. Further, a reference generator, accounting for losses due to nonzero advance

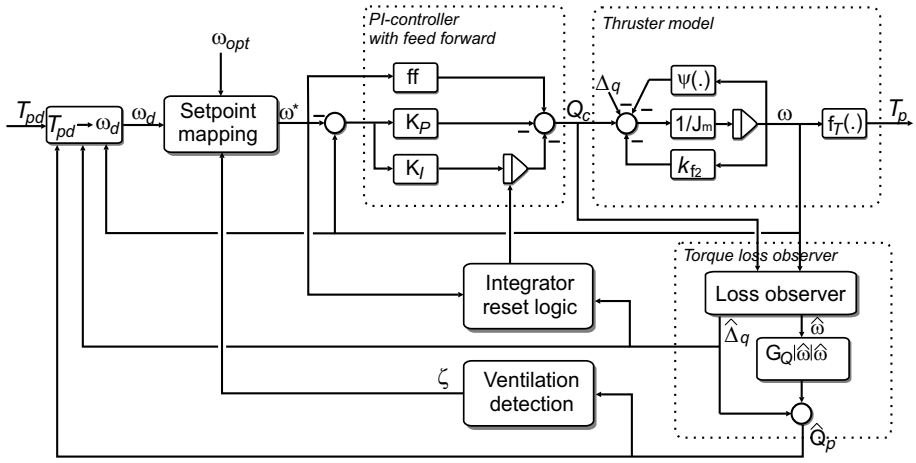

Figure 5.2: LTC system with controller state reset mechanism for transit operation. The approach is similar to the one presented in Figure 4.4. A PI-controller equipped with feed forward term works as a backbone for the strategy. The static mapping presented in Figure 4.4 is here replaced with a dynamic one, in order to cope for changes in vessel speed. The loss estimator is also changed due to the same reason.

speed, maps the desired thrust into the desired shaft speed ω_d. This is in turn fed into a set-point mapping, limiting the value of the desired shaft speed to some optimal value ω_{opt} when ventilation is detected. A PI-controller with feed-forward from the desired shaft speed gives the commanded torque Q_c to the motor driving the propeller shaft. The main idea in this chapter is, as in Chapter 4, that the integrator state in the PI-controller may be instantaneously reset to a different value, if appropriate. Consequently, the propeller shaft speed may track the desired one given by the reference generator more accurately.

The proposed controller for the transit case is heavily related to the one in the DP case presented in Chapter 4. However, they do differentiate in way of modelling the thruster and selection of dynamic controller followed by obtaining a suitable Lyapunov function, hence handled as two different applications presented in two different chapters.

5.2.1 Thruster Model

The thruster model to be considered is given by a first-order dynamic system

$$J_m\dot{\omega} = Q_c - \psi(\omega) - k_{f_2}\omega - \Delta_q \tag{5.1}$$

$$\dot{\Delta}_q = 0 \tag{5.2}$$

where ω is propeller shaft speed, J_m is shaft moment of inertia and Q_c is commanded torque to the motor drive. This model assumes the dynamics of the electrical part to be negligible when

compared to the shaft dynamics. All the nonlinearities are included in the function

$$\psi(\omega) = G_Q|\omega|\omega + k_{f_1}\arctan\left(\frac{\omega}{\epsilon}\right) + k_{f_3}\arctan\left(k_{f_4}\omega\right) \tag{5.3}$$

where the first term is the nominal propeller torque at zero advance speed in normal conditions, where

$$G_Q = \begin{cases} G_{Q_+}, & \omega \geq 0 \\ G_{Q_-}, & \omega < 0. \end{cases} \tag{5.4}$$

The constants G_{Q_+} and G_{Q_-} are positive and in general different since the propeller usually is not symmetric with respect to the shaft speed ω. Further, k_{f_i} and ϵ are constant and positive, included in order to model the system friction torque, see Pivano et al. (2007) for more details.

The model in (5.1)-(5.2) is representing the same system as the one presented in (4.1). The only difference is the way of modelling. The purpose of Δ_q in (5.1)-(5.2) is to model unknown torque losses due to variations in the vessel speed, propeller submergence, cross flows, wave-induced water velocities, interaction between the vessel hull and the propeller etc. All these losses are included in Δ_q in order to make the controller work in the total operation region in the four quadrants, unlike the controller system in Chapter 4. The advantage of the propeller model in (5.1)-(5.2) is the relaxation of a priori model knowledge.

Remark 5.1 *It is assumed that Δ_q is constant. This is a simplification. In reality Δ_q varies slowly due to the changes in advance speed, and quickly, almost discrete, due to losses caused by ventilation and in-and-out-of-water effects. The controller state reset procedure proposed in this chapter makes use of an estimate of Δ_q. This estimate $\hat{\Delta}_q$ triggers the reset procedure only by sudden changes in $\hat{\Delta}_q$. During transients caused by such an incident, we may assume Δ_q being constant due to slowly varying advance speed dynamics, see Section 2.1.4.*

5.2.2 PI-controller with Feed Forward Term

Assume ω_d is a smooth and bounded reference, the controller is given as

$$\begin{aligned} Q_c &= J_m\dot{\omega}_d + \psi(\omega_d) + k_{f_2}\omega_d - z - k_P\left(\omega - \omega_d\right) \\ \dot{z} &= k_I\left(\omega - \omega_d\right) \end{aligned} \tag{5.5}$$

including a feed forward part from ω_d and a regular PI-controller part on the error $\omega - \omega_d$, where $k_P > 0$ and $k_I > 0$ are the proportional and integral gains, respectively. The integrator state z can be interpreted as an estimate for $-\Delta_q$, used in the feed forward compensation in (5.5), hence similar to the adaptive case. The two states z and ω are stacked into the vector $x = [x_1,\, x_2]^T$, where $x_1 = z$ and $x_2 = \omega$.

The closed-loop error states are defined as $\tilde{x}_1 = z + \Delta_q$ and $\tilde{x}_2 = \omega - \omega_d$, hence from (5.1) and (5.5) the error system becomes

$$\dot{\tilde{x}}_1 = k_I\tilde{x}_2 \tag{5.6a}$$

$$\dot{\tilde{x}}_2 = \frac{1}{J_m}\left(-\left(k_{f_2} + k_P\right)\tilde{x}_2 - g(\tilde{x}_2, \omega_d) - \tilde{x}_1\right) \tag{5.6b}$$

where the nonlinear function $g(\tilde{x}_2, \omega_d) = \psi(\tilde{x}_2 + \omega_d) - \psi(\omega_d)$ is nondecreasing and inside the sector $[0, \infty]$ in the variable $\tilde{x}_2$, for any fixed ω_d.

5.2.3 Lyapunov Function

A Lyapunov function is needed both in order to prove the closed-loop system to be stable and as a measure of the remaining transient "energy". A quadratic Lyapunov function turns out to satisfy this property:

Lemma 5.1 *The following Lyapunov function proves the origin of the error system (5.6) to be uniformly globally stable (UGS) and convergent:*

$$V = \frac{1}{2}p_{11}\tilde{x}_1^2 + \frac{1}{2}p_{22}\tilde{x}_2^2 \tag{5.7}$$

where p_{11} and p_{22} are two positive constants, selected such that

$$p_{11} = \frac{p_{22}}{k_I J_m}. \tag{5.8}$$

Proof. The time derivative of (5.7) along the trajectories of (5.6) becomes

$$\begin{aligned}\dot{V} &= p_{11}k_I\tilde{x}_1\tilde{x}_2 \\ &\quad + \frac{p_{22}}{J_m}\tilde{x}_2\left[-\left(k_{f_2}+k_P\right)\tilde{x}_2 - \tilde{x}_1 - g(\tilde{x}_2,\omega_d)\right].\end{aligned} \tag{5.9}$$

Using the fact that $g(\tilde{x}_2,\omega_d)\tilde{x}_2 \geq 0\,\forall\omega_d,\ \tilde{x}_2$, and selecting p_{11} as in (5.8), (5.9) becomes

$$\dot{V} \leq -\frac{p_{22}}{J_m}\left(k_{f_2}+k_P\right)\tilde{x}_2^2 \tag{5.10}$$

hence the origin of (5.6) is UGS. Since $V \geq 0$ is bounded and non-increasing in time we have that $\lim_{t\to\infty}V(\tilde{x}(t)) = V_\infty$ exists and

$$\begin{aligned}&\int_0^\infty K\tilde{x}_2^2(\tau)d\tau = K\int_0^\infty \tilde{x}_2^2(\tau)d\tau \\ &\leq -\int_0^\infty \dot{V}(\tau)d\tau = V_0 - V_\infty\end{aligned} \tag{5.11}$$

where $K = \frac{p_{22}}{J_m}\left(k_{f_2}+k_P\right)$ and $V_0 = V(\tilde{x}(0))$. The expression in (5.11) implies that $\tilde{x}_2 \in \mathcal{L}_2$. Since $\omega_d \in \mathcal{L}_\infty$ and $\tilde{x}_1,\ \tilde{x}_2 \in \mathcal{L}_\infty$, due to UGS of the origin (5.6), from (5.6b) also $\dot{\tilde{x}}_2 \in \mathcal{L}_\infty$. These conditions imply that $\lim_{t\to\infty}\tilde{x}_2(t) = 0$ from Barbalat's lemma, see Khalil (2002). Further, using the fact that $g(\cdot,\cdot)$ is differentiable and $\dot{\omega}_d \in \mathcal{L}_\infty$, from (5.6b) $J_m\ddot{\tilde{x}}_2 = -\left(k_{f_2}+k_P\right)\dot{\tilde{x}}_2 - \frac{\partial g}{\partial\tilde{x}_2}(\tilde{x}_2,\omega_d)\dot{\tilde{x}}_2 - \frac{\partial g}{\partial\omega_d}(\tilde{x}_2,\omega_d)\dot{\omega}_d - k_I\tilde{x}_2$ leading to $\ddot{\tilde{x}}_2 \in \mathcal{L}_\infty$, hence $\dot{\tilde{x}}_2$ being uniformly continuous (UC). Next, we know that $\int_0^\infty \dot{\tilde{x}}_2(\tau)d\tau = \tilde{x}_2(\infty) - \tilde{x}_2(0)$ exists and is finite, and in combination with $\dot{\tilde{x}}_2$ being UC, $\dot{\tilde{x}}_2(t) \to 0$ as $t \to \infty$ using Barbalat's lemma. From (5.6b) we conclude that also $\lim_{t\to\infty}\tilde{x}_1(t) = 0$, hence the origin of the error system (5.6) is convergent. ■

Remark 5.2 *If ω_d is constant, the origin of (5.6) will be GAS.*

5.2.4 Torque Loss Observer

The need for an observer estimating the torque losses Δ_q is twofold; one for using it as a fast estimator in order to apply the controller state resetting procedure described in Section 2.1.4, and another to include Δ_q in the reference generator developed in Pivano et al. (2007).

A nonlinear observer with gain l_1 and l_2 is designed in order to estimate the torque loss $\hat{\Delta}_q$ and the shaft speed $\hat{\omega} = \hat{y}$:

$$\begin{aligned} J_m\dot{\hat{\omega}} &= Q_c - \psi(\hat{\omega}) - k_{f_2}\hat{\omega} - \hat{\Delta}_q + l_1\,(y - \hat{y}) \\ \dot{\hat{\Delta}}_q &= l_2\,(y - \hat{y}) \\ y &= \omega \end{aligned} \tag{5.12}$$

Defining the observer error variables as $\tilde{\omega} = \omega - \hat{\omega}$ and $\tilde{\Delta}_q = \Delta_q - \hat{\Delta}_q$, the observer error dynamics becomes

$$J_m\dot{\tilde{\omega}} = -\left(\psi(\omega) - \psi(\hat{\omega})\right) - l_1\tilde{\omega} - k_{f_2}\tilde{\omega} - \tilde{\Delta}_q \tag{5.13}$$

$$\dot{\tilde{\Delta}}_q = -l_2\tilde{\omega}. \tag{5.14}$$

Lemma 5.2 *If the gains l_1 and l_2 are chosen such that*

$$\begin{aligned} &A1 \quad l_1 > -k_{f_2} \\ &A2 \quad l_2 < 0 \end{aligned} \tag{5.15}$$

then the origin of (5.13)-(5.14) is UGS and convergent.

Proof. Consider the following Lyapunov function for the observer error dynamics (5.13)-(5.14)

$$V_o = \frac{1}{2}a_{11}\tilde{\omega}^2 + \frac{1}{2}\tilde{\Delta}_q^2 \tag{5.16}$$

where $a_{11} = -J_m l_2$ a positive constant. The time derivative of (5.16) along the trajectories of (5.13)-(5.14) is

$$\dot{V}_o = l_2\left(\psi(\omega) - \psi(\hat{\omega})\right)\tilde{\omega} + l_2\left(k_{f_2} + l_1\right)\tilde{\omega}^2. \tag{5.17}$$

Furthermore, the function $\psi(\cdot)$ belongs to the sector $[0,\ \infty]$ and is non-decreasing, hence $\forall\omega,\ \hat{\omega}$ $[\psi(\omega) - \psi(\hat{\omega})]\,(\omega - \hat{\omega}) \geq 0$, hence $\dot{V}_o \leq l_2\left(k_{f_2} + l_1\right)\tilde{\omega}^2$ being negative semi-definite. Using the same argument as in the proof of Lemma 5.1, (5.16) will prove the origin of the error system (5.13)-(5.14) UGS and convergent. ■

The estimates $\hat{\omega}$ and $\hat{\Delta}_q$ can be used to compute an estimate of the propeller torque from

$$\hat{Q}_p = G_Q|\hat{\omega}|\hat{\omega} + \hat{\Delta}_q. \tag{5.18}$$

5.2.5 Dynamic Reference Generator

As in Chapter 4, the reference is given as desired propeller thrust T_{pd}, hence a reference generator mapping T_{pd} to the desired propeller speed ω_d is needed. In Chapter 4, however, this mapping was assumed to be constant due to the assumption of zero advance speed. In transit operation, nominal thrust and torque coefficients K_{T0} and K_{Q0} in (4.29) and (4.3) are no longer appropriate. In Pivano et al. (2007) a dynamic reference generator for nonzero advance speed is proposed. The reference generator is using thrust and torque coefficients K_T and K_Q, given as a function of the advance number

$$J = \frac{2\pi u_a}{\omega D} \tag{5.19}$$

where D is propeller diameter and u_a is the advance speed. The coefficients K_T and K_Q are computed as

$$K_T = \frac{4\pi^2 T_p}{\rho|\omega|\omega D^4} \tag{5.20}$$

$$K_Q = \frac{4\pi^2 Q_p}{\rho|\omega|\omega D^5}. \tag{5.21}$$

The proposed reference generator is divided into three main parts. The first part maps T_{pd} into the desired propeller torque

$$Q_{pd} = \frac{1}{\hat{G}_{QT(\hat{J})}} T_{pd} \tag{5.22}$$

where

$$\hat{G}_{QT(\hat{J})} = \frac{K_T|_{\hat{J}}}{DK_Q|_{\hat{J}}} \tag{5.23}$$

is an estimate of the actual thrust-torque ratio. An estimate of the advance number $\hat{J}$ is used instead of the real value J, because the advance speed u_a is not available in practise, see Pivano et al. (2007) for more details.

The second part maps Q_{pd} into $\bar{\omega}_d$:

$$\bar{\omega}_d = \sqrt{\frac{\left|Q_{pd} - \hat{\Delta}_q\right|}{G_Q}} \text{sign}(Q_{pd} - \hat{\Delta}_q). \tag{5.24}$$

The final part is a second order low pass filter that generates smooth reference signals ω_d and $\dot{\omega}_d$:

$$\ddot{\omega}_d + 2\omega_c \xi \dot{\omega}_d + \omega_c^2 \omega_d = \omega_c^2 \bar{\omega}_d \tag{5.25}$$

where ω_c is the cutoff frequency and ξ is relative damping factor.

5.2.6 Reset Procedure

Resetting of the integrator state z to a properly chosen different value z_i may improve the transient performance of the proposed controller in (5.5).

Lemma 5.3 *A reset of the integrator value $z(t^+)$ to z_i, where t^+ denotes an infinitely small time increment of t, of the system in (5.6) leads to a jump in the Lyapunov function (5.7) as follows:*

$$\Delta V_i(t) = \frac{p_{11}}{2}\left(z_i^2 + 2\Delta_q\left(z_i - z(t)\right) - z^2(t)\right). \tag{5.26}$$

Proof. *Proof:* Let $\tilde{x}_{1i} = z_i + \Delta_q$. The jump in the Lyapunov function becoms

$$\begin{aligned}\Delta V_i(t) &= V(\tilde{x}_{1i}, \tilde{x}_2(t^+)) - V(\tilde{x}_1(t), \tilde{x}_2(t)) \\ &= \frac{p_{11}}{2}\left((z_i + \Delta_q)^2 - \left(z(t) + \Delta_q\right)^2\right) \\ &= \frac{p_{11}}{2}\left(z_i^2 + 2\Delta_q\left(z_i - z(t)\right) - z^2(t)\right)\end{aligned} \tag{5.27}$$

where the fact that $\tilde{x}_2(t^+) = \tilde{x}_2(t)$, due to the continuity of solutions of ordinary differential equations, has been used. ■

We assume a finite set of integrator reset candidates, $\mathcal{H} = \{z_1, \ldots, z_n\}$. The following result states stability when the integrator is reset.

Proposition 5.1 *Given a closed-loop system with a PI-controller as in (5.1) and (5.5). Assume that $V(\tilde{x})$ in (5.7) is a Lyapunov function that proves the equilibrium point of the nonlinear system in (5.6) to be UGS and convergent. Further assume that $\Delta V_i(t)$ denotes the jump in the Lyapunov function value if the integrator of the PI-controller in (5.5) is reset to a different value $z_i \in \mathcal{H}$. Then if $z(t)$ is reset to the value z_i only if $\Delta V_i(t) < 0$, the equilibrium point of the nonlinear system in (5.6) is UGS and convergent.*

Proof. The reader is referred to the proof of Theorem 2.1. ■

Note that Δ_q in (5.26) is unknown. Instead the estimate $\hat{\Delta}_q$ in (5.12) is used in the implementation of the reset algorithm. Analyzing the effect of noise in calculation of (5.26) is neglected. However, in order to reduce erroneous resets and scattering effects due to this issue, a positive threshold δ is added in the resetting procedure. The criterion for performing reset then becomes $\Delta V_i(t) + \delta < 0$.

5.2.7 Ventilation Detection

An estimate of the torque loss factor β_Q is calculated based on the estimated propeller load torque $\hat{Q}_p$ from (5.18) and the nominal load torque Q_n:

$$\hat{\beta}_Q = \alpha_b(\omega) + (1 - \alpha_b(\omega))\frac{\hat{Q}_p}{Q_n}. \tag{5.28}$$

where $\alpha_b(\omega)$ is a weighting function of the type

$$\alpha_b(y) = e^{-k|py|^r}. \tag{5.29}$$

k, p and r are positive tuning gains, needed because the estimate otherwise would be singular for zero shaft speed. The nominal torque, i.e. in case of no ventilation, is computed from the K_Q coefficient through (5.21) as

$$Q_n = K_Q \frac{\rho|\omega|\omega D^5}{4\pi^2}. \tag{5.30}$$

The nominal value of K_Q in (5.30) is derived from the K_Q characteristic where the nominal value of J is computed from (5.19) using the steady-state relation

$$u_a = (1 - w_f)\, u \tag{5.31}$$

where $0 < w_f < 1$ is the wake fraction number, often identified from experimental tests, and u is the vessel speed. The wake fraction number accounts for the reduction of water velocity to the propeller caused by the vessel hull.

As noted in Chapter 4, the estimated loss factor $\hat{\beta}_Q$ may be subject to some fluctuations during the period of ventilation. A translation of this value into a discrete value ζ is done in a similar way as described in Section 4.2.7.

5.2.8 Set-point Mapping

The reference generator (5.24), designed to counteract the losses due to nonzero advance speed, fails when ventilation occurs. This is so because losses due to ventilation are not accounted for. Anti-spin set-point mapping is used in order to reduce the shaft speed reference in case of ventilation

$$\omega^* = \begin{cases} \omega_{opt}, & \text{if } \zeta = 1 \text{ and } \omega_d \geq \omega_{opt} \\ \omega_d, & \text{otherwise} \end{cases} \tag{5.32}$$

where ω_{opt} is some optimal propeller shaft speed during ventilation, see Smogeli (2006) for models used to compute ω_{opt}.

5.3 Experimental Test Results

A thruster setup with propeller disc diameter $D = 0.25m$ and shaft moment of inertia $J_m = 0.006kgms^2$ was used to experimentally test the proposed strategy in the Marine Cybernetics Laboratory (MCLab) at NTNU, see Figure 5.3.

The tuning of the overall controller was performed in several steps. The friction parameters k_{f_i} and ϵ were identified by running the propeller in free air at different speeds ω. The parameters for the PI-controller were found by focusing on the control performance in calm and moderate seas. The resulting parameters led to a relatively slow controller response, where the commanded torque Q_c avoids wear-and-tear on the mechanical components. Next, the loss observer and reference generator were tuned in order to operate in calm sea conditions. Further, the ventilation detection with set-point mapping was tuned in order to handle extreme sea situations. Finally, the parameters of the reset procedure were tuned in extreme sea conditions.

The resulting parameters for the PI-controller were $k_P = 0.07$ and $k_I = 0.8$. The observer parameters were selected to be $l_1 = 3.2$, satisfying **A1** in Lemma 5.2, and $l_2 = -160$,

Figure 5.3: A test setup in MCLab at NTNU. The LTC for transit operation in extreme sea conditions with integrator reset was tested in a basin. The nonzero advance speed was effectuated by moving the thruster horizontally using a towing carriage. Also the thruster vertical position was moved in order to trigger ventilation and in-and-out-of-water effects.

satisfying **A2** in Lemma 5.2. The optimal controller speed during ventilation was selected to be $\omega_{opt_+} = 45$ and $\omega_{opt_-} = 54$ for positive and negative shaft speed, respectively. The Lyapunov function coefficients were selected to be $p_{11} = 21$ and $p_{22} = 0.1$, hence satisfying (5.8). The tuning of the resetting procedure was then restricted to select a suitable δ in order to yield acceptable performance, where $\delta = 100$ turned out to work fine. The reset candidates $\mathcal{H} = \{z_1, \ldots, z_n\}$ both need to span the working area of the integrator state z and to address robustness properties for the reset procedure by appropriately selection of candidate sparseness. $\mathcal{H} = \{-6.6, -4.4, -2.2, 0, 2.2, 4.4, 6.6\}$ gave satisfactory performance.

A thruster mounted on a moving towing carriage was employed in order to demonstrate the strategy. Extreme sea conditions were simulated by raising and lowering the thruster into the water with a period of $6.6s$ and amplitude of $15cm$. This way of emulating waves gave total control of the environmental interaction with the thruster setup, hence a more accurate way of comparing different controller algorithms.

Figures 5.4-5.5 and Figures 5.6-5.7 show data from the test without and with resetting the integrator state, respectively. The thruster vertical position was moved in order to trigger ventilation and in-and-out-of-water effects, presented as relative submergence h/R, where $R = D/2$ is the propeller radius and h is the submergence of the propeller shaft, see Figure 4.5. The time series of σ shows integrator reset incidents. When σ is nonzero, say $\sigma = i$, a reset to candidate $z_i \in \mathcal{H}$ is performed. Motor power P_m is included in order to show power fluctuations generating power peaks on the power network.

The test scenario was the same for both cases. The commanded thrust T_{pd} had the pattern seen in Figure 5.5, with amplitude $120N$. The emulated resulting speed of the towing carriage u had

an amplitude $0.7m/s$, dephased from the commanded thrust. The combination of the behavior of T_{pd} and u yields operation in 4 quadrants. In this case, $u_a = u$.

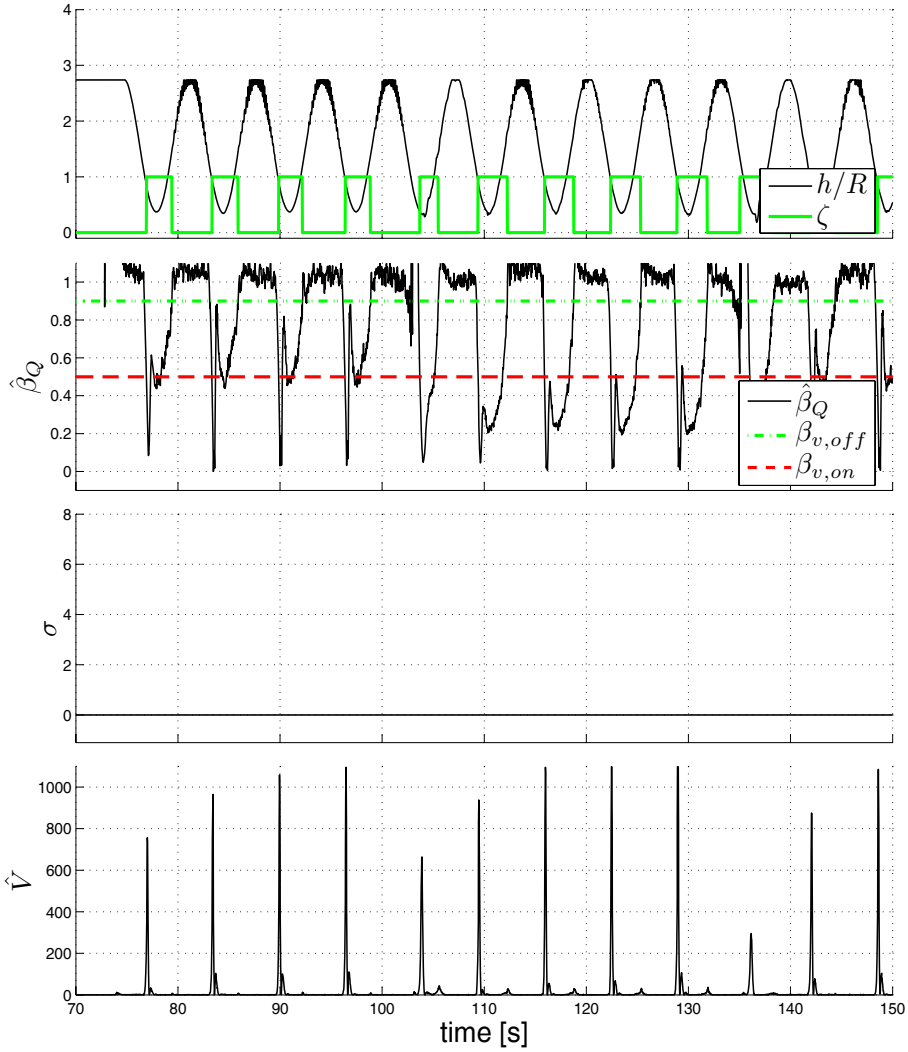

Figure 5.4: Experimental results of shaft speed PI-control without reset. The plot shows relative submergence h/R, ventilation detection signal ζ, estimated loss value $\hat{\beta}_Q$, reset index value σ and estimated Lyapunov function value $\hat{V}$. Figure 5.5 presents the rest of the plots for this situation.

In Figures 5.4-5.5 the controller is tuned for operating in calm sea. As seen in Figure 5.5, the propeller speed increases when the propeller rotates close to the water surface. These peaks in rotational speed are reduced when the integrator reset is made active, see Figure 5.7. Also

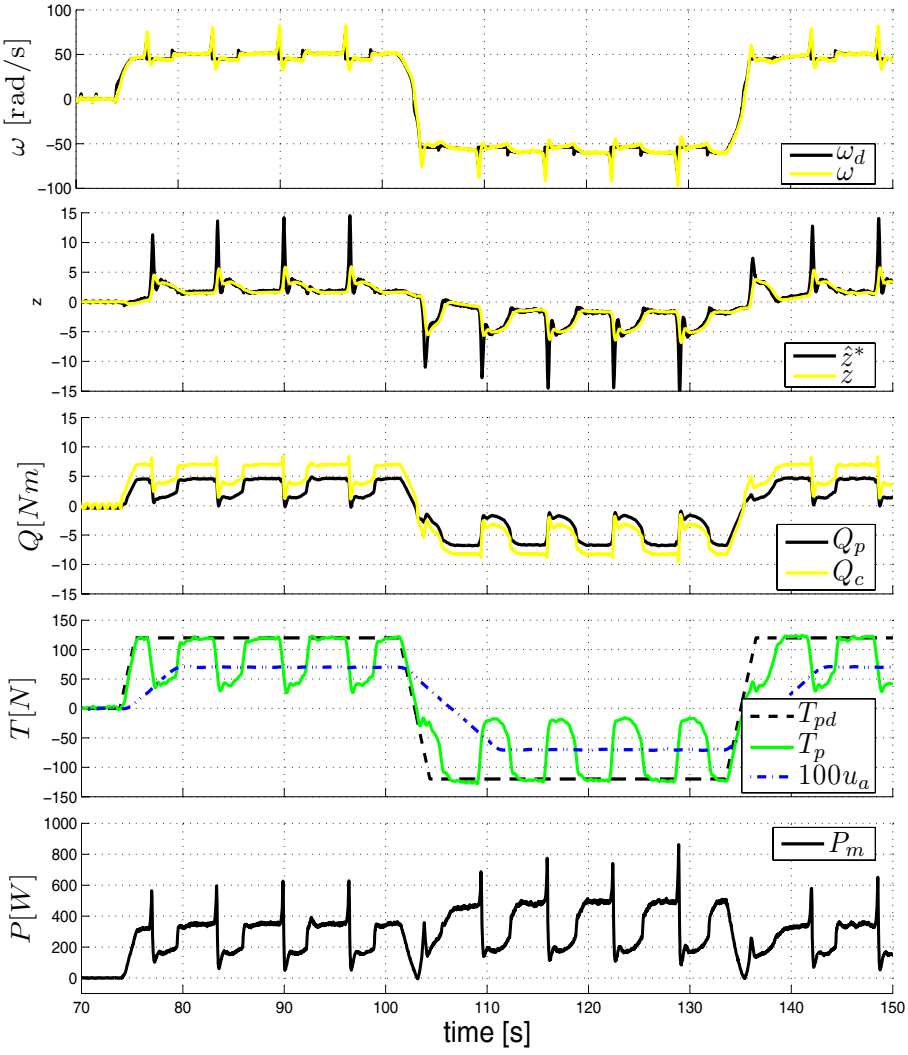

Figure 5.5: The rest of the plots of the situation presented in Figure 5.4. The figure shows the desired shaft speed ω_d, actual shaft speed ω, estimated integrator value $\hat{z}^*$, actual integrator value z, measured propeller torque Q_p, commanded torque Q_c, desired thrust T_{pd}, measured thrust T_p, propeller advance speed u_a and motor power P_m.

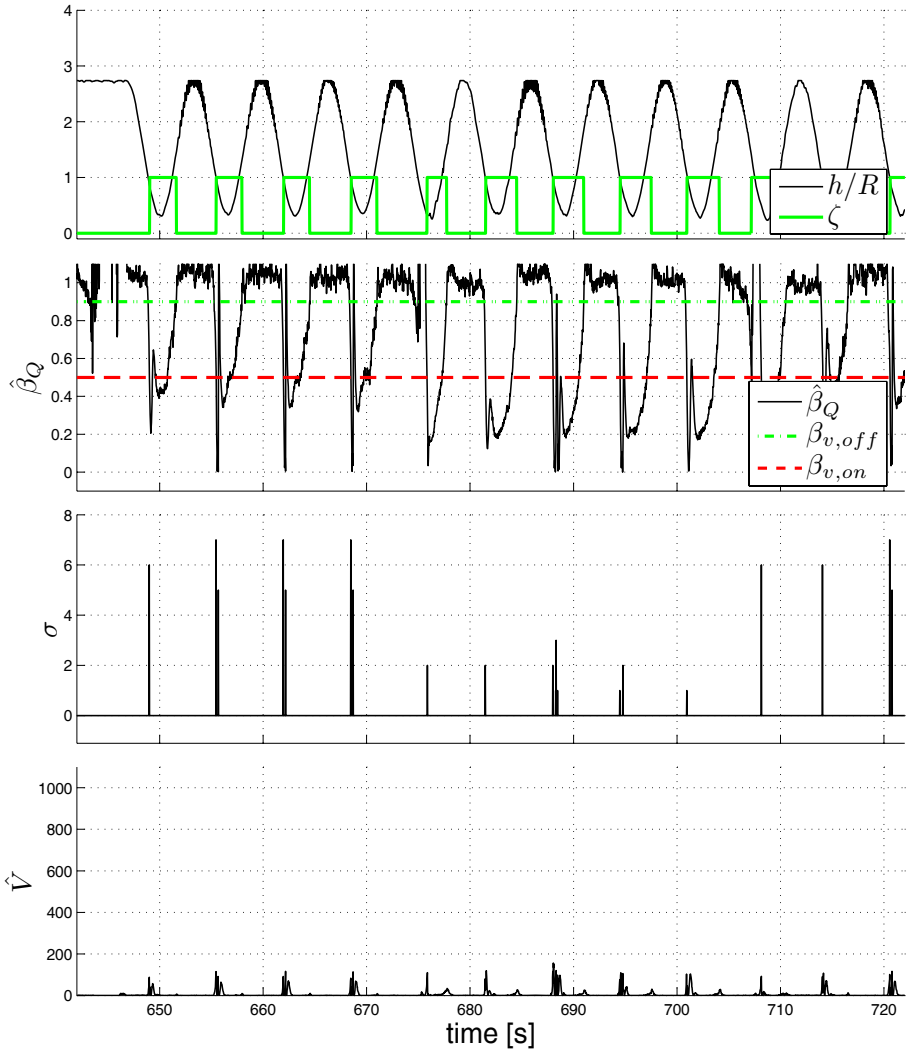

Figure 5.6: Same as Figure 5.4, but with integrator reset made active.

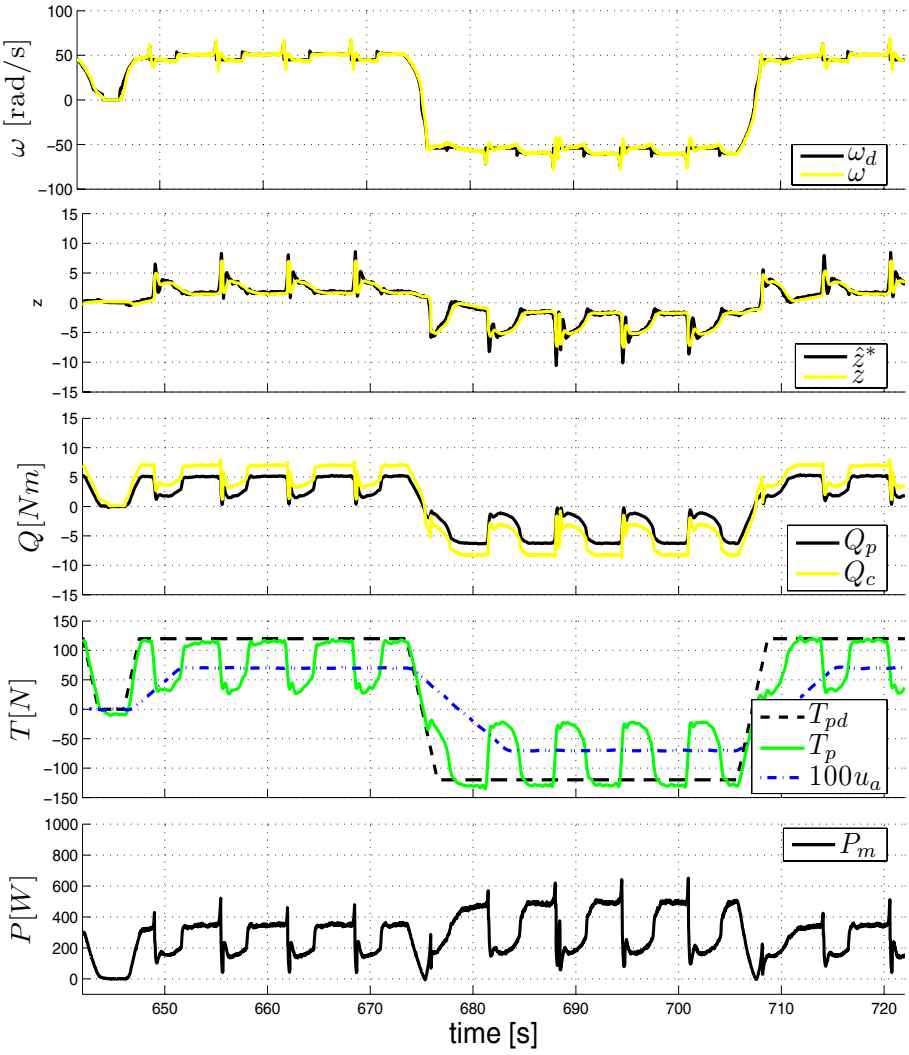

Figure 5.7: Same as Figure 5.5, but with integrator reset made active.

note the reduction in power peaks, hence reducing the risk of blackouts due to fluctuations on the electric power network. Despite this reductions in power peaks, the average thrust production is kept more or less constant.

5.4 Concluding Remarks

A Lyapunov-based integrator reset strategy for a PI shaft speed thruster controller has been presented. It deviates from the predecessor, a controller for propeller operating in DP, by also being optimized for transit operations. This was done by including a dynamic reference generator and a new way of modelling the thruster dynamics leading to a slightly different observer. The strategy handled the dynamic parameters K_Q and K_T by incorporate the losses due to nonzero advance speed into a common loss factor.

In order to emulate operation in 4 quadrants and extreme seas conditions, the propeller was towed through the water and at the same time moved along its vertical axis. Tests showed reduced peaks in propeller speed, hence reduction of structural loads on propeller blades, while not changing the mean propeller thrust significantly. The improved performance in propeller speed compared to the one without reset was not that significant as for the controller optimized for DP operations. The reason to this is that the feed forward term in the current controller gives fast reactions to thrust losses. This reduces the importance of the resetting mechanism regarding improving propeller speed transient performance. The reduction of power peaks, however, was greatly improved, hence reduced risk of blackouts due to fluctuations on the electric power network.

Chapter 6

Conclusions and Future Work

6.1 Conclusions

A strategy for improving transient performance for systems with a dynamic controller has been presented. The strategy leaned on finding a Lyapunov function. This was used both in order to prove the controller system without controller state reset being asymptotically stable, and to decide when to preform a controller state reset. Prediction of negative jump in the Lyapunov function lead to a reset of the controller state. In this way, AS was preserved in occurrences of controller state reset.

A framework for the controller state reset strategy was presented. A simple example was given in order to motivate for the control method. The improved performance was seen as reduced time for the system to settle after some sudden changes in the environmental states or the controller set-points, given an appropriately selected Lyapunov function.

The strategy was employed on a parametric-strict-feedback system, where the effects of filtering noisy measurements were studied in details. This led into a tuning guideline in order to prevent erroneous reset due to these effects. Simulations of an idealized anti brake system showed improved transient performance when braking on heterogeneous road conditions.

The resetting mechanism was also implemented on a LTC for DP and low speed manoeuvering for ships operating in extreme sea conditions. The continuous controller used as the backbone for the resetting mechanism, was a shaft speed PI-controller, being today's typical installation in mechanically and electrically driven vessels. Tests carried out in a test basin showed improved performance by reduction of propeller spin in case of ventilation and in-and-out-of-water effects. The produced propeller thrust was shown to be constant or even increased by up to 10% compared to the controller without reset mechanism. A reduction of the power peaks was also shown but, on the other hand, increased fluctuations in the power plots was observed. Hence, tradeoffs between the motor power fluctuations and improved performance of the propeller speed transients need to be considered. The latter may reduce the wear-and-tear of the mechanical parts.

The strategy was further augmented to transit vessel operations in extreme sea conditions. The PI-controller was slightly changed in order to handle additional losses due to nonzero speed of water hitting the propeller disc. Experimental tests were carried out in a towing tank in order to show the increased transient performance of propeller speed. In this case, a considerably

reduction in the power peaks were observed in the power consumption. This may be an important issue in preventing blackout in the ship's power generation and distribution system.

Despite the controller strategy for transit operation is suitable both in DP and transit situations, the pure DP controller does have some advantages overall. It turned out that the process of tuning the controller parameters when in DP operation, was much easier for the DP controller compared to the one also suitable for transit operation. The reason to this is that the model used in the pure DP controller is more accurate in DP operation than the controller applicable for both DP and transit operations. A solution to this may be to switch from the pure DP controller to the one suitable both for DP and transit operation when going from DP to transit operation, and vice versa. In this way we may achieve an optimal controller for the full four-quadrant range.

The appendix of the thesis contains three papers made during the work of this PhD study. These papers are complementary to the presented framework, and included since they describe alternative solutions to the control problems presented in the application part of the thesis.

Appendix A and Chapter 3 consider the same wheel slip control problem to exemplify the given strategies. In fact, these examples are not included in order to serve as satisfactory solutions to the wheel slip problem. In Appendix A, the wheel slip example is included in order to study how the quarter car can be modelled by nonparametric identification tools. The likelihood of the controller robustness is mapped into a pole placement graph. In Chapter 3, however, the wheel slip control problem is used to illustrate the Lyapunov resetting mechanism for parametric-strict-feedback systems.

Appendix B shows an alternative way of solving the anti-spin control problem in DP operations presented in Chapter 4. A combined power/torque controller with anti-spin is used in order to handle extreme sea conditions. Since only simulation results are included in Appendix B, no direct comparison to the experimental results presented in Chapter 4 is possible. However, by comparing the combined power/torque strategy presented in Smogeli (2006), there is little difference to report regarding performance. The difference lies in the way of solving the control problem. The Lyapunov-based reset strategy has, however, an advantage in terms of implementation in that it allows tuning of the reset algorithm as a separate module.

Appendix C shows an alternative way of solving the anti-spin control problem in transit operations presented in Chapter 5. Both approaches are similar in way of modelling the thruster dynamics and how to handle nonzero advance speed, using a dedicated loss estimator. The loss estimator enters into the controllers in two separate missions. In both approaches, the loss estimator constitutes as a part of a dynamic reference generator, counteracting for the torque loss due to nonzero advance speed. The other use of the loss estimator is however distinct in the two approaches. In Chapter 5, the loss estimator is used in the resetting mechanism, while in Appendix C it constitutes as a part of the dynamic PI-controller as a feed forward term. Studying the performance of the two approaches leads to the same conclusion as in the pure DP controllers above; the difference lies mainly in the way of solving the control problem.

The main benefit of the presented strategy is the separation of the specification, design, implementation and tuning procedure into two distinct operations, within a common theoretical framework. First, the dynamic controller without reset may be developed for optimal performance in normal conditions. In this way, the controller performance may leave out the need for reacting with sufficient performance in extreme conditions, hence be less sensitive to measurement noise. Second, the resetting strategy detects when an extreme situation occur, e.g. a sudden change in the plant parameter, and takes action to this. It is, however, important to tune the reset mechanism

in such a way that it is not triggered by measurement noise. If properly tuned, we achieve a controller that is optimal both in normal and extreme conditions. The presented strategy may apply for all kinds of dynamic controllers, given that there is room for transient improvements.

There are however some drawbacks of the presented strategy.

It leans on finding a Lyapunov function for a given system. This is the main weakness of the strategy, since there are no general way of finding such a function. This is easily seen by going from the controller strategy for DP and low speed manoeuvering in Chapter 4 to the one handling the transit situation in Chapter 5. This transition led to a totally different way of finding a suitable Lyapunov function and also the way of stating the system's stability properties. The way of using the Lyapunov function is, however, unchanged in the different cases.

Another drawback is the need for a fast estimator in order to estimate the Lyapunov function value, since this is not available for measurement. This may lead to erroneous resets due to the potential discrepancy between the estimated and actual Lyapunov function value. Different techniques may apply in order to secure the reset algorithm not performing erroneous resets, like the one presented in Chapter 3, but this may change from one control problem to another. No such universal technique exists so far.

Despite there are some questions to be answered, the main conclusion is however that this reset strategy may be applied on industrial control problems, with a potential of improving the transient performance. The main goal of this thesis is to be a small piece in the puzzle of bringing theoretical results into real life applications. One may say that the example applications presented in this thesis are carried out in idealized conditions, i.e. they are either been tested as simulation on a computer or been tested in a basin in a laboratory environment, but it is a start in approaching the conditions encountered in the industry.

6.2 Suggestions for Future Work

The following is a list of suggestions for future work.

- Establish techniques in order to verify if a given Lyapunov function is suitable for being a measure for the systems transient energy. This may be done by having a closer link to optimal control theory, allowing the reset to be associated with optimization criteria.

- Utilizing the fact that by online deactivating and activating some of the reset candidates, does not violate the overall stability property. This can be done in order to, for instance, preventing repeatedly resets between two neighboring reset candidates. Further for the LTC application, by online removing those candidates that are potential dangerous in generating severe power fluctuations on the net, reduced risk of blackout may be achieved. Removing candidates may also reduce the computational burden, by ignoring calculations that deals with the deactivated candidates.

- A more systematic method is also needed to find the reset candidates.

- Include the reset mechanism on the combined power/torque controller proposed in Smogeli (2006).

- Establish systematic methods for design of fast estimators. The methods need to address the problem of preventing erroneous resets due to lack of measurable Lyapunov function value.

Part III

Other Publications

Appendix A

Nonparametric Identification

This chapter includes the paper Bakkeheim, Murray-Smith & Johansen (2005). The paper deals with nonparametric identification. The case study at the end of the paper is motivated by the case study in Chapter 3. The following paper uses, however, a nonparametric model of the friction curve, in contrast to the modelling in Chapter 3, being a parametric one. In this way, the uncertainty of the nonlinear model is included in the process of tuning the given controller.

A.1 Abstract

Gaussian process prior (GP) models offer a nonparametric approach to modelling unknown nonlinear systems from experimental data. These are flexible models which automatically adapt their model complexity to the available data, and which give not only mean predictions but also the variance of these predictions. A further advantage is the analytical derivation of derivatives of the model with respect to inputs, with their variance, providing a direct estimate of the locally linearized model with its corresponding parameter variance. We show how this can be used to tune a controller based on the linearized models, taking into account their uncertainty. The approach is applied to a simulated wheel slip control task illustrating controller development based on a nonparametric model of the unknown friction nonlinearity. Local stability and robustness of the controllers are tuned based on the uncertainty of the nonlinear models' derivatives.

A.2 Introduction

Robust control is a fairly mature field, in particular for the controller synthesis problem for linear systems, where numerous approaches exist, see e.g. Zhou, Doyle & Glover (1996) and Skogestad & Postlethwaite (1996). However, robust control synthesis relies on a description or model of plant uncertainty. Although system identification methods as in Garulli, Tesi & Vicino (1999) and Reinelt, Garulli & Ljung (2002), may provide uncertainty information, this may be difficult to apply directly in robust control synthesis since this information may prove to be misleading in case of structural model mismatch. The availability of reliable uncertainty estimates is a major concern in applications of robust control, in particular for nonlinear systems.

Many model-based nonlinear control problems are still based on parametric models, where the functional form is fully described by a finite number of parameters, often a linear function of the parameters. Even in the cases where flexible parametric models are used, such as neural networks, spline-based models, multiple models etc., the uncertainty is usually expressed as uncertainty of parameters (even though the parameters often have no physical interpretation), and do not take into account uncertainty about model structure, or distance of current prediction point from training data used to estimate parameters.

In such cases, an alternative approach is that some parts or even the whole structure, may be given by nonparametric models, such as GP models. In this paper, we study an approach which has the following properties. It is a non-parametric model which retains the available data and performs inference conditional on the current state and local data (called smoothing in some frameworks). The uncertainty of model predictions is dependent on local data density, noise on data, and model mismatch. The final model complexity is automatically related to the amount and distribution of available data (more complex models need more evidence to make them likely), as well as the complexity of the target system. These aspects are especially useful in transient regimes with sparse data, in system identification tasks.

A.3 Gaussian Process Prior

In a Bayesian framework the model must be based on a prior distribution over the infinite-dimensional space of functions. As illustrated in O'Hagan (1978), such priors can be defined as Gaussian processes. These models have attracted a great deal of interest recently, in for example reviews such as Williams (1998*b*). Rasmussen (1996) showed empirically that Gaussian processes were extremely competitive with leading nonlinear identification methods on a range of benchmark examples.

The further advantage that they provide analytic predictions of model uncertainty makes them very interesting for control applications. Early use of GPs in a control systems context is discussed in Murray-Smith, Johansen & Shorten (1999) and Leith, Murray-Smith & Leithead (2000). A variation which can include ARMA noise models is described in Murray-Smith & Girard (2001). k-step ahead prediction with GP's is described in Girard, Rasmussen, Candela & Murray-Smith (2003) and Kocijan, Murray-Smith, C.Rasmussen & Girard (2004). Murray-Smith & Shorten (2005) provides a number of chapters on recent applications of Gaussian processes in control contexts.

A.3.1 Inference with Gaussian Processes

Assume we are modelling a nonlinear target function $f(\mathbf{x})$ where the observed outputs y^i to inputs $\mathbf{x}^i$, subject to noise ϵ_i can be described by the equation

$$y^i = f(\mathbf{x}^i) + \epsilon_i \tag{A.1}$$

and that we can observe a set S of input/output pairs $X, \mathbf{y}$, or $\{(\mathbf{x}^i, y^i)\}$ are given, where $\mathbf{x}^i \in \mathbf{R}^D,\ y^i \in \mathbf{R},\ i = 1 \ldots N$, hence:

$$X = \begin{bmatrix} \mathbf{x^1} \\ \vdots \\ \mathbf{x^i} \\ \vdots \\ \mathbf{x^N} \end{bmatrix}, y = \begin{bmatrix} y^1 \\ \vdots \\ y^i \\ \vdots \\ y^N \end{bmatrix}. \tag{A.2}$$

Instead of parameterising the system as a parametric model, we are placing a prior directly on the space of functions where f is assumed to belong. A Gaussian process represents the simplest form of prior over functions, we assume that any N points have a N-dimensional multivariate Normal distribution. In the GP framework, the output values y^i are viewed as being drawn from a zero-mean multivariable Gaussian distribution whose covariance matrix is a function of the input vectors $\mathbf{x}^i$. Namely the output distribution is

$$(y^1, \ldots, y^N | \mathbf{x}^1, \ldots, \mathbf{x}^N) \sim \mathcal{N}(0, \Lambda(X, X)).$$

Where $\Lambda(\mathbf{x}^i, \mathbf{x}^j) = \mathrm{cov}(y^i, y^j)$ is the covariance matrix of the function observations. A general model, which reflects the higher correlation between spatially close (in some appropriate metric) points – a smoothness assumption in target function $f(\mathbf{x})$ – uses a covariance matrix with the following structure;

$$\Lambda(\mathbf{x}^i, \mathbf{x}^j) = \alpha \exp(-\frac{1}{2}\|\mathbf{x}^i - \mathbf{x}^j\|_\Gamma^2) + v_0 \delta_{i,j}, \tag{A.3}$$

where $\delta_{i,j} = 1$ for $i = j$, and zero otherwise. The norm $\|\cdot\|_\Gamma$ is defined as

$$\|\mathbf{u}\|_\Gamma = (u^T \Gamma u)^{\frac{1}{2}},\ \ \Gamma = \mathrm{diag}(\gamma_1, \ldots, \gamma_D).$$

The $D + 2$ variables, $\alpha, \gamma_1, \ldots, \gamma_D, v_0$ are the hyper-parameters of the GP model, which are constrained to be non-negative. In particular v_0 is included to capture the noise component of the covariance. The GP model can be used to calculate the distribution of an unknown output y^{N+1} corresponding to known input $\mathbf{x}^{N+1}$ as

$$(y^{N+1} | \mathbf{x}^1, \ldots, \mathbf{x}^N, \mathbf{x}^{N+1}, y^1, \ldots, y^N) \sim \mathcal{N}(\mu, \bar{\Lambda}),$$

where

$$\mu = \Lambda(\mathbf{x}^{N+1}, X)\Lambda^{-1}(X, X)\mathbf{y}, \tag{A.4}$$

$$\bar{\Lambda} = \Lambda(\mathbf{x}^{N+1}, \mathbf{x}^{N+1}) - \Lambda(\mathbf{x}^{N+1}, X)\Lambda^{-1}(X, X)\Lambda(X, \mathbf{x}^{N+1}) \tag{A.5}$$

so we can use μ as the expected model output, with a variance of $\bar{\Lambda}$. Note that the covariance matrix $\Lambda(X, X)$ will be $N \times N$ dimensional, so the computational cost of its inversion grows rapidly with the number of data points N.

Nonstationary Covariance Function

In this paper, instead of the stationary covariance function of (A.3) we use a nonstationary one,

$$\Lambda(\mathbf{x}^i, \mathbf{x}^j) = v_1 \sin^{-1}\left(\frac{\mathbf{x}^{iT}\Gamma\mathbf{x}^j}{\sqrt{(1+2\mathbf{x}^{iT}\Gamma\mathbf{x}^i)(1+\mathbf{x}^{jT}\Gamma\mathbf{x}^j)}}\right) + v_0\delta_{i,j} \tag{A.6}$$

as described in Williams (1998*a*), using Rasmussen's Matlab implementation.[1] Further, $\Gamma = \mathrm{diag}(\gamma_1, \ldots, \gamma_{D+1})$ where the positive γ_i, weight each input i (and an additional constant one acting as a bias term). The parameter vector $\Theta = \log[v_1, \gamma_{1,..,D+1}, v_0]^T$ (the log is applied elementwise and ensures positivity in the parameters) and D is the dimension of vector $\mathbf{x}$. The hyperparameters Θ, can be adapted as the model is fit to the identification data, using numerical methods such as standard gradient-based optimisation tools to optimise hyperparameters.

A.3.2 Gaussian Process Derivatives

Differentiation is a linear operation, so the derivative of a Gaussian process remains a Gaussian process. We now use this fact to infer from and to a mixture of observations of values and derivatives. Suppose we are given new sets of pairs $S'_j = \{(\mathbf{x}^{j,i}, \omega^{j,i})\},\ j = 1, \ldots, D,\ i = 1, \ldots K$, each S'_j corresponding to the K points of j^{th} partial derivative of the underlying function $y = f(\mathbf{x})$. In the noise-free setting this corresponds to the relation

$$\omega^{j,i} = \frac{\partial f(\mathbf{x})}{\partial x_j}|_{\mathbf{x}=\mathbf{x}^{j,i}},\ i = 1, \ldots, K.$$

We now wish to find the joint probability of the vector of y's and ω's, which involves calculation of the covariance between the function and the derivative observations as well as the covariance among the derivative observations. Covariance functions are typically chosen to be differentiable, so the covariance between a derivative and function observation and the one between two derivative points satisfy

$$\mathrm{cov}(\omega^{j,m}, y^n) = \frac{\partial}{\partial x_j}\mathrm{cov}(y^m, y^n) \tag{A.7}$$

$$\mathrm{cov}(\omega^{j,m}, \omega^{i,n}) = \frac{\partial^2}{\partial x_j \partial x_i}\mathrm{cov}(y^m, y^n). \tag{A.8}$$

Including these in our covariance function allows us to identify and predict from a data set which includes a mixture of function and derivative observations. Predictions can be inferred function values or inferred derivative values, with standard deviations in both cases.

The use of derivatives of Gaussian processes is described in O'Hagan (1992) and Rasmussen (2003), and in engineering applications in Murray-Smith et al. (1999), Murray-Smith & Sbarbaro (2002), Leith, Leithead, Solak & Murray-Smith (2002) and Solak, Murray-Smith, Leithead, Leith & Rasmussen (2003). This allows the integration of prior information in the form of state or control linearisations, as presented in Solak et al. (2003), and importantly for this paper, GP

[1] Code available at http://www.kyb.tuebingen.mpg.de/bs/people/carl/code/gp/

models can provide local linearisation information with mean and uncertainty estimates. This is useful for controller development with robustness analysis in small regions around the point of operation, and make GP models interesting candidates for nonlinear robust control problems.

A.4 Case Study; Wheel Slip Control

An application to wheel slip control is studied to illustrate the controller development for a non-parametric nonlinear model.

A.4.1 Equations of Motion of a Quarter Car

With reference to Figure A.1, the quarter car model consists of a single wheel attached to a mass m. A tyre reaction force F_x is generated by the friction between the tyre surface and the road surface, while the wheel moves driven by inertia of the mass m in the direction of the velocity v. A rolling motion of the wheel ω will be initiated by a torque caused by the tyre reaction force. A brake torque applied to the wheel will act against the spinning of the wheel causing a negative angular acceleration. The equations of motion of the quarter car are

$$m\dot{v} = -F_x \tag{A.9}$$
$$J\dot{\omega} = rF_x - T_b sign(\omega) \tag{A.10}$$

where

v	longitudinal speed at which the car travels
ω	angular speed of the wheel
F_z	vertical force
F_x	tyre friction force
T_b	brake torque
r	wheel radius
J	wheel inertia

Further, the tyre friction force is given by $F_x = F_z \cdot \mu(\lambda, \mu_H, \kappa)$ where the friction coefficient μ is a nonlinear function of

λ	tyre slip
μ_H	maximum friction coefficient between tyre and road
κ	slip angle of the wheel

The slip $\lambda = (v - \omega r)/v$ describes the normalized difference between horizontal speed v and speed of the wheel perimeter ωr. Note that this value is not measurable in practical applications, hence some type of observer is needed in order to obtain this value. The slip value of $\lambda = 0$ indicates that the wheel is in free motion and no friction force F_x is exerted. If the slip attains the value $\lambda = 1$ then the wheel is locked which means that it has come to a standstill. A change of

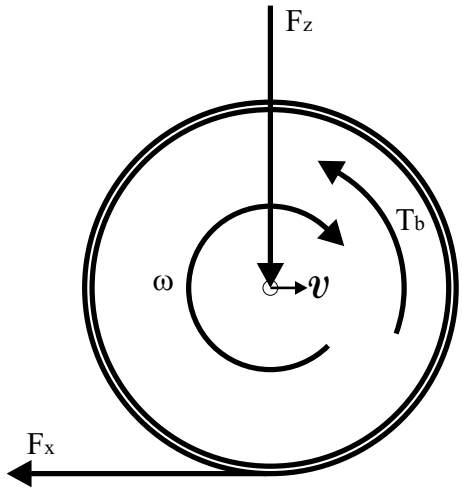

Figure A.1: Quarter car forces and torques.

variables is carried out where the angular speed of the wheel ω is replaced by the slip λ (assuming $\omega \geq 0$ and $v > 0$):

$$\dot{\lambda} = -\frac{1}{v}\left\{\frac{1}{m}(1-\lambda) + \frac{r^2}{J}\right\} F_z \mu(\lambda, \mu_H, \kappa) + \frac{1}{v} \cdot \frac{r}{J} T_b \tag{A.11}$$

$$\dot{v} = -\frac{1}{m} F_z \mu(\lambda, \mu_H, \kappa). \tag{A.12}$$

It can be seen that the time scale of the slip dynamics (A.11) scales with speed v. The qualitative dynamic behavior of slip is not affected by speed. Further assuming the slip angle of the wheel, κ, being zero, an example of such nonlinear tyre slip/friction curve, $\mu(\lambda, \mu_H)$, is shown in Figure A.4. Several structural models of different complexities exist in the literature, e.g. Bakker, Nyborg & Pacejka (1987), Pacejka & Sharp (1991), Daiss & Kiencke (1996) and Burckhardt (1993), but the detailed friction curve also depend on highly uncertain properties such as wear-and-tear of the tyres. A non-parametric GP model may therefore be a suitable alternative.

A.4.2 Control Strategy

As in Solyom (2004), assuming the velocity of the car varies much more slowly than the other variables involved and in addition that we have in general $\frac{J}{mr^2}(1-\lambda) \ll 1$, one obtains the dynamics of the tyre slip:

$$\dot{\lambda} v = -\frac{r^2 F_z}{J} \mu(\lambda, \mu_H) + \frac{r}{J} T_b. \tag{A.13}$$

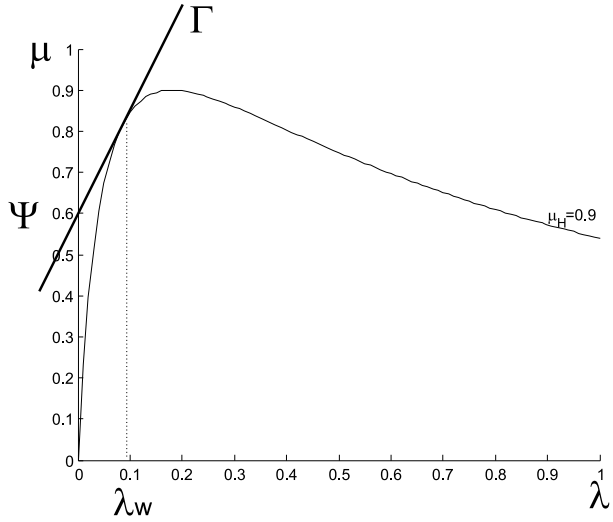

Figure A.2: Linearization $\mu_0(\lambda) = \Gamma\lambda + \Psi$ (solid line) of the nonlinear function $\mu(\lambda, \mu_H)$ (thin line) at $\mu_H = 0.9$ and $\lambda = \lambda_w$.

Further denoting $\beta = r^2 F_z/J$, $\alpha = r/J$ and adding hydraulic actuator dynamics, with time constant T_a:

$$\dot{T}_b = -\frac{1}{T_a}T_b + \frac{1}{T_a}u \tag{A.14}$$

$$\dot{\lambda}v = -\beta\mu(\lambda, \mu_H) + \alpha T_b. \tag{A.15}$$

Further, a simplification is made by linearizing the nonlinear function $\mu(\cdot)$ at a point of operation λ_w, as seen in Figure A.2. This new linearized function is given by $\mu_0(\lambda) = \Gamma\lambda + \Psi$, where Γ is the slope of the line and Ψ is the μ-intercept.

The total slip dynamics model may now be written as:

$$\dot{T}_b = -\frac{1}{T_a}T_b + \frac{1}{T_a}u \tag{A.16}$$

$$\dot{\lambda}v = -\beta(\Gamma\lambda + \Psi) + \alpha T_b. \tag{A.17}$$

Assuming zero initial conditions the transfer function of (A.16) and (A.17) is:

$$h_p(s) = \frac{\frac{\alpha}{v}}{(s + \frac{\beta}{v}\Gamma)(1 + T_a s)}. \tag{A.18}$$

We remark that Γ is to be considered a highly uncertain parameter, depending on both the operating point (reference slip value λ^*), and tyre/road properties. A GP model of the friction curve will be used to extract information about the uncertain parameters.

PID-controller

The literature presents a range of approaches to the use of PID-controllers in ABS problems, see Jiang & Gao (2001) and Wang, Schmitt-Hartmann, Schinkel & Hunt (2001), to mention some. Here a different approach using a PID-controller to solve the ABS problem is presented.

An ideal PID-controller is given by:

$$h_c(s) = K_p \frac{(1+T_i s)(1+T_d s)}{T_i s}. \tag{A.19}$$

Choosing $T_d = T_a$ leads to the open loop transfer function

$$h_0(s) = \frac{K_p \frac{\alpha}{v} s + \frac{K_p \alpha}{T_i v}}{s^2 + \frac{\beta}{v}\Gamma s} \tag{A.20}$$

which gives the following closed-loop transfer function:

$$G(s) = \frac{Ts+1}{1 + 2\zeta \frac{s}{\omega_0} + \left(\frac{s}{\omega_0}\right)^2} \tag{A.21}$$

where $2\zeta\omega_0 = \frac{\beta}{v}\Gamma + K_p \frac{\alpha}{v}$, $\omega_0^2 = \frac{K_p \alpha}{T_i v}$ and $T = T_i$. This gives the relative damping $\zeta = \left(\frac{\beta}{2v}\Gamma + K_p \frac{\alpha}{2v}\right)\sqrt{\frac{T_i v}{K_p \alpha}}$ and undamped resonance frequency $\omega_0 = \sqrt{\frac{K_p \alpha}{T_i v}}$.

Control Performance Requirement

For the closed-loop system (A.21), the poles are given by the solutions of its characteristic equation. If the parameters of the characteristic equation of (A.21) is given as random variables with an expectation and variance, the poles are then also given as random variables.

Example 1 *First assume for the system in (A.21) the parameter ζ is given as a random number with an expectation $E(\zeta)$ and a variance $\sigma^2(\zeta)$ and the parameter ω_0 is known exactly. The locations of the two complex conjugated poles are given by mean and standard deviation in a set of two arcs as seen in Figure A.3 a). If instead the uncertainty is in the parameter ω_0, and ζ is known exactly, two lines will characterize locations of the mean and standard deviation of the poles, Figure A.3 b). Finally, if ω_0 and ζ are independent random parameters, the mean and standard deviation of the poles are given as two areas, illustrated in Figure A.3 c).*

Controller Parameter Tuning

Assume the controller is supposed to regulate the set-point $\lambda = \lambda^*$. The controller parameters may be tuned according to a linear model of the quarter car around this point. The GP model provides estimates of the expectation $E(\Gamma)$ and variance $\sigma^2(\Gamma)$.

In this case study, Γ is randomly given, hence the relative damping ζ will be a random parameter in (A.21), i.e $E(\zeta) = \left(\frac{\beta}{2v}E(\Gamma) + K_p \frac{\alpha}{2v}\right)\sqrt{\frac{T_i v}{K_p \alpha}}$. This is exactly the situation depicted in Figure A.3 a).

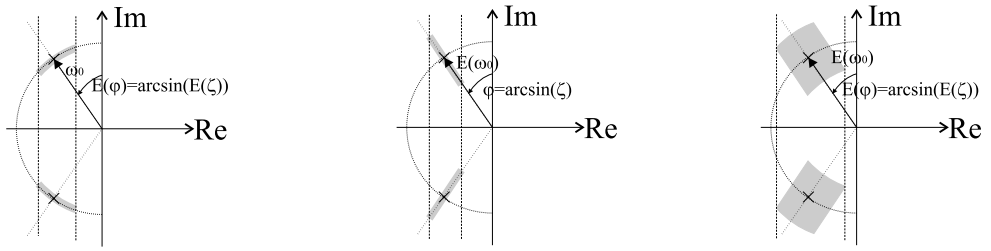

Figure A.3: Different pole locations. The vertical dotted lines indicates the real part of the mean with standard deviation of the pole placement. The uncertainties are shown as gray arcs, lines and areas. a) ζ uncertain. b) ω_0 uncertain. c) both ω_0 and ζ uncertain.

Assume the desired bandwidth and the desired nominal relative damping are given by ω_{0d} and ζ_d respectively. The bandwidth ω_0 is known exactly, and given by $\omega_0 = \sqrt{\frac{K_p}{T_i}\frac{\alpha}{v}}$. If the relative damping ζ is assumed to be less than 1, the bandwidth may be chosen to be equal to ω_{0d}. Further, since the best we can do regarding tuning the relative damping, is given by $E(\zeta) = \zeta_d$, we get the following expressions for the controller parameters:

$$K_p = \zeta_d \omega_{0d} \frac{2v}{\alpha} - \frac{\beta}{\alpha} E(\Gamma) \tag{A.22}$$

$$T_i = \frac{K_p}{\omega_{0d}^2} \frac{\alpha}{v}. \tag{A.23}$$

Given the above and the assumption of Γ being normally distributed with variance $\sigma^2(\Gamma)$, stability is ensured with at least 95% of confidence, i.e. behavior inside 2σ-contours, if $0 < \zeta^- < \zeta^+ < 1$ where:

$$\zeta^+ = \left(\frac{\beta}{2v}(E(\Gamma) + 2\sigma(\Gamma)) + K_p \frac{\alpha}{2v} \right) \sqrt{\frac{T_i v}{K_p \alpha}} \tag{A.24}$$

$$\zeta^- = \left(\frac{\beta}{2v}(E(\Gamma) - 2\sigma(\Gamma)) + K_p \frac{\alpha}{2v} \right) \sqrt{\frac{T_i v}{K_p \alpha}}. \tag{A.25}$$

A.4.3 Results

In the simulation that follows, a simplified model by Daiss & Kiencke (1996) is used for the tyre friction curve $\mu(\lambda, \mu_H)$,

$$\mu(\lambda) = \frac{k\lambda}{a\lambda^2 + b\lambda + 1}. \tag{A.26}$$

Note that this model is linear in the parameters a and b, where k is the slope at $\lambda = 0$.

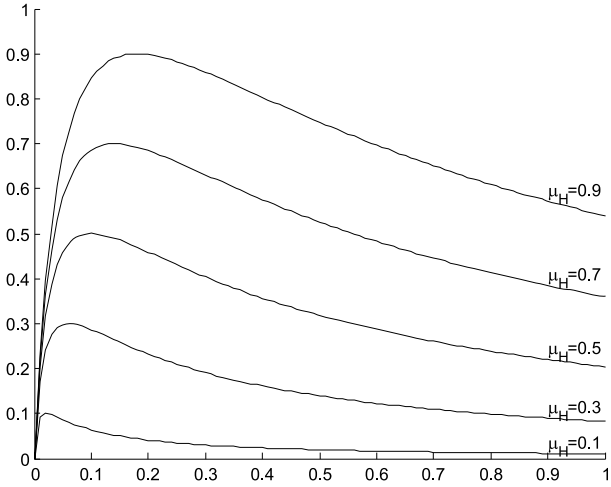

Figure A.4: Simplified tyre slip/friction curves $\mu(\lambda, \mu_H)$ by Daiss and Kiencke 1996.

First assuming the slope to be $k = 28$, and the slip at maximum friction to be given by $\lambda_0 = 0.2\mu_H$, where μ_H denotes the maximum friction coefficient at slip value λ_0. Further assuming the two parameters in (A.26) to be given as $a = 1/(\lambda_0^2)$ and $b = (k\lambda_0 - 2\mu_H)/(\lambda_0\mu_H)$, one obtains the following friction curve:

$$\mu(\lambda, \mu_H) = \frac{k\lambda}{\left(\frac{\lambda}{0.2\mu_H}\right)^2 + \frac{k0.2\mu_H - 2\mu_H}{0.2\mu_H}\lambda + 1}. \tag{A.27}$$

This simplified tyre friction curve is shown in Figure A.4.

Modelling Simulated Data with a Gaussian Process

A set of only 10 noisy (Gaussian noise, zero mean with standard deviation, $\sigma = 0.05$) observations of the simulated curve is used to train a GP model. Figure A.4 shows curves which have significantly nonuniform curvatures, showing a rapid change for small values of λ, with more gradual change later. Because of this, we use a nonstationary covariance function, as defined in (A.6). The parameters Θ were optimized for the given training data using a conjugate-gradient algorithm.

Figures A.5 and A.6 show the resulting GP model of the function value Ψ and the corresponding slope Γ. In addition to the noise property described above, also the *a priori* knowledge of the friction curve vanishing at the origin is included in the training data set.

The advantage of using a GP as a modelling tool is easily motivated by looking at Figure A.5. Even with no structural knowledge of the nonlinear function and with fairly small, sparsely populated training set, the GP model is close to the correct one. The GP model in Figure A.5 is based on a training set of 10 noisy data points, taken from a region where data typically are accessible. Note how the uncertainty increases in regions with no data, as would be expected.

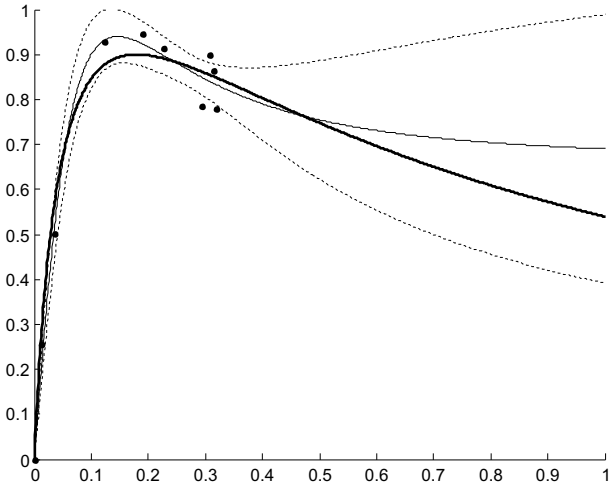

Figure A.5: GP model of friction coefficient. In addition to the set of accessible training data (sparsely populated dots), the model mean (thin line) and 2σ contours (dashed pair of lines) are shown. Also the real model curve (bold line) is shown for reference.

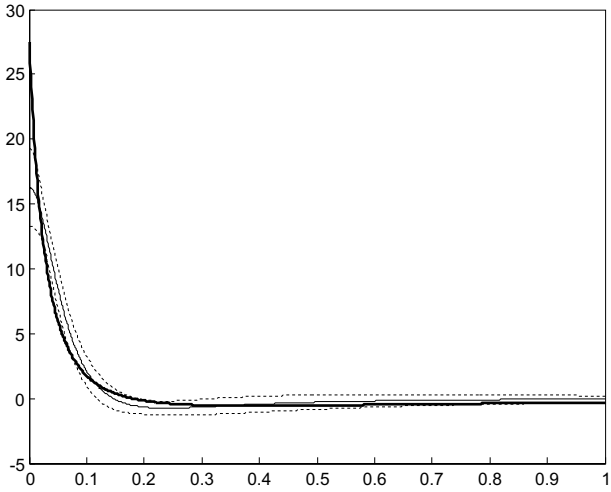

Figure A.6: Friction coefficient derivative $\frac{\partial \mu}{\partial \lambda}(\lambda)$. The model mean derivative (thin line) and 2σ contours (dashed pair of lines) are shown. Also the real model derivative curve (bold line) is shown for reference.

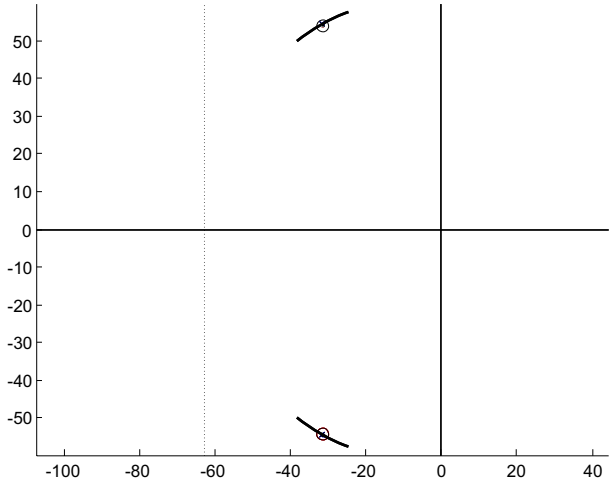

Figure A.7: Pole placement calculation. Mean placement of the poles are indicated with an x, the 95% confidence interval is indicated with the arc. The actual pole is indicated with the circle. The GP model is based on a training set of size 10. The dotted line is the line of ω_0.

Assume the controller is supposed to control a fixed slip $\lambda^* = 0.15$. At the point of linearization (selected to be equal to the slip set-point, i.e. $\lambda_w = \lambda^*$) the nominal slope is $\Gamma = 0.3882$ with $\mu_H = 0.9$. But instead knowledge of an expectation and variance exist at this point, from our GP model. $E(\Gamma) = -0.0787$ and $\sigma^2(\Gamma) = 0.1610$. Further assume the parameters of the quarter car are given by $r = 0.35$, $F_z = 250 \cdot 9.81$ and $J = 0.68$. Hence $\beta = 441.8$ and $\alpha = 0.51$. The time constant of the actuator dynamics is $T_a = 0.014$ s. The desired closed-loop property is given by $\omega_{0d} = 20\pi$ and $\zeta_d = 0.5$. Since the relative damping is assumed to be less than 1, the bandwidth may be selected to be equal to the desired one, i.e. $\omega_0 = \omega_{0d}$. Plugging the mean into (A.22) and (A.23), a set of controller parameters, scheduled with speed v, are inferred:

$$K_p = \zeta_d \omega_{0d} \frac{2v}{\alpha} - \frac{\beta}{\alpha} E(\Gamma) = 122.07v + 67.55 \tag{A.28}$$

$$T_i = \frac{K_p}{\omega_{0d}^2} \frac{\alpha}{v} = 0.0159 + 0.0088 \frac{1}{v} \tag{A.29}$$

also with this given set of controller parameters, a 95% boundary of where the poles may be located inside is given by an upper and lower bound. For a given speed $v = 30$ m/s, these bounds are $\zeta^+ = 0.5940$ and $\zeta^- = 0.4060$, obtain from (A.24) and (A.25).

Figure A.7 shows the pole placement of the controller parameter calculations with the 95% confidence interval, and the actual placement of the nominal poles. The are only 10 training points and we have set $v = 30$ m/s. The confidence interval is entirely inside the region of stability, hence stability is ensured with at least 95% of confidence.[2] Increasing the size of the

[2]On a cautionary note, however, where we state e.g. '95% confidence intervals', these are conditioned on the GP with

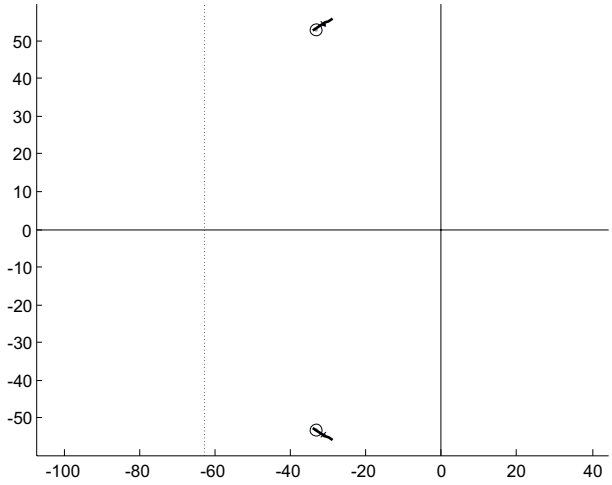

Figure A.8: Pole placement calculation. Mean placement of the poles are indicated with an x, the 95% confidence interval is indicated with the arc. The actual pole is indicated with the circle. The GP model is based on a training set of size 100. The dotted line is the line of ω_0.

training set, will tend to decrease the 95% confidence interval, Figure A.8 shows the situation with 100 training points.

Only one road condition is considered in the case study, i.e. μ_H fixed. An alternative approach would be to include other road conditions as well. By training the model using data from different road conditions, a less certain model will lead to a more robust but hence a more conservative controller. Alternatively, an adaptive control approach with online training of the GP model could be implemented. In this case, tradeoffs between computational capacity and model update rate must be considered. Also, precautions due to persistence of excitation must be made, e.g by turning off the estimator when information loss.

A.5 Conclusions

We have shown that a nonparametric GP model can be used to model nonlinear, simulated tyre slip/friction curves, to a high degree of accuracy considering the sparseness of the training data. The inference based on the GP model provides not only mean predictions, with uncertainty estimates for the curves themselves, but also mean and uncertainty estimates of local linearisations of these curves, which is useful for robust control. We illustrate this with a pole-placement task for a PID-controller.

covariance parameters being an appropriate model. For simplicity, the examples in this paper used Maximum likelihood optimisation to find appropriate parameters for GP covariance function parameters. GPs are very flexible models, but optimisation will tend to make the model overconfident in its predictions. Taking the Bayesian approach of integrating over hyperparameter distributions, possibly implemented using MCMC algorithms, would be more robust, especially for small data sets, see Rasmussen (1996).

A.6 Acknowledgements

This work was in part sponsored by the European Commission through the RTN project **MAC** (Multi Agent Control) HPRN-CT-1999-00107 , the STREP project **CEmACS** (Complex Embedded Automotive Control Systems), the Research Council of Norway and Science Foundation Ireland grant 00/PI.1/C067.

Appendix B

Alternative Anti-spin Controller in DP Operation

An alternative approach to the controller problem discussed in Chapter 4 is given in the paper Smogeli, Hansen, Sørensen & Johansen (2004), repeated here. In contrast to the core controller used in Chapter 4, being a shaft speed PI-controller, the core controller in this paper is a combined power/torque controller. The power/torque controller has some advantages in operation where high thrust is demanded, compared to the propeller shaft speed controller. However, it has some limitations if used in extreme sea conditions. In case of ventilation and in-and-out-of-water effects, the power/torque controller will lead to extreme propeller spin and motor racing. In contrast to the shaft speed controller, the power/torque controller will fail working if operating in extreme sea conditions without an anti-spin mechanism. This paper was the seed initiating my interest of anti-spin in marine propulsion systems, but here solved without using the Lyapunov-based controller state reset strategy.

B.1 Abstarct

An anti-spin controller for marine propulsion systems in rough seas is developed. From measurements of motor torque and propeller shaft speed, an observer providing an accurate estimate of the propeller load torque is used to calculate an estimate of the torque loss. A monitoring algorithm utilizing the estimated torque loss detects ventilation incidents, and activates the anti-spin control action. When a ventilation situation is detected, the anti-spin control action will reduce the propeller shaft speed to some optimal value, using a combined power/torque controller. The ultimate goal is to minimize the effect of ventilation, and hence increase the thrust production, limit the transients in the power system and reduce the mechanical wear-and-tear of the propulsion system components. Simulations are provided to validate the performance of the control scheme.

B.2 Introduction

Presently, DP systems have limitations in rough seas. The reasons for this are limitations in the thrust capability and the available power, and reduced performance of the control system due to thrust losses and unmodelled nonlinearities. The most severe thrust loss effects that may be experienced are due to ventilation, which in this work is used to describe air suction to a submerged propeller and in-and-out-of-water effects. Ventilation leads to an abrupt and large loss of propeller thrust and load torque, see Minsaas, Thon & Kauczynski (1987) for more details. This is challenging for the LTC, which is trying to fulfill the high-level control commands from the DP system. The effects of ventilation are loss of thrust, excessive wear-and-tear of mechanical components and undesired power transients. It is typically induced by large vessel motions and large waves encountered during harsh weather conditions, and is frequently experienced by e.g. tunnel thrusters and main propellers on offshore supply vessels and shuttle tankers.

In order to counteract the problem of ventilation, the concept of anti-spin thruster control was introduced in Smogeli, Aarseth, Overå, Sørensen & Minsaas (2003). Model tests and simulations of a marine thruster showed the feasibility of increasing thrust production, reducing wear-and-tear on the mechanical propulsion system and limiting transients in the power system during severe thrust loss incidents by means of controlling the thruster spin. The anti-spin concept was divided in three: *Detection*, *Switching* and *Control*. However, no explicit control scheme for a general operational setting was presented.

This paper provides an anti-spin control scheme that improves all three parts of the concept, utilizing recent results in thruster control. There are many similarities to car wheel anti-spin control, see e.g. Haskara, Özgüner & Winkelman (2000), which has served as motivation for the research presented here. The ventilation detection scheme, which triggers the anti-spin control action, is implemented by monitoring an estimate of the propeller torque loss. The estimated torque loss is based on a propeller load torque observer, reported in Smogeli, Sørensen & Fossen (2004). The torque loss estimate is a convenient variable for detecting the ventilation situations, as it gives explicit and instantaneous information on the thruster load condition. In this work the switching algorithm is by a large part bypassed, as the thruster controller presented here is valid for all load conditions. This simplifies the overall control scheme, and removes any concerns about ensuring bumpless transfer between the various controllers. The torque loss estimate is also used as a basis for the anti-spin control action.

This work is a continuation of the research on propulsion control, where contributions have been made by for example Fossen & Blanke (2000), Whitcomb & Yoerger (1999*b*) and the references therein. The LTC used in this work is a combined power/torque control scheme. Power and torque thruster control in marine propulsion systems were first introduced by Sørensen, Ådnanes, Fossen & Strand (1997), and recently refined to the combined power/torque control scheme by Smogeli, Sørensen & Fossen (2004).

B.3 Thruster Modelling

The thruster is modelled as an electric motor, a shaft with friction and a hydrodynamically loaded propeller. The rotational dynamics are described by the following equations:

$$\begin{aligned} \dot{Q}_m &= \frac{1}{T_m}(Q_c - Q_m), \\ J\dot{\omega} &= Q_m - Q_p - K_\omega \omega, \\ Q_p &= f_Q(\theta, \xi), \end{aligned} \tag{B.1}$$

where T_m is the motor time constant, Q_c is the commanded torque, Q_m is the motor torque, J is the rotational inertia of the propeller including added mass, shaft, gears and motor, K_ω is a linear friction coefficient, ω is the rotational speed of the propeller in rad/s, and Q_p is the propeller load torque. The load torque is modelled as a general function f_Q of fixed thruster parameters θ (i.e. propeller diameter, position, number of propeller blades, pitch ratio, propeller blade expanded-area ratio) and variables ξ (i.e. shaft speed, submergence). The actually produced propeller thrust T_p is modelled in a similar manner as:

$$T_p = f_T(\theta, \xi). \tag{B.2}$$

The nominal thrust T_n and torque Q_n are typically found from open-water tests with a deeply submerged thruster, expressed by the nominal thrust and torque coefficients K_{T0} and K_{Q0} or other equivalent mappings. In Carlton (1994), the following mapping is used:

$$\begin{aligned} T_n &= sgn(n) K_{T0} \rho D^4 n^2, \\ Q_n &= sgn(n) K_{Q0} \rho D^5 n^2. \end{aligned} \tag{B.3}$$

Here, n is the propeller shaft speed in rps, D is the propeller diameter, and ρ is the density of water. Thrust losses may be expressed by the thrust and torque reduction coefficients β_T and β_Q, which express the ratio of actual to nominal thrust and torque, see Minsaas et al. (1987):

$$\beta_T = \frac{T_p}{T_n} = \frac{f_T(\theta, \xi)}{T_n}, \;\; \beta_Q = \frac{Q_p}{Q_n} = \frac{f_Q(\theta, \xi)}{Q_n}. \tag{B.4}$$

In Smogeli et al. (2003) experiments with a ducted propeller in a cavitation tunnel were performed to investigate the effect of ventilation. Fig. B.1 shows the nondimensional load torque versus relative submergence h/R and relative shaft speed $n/n_{\max}$, where h is the propeller shaft submergence, R the propeller radius and $n_{\max}$ the maximum shaft speed of the propeller. Based on these results, a generic loss model capturing the main characteristics of ventilation may be formulated. Submergence larger than $h/R \approx 1.5$ should give the conventional quadratic thrust and torque curves as in (B.3). Decreasing submergence should lead to gradually decreasing thrust and torque for low propeller loading (loss of effective disc area), and a sharp loss of thrust and torque for high propeller loading (air suction). The loss factors β_T and β_Q are therefore formulated as functions of the relative submergence and the relative shaft speed, see Fig. B.4 later in the text.

From this, it is clear that a highly loaded thruster operating close to the surface may experience a sudden drop of thrust and torque as ventilation starts. Other loss effects that may be encountered are losses due to in-line and cross-flow velocity fluctuations, thruster-thruster interaction and the Coanda effect. However, for sudden and large load fluctuations giving mechanical wear-and-tear and large power fluctuations, ventilation is the most important loss effect.

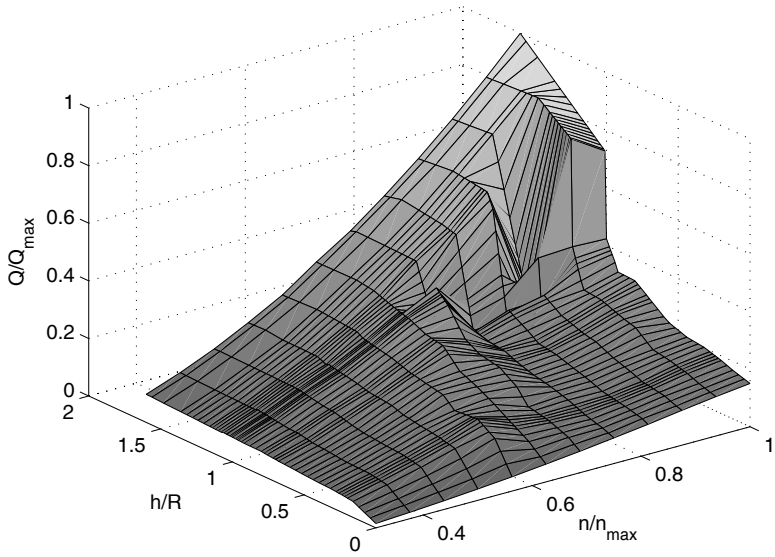

Figure B.1: Experimental results showing nondimensional propeller load torque as a function of relative submergence h/R and relative shaft speed $n/n_{\max}$.

B.4 Loss Estimation and Ventilation Detection

B.4.1 Propeller Load Torque Observer

An estimate of the propeller load torque is essential for torque loss estimation and ventilation detection. The propeller load torque observer using feedback from motor torque and shaft speed presented in Smogeli, Sørensen & Fossen (2004) is shortly summarized in the following. Based on (B.1), the propeller shaft control plant model is written as:

$$\begin{aligned} J\dot{\omega} &= Q_m - Q_p - K_\omega \omega, \\ \dot{Q}_p &= -\frac{1}{T_Q} Q_p + w_Q, \\ y &= \omega, \end{aligned} \tag{B.5}$$

where the propeller load torque Q_p has been modelled as a first order Markov process with time constant T_Q driven by white noise w_Q. With the motor torque Q_m as input u and the shaft speed ω as the measured output y, the observer equations for the estimated propeller load torque $\hat{Q}_p$ are written as:

$$\begin{aligned} \dot{\hat{\omega}} &= \frac{1}{J}(-\hat{Q}_p - K_\omega \hat{\omega} + u) + k_1(y - \hat{y}), \\ \dot{\hat{Q}}_p &= -\frac{1}{T_Q}\hat{Q}_p + k_2(y - \hat{y}), \\ \hat{y} &= \hat{\omega}. \end{aligned} \tag{B.6}$$

The equilibrium point of the observer error dynamics is GES if $w_Q = 0$ and the observer gains k_1 and k_2 are chosen according to Smogeli, Sørensen & Fossen (2004):

$$k_1 > -K_\omega/J, \;\; k_2 < (K_\omega + k_1 J)/T_Q. \tag{B.7}$$

If w_Q is a Gaussian white noise process, uniform ultimately boundedness (UUB) follows.

B.4.2 Torque Loss Calculation

An estimate of the torque loss factor β_Q may be calculated based on the estimated propeller load torque $\hat{Q}_p$ from (B.6). For DP operation the expected nominal load torque Q_{n0} is given from (B.3) by feedback from the propeller shaft speed n as:

$$Q_{n0} = sgn(n) K_{Q0} \rho D^5 n^2. \tag{B.8}$$

The estimated torque loss with respect to the nominal torque expected from the measured shaft speed is then:

$$\hat{\beta}_Q = \alpha_b(n) + (1 - \alpha_b(n)) \frac{\hat{Q}_p}{Q_{n0}}. \tag{B.9}$$

$\alpha_b(n)$ is a weighting function of the type:

$$\alpha(z) = e^{-k|pz|^r} \quad for \quad z \in \mathbb{R}, \tag{B.10}$$

where k, p and r are positive tuning gains. The weighting function is needed because the estimate otherwise would be singular for zero shaft speed, see Smogeli, Sørensen & Fossen (2004) for more details.

B.4.3 Ventilation Detection

The thrust loss detection is based on the torque loss estimate $\hat{\beta}_Q$. By defining limits for beginning and termination of the ventilation, $\beta_{v,on}$ and $\beta_{v,off}$, a detection signal may be generated by monitoring $\hat{\beta}_Q$. This approach is intuitive and robust, and may also be combined with the motor torque detection algorithm in Smogeli et al. (2003). The loss detection sets the detection flag ζ to high or low, i.e. $\zeta \in \{0, 1\}$. For a single ventilation incident ζ will have the following evolution, with $t_1 < t_2 < t_3$:

$$\begin{aligned} t_1: &\quad \hat{\beta}_Q \geq \beta_{v,on} \Rightarrow \quad \zeta = 0, \quad \text{(no ventilation)}, \\ t_2: &\quad \hat{\beta}_Q < \beta_{v,on} \Rightarrow \quad \zeta = 1, \quad \text{(ventilation)}, \\ t_3: &\quad \hat{\beta}_Q \geq \beta_{v,off} \Rightarrow \quad \zeta = 0, \quad \text{(no ventilation)}. \end{aligned}$$

See also Fig. B.2 later in the text.

B.5 Thruster Control

B.5.1 Conventional Thruster Control

The three thruster control schemes; *shaft speed* (B.11), *torque* (B.12) and *power control* (B.13), are shortly summarized:

$$n_d = sgn(T_d)\sqrt{\frac{|T_d|}{\rho D^4 K_{T0}}},$$

$$Q_{cn} = f(n - n_d), \tag{B.11}$$

$$Q_{cq} = Q_d = \frac{K_{Q0}}{K_{T0}} D T_d, \tag{B.12}$$

$$\begin{aligned} Q_{cp} &= \frac{P_d}{2\pi|n|} = \frac{Q_d 2\pi n_d}{2\pi|n|} \\ &= \frac{K_{Q0}}{\sqrt{\rho} D K_{T0}^{3/2}} \frac{sgn(T_d)|T_d|^{3/2}}{|n|}, \quad n \neq 0. \end{aligned} \tag{B.13}$$

For details, see Sørensen et al. (1997) and Smogeli, Sørensen & Fossen (2004). In shaft speed control, shaft speed feedback n from the thruster and the desired shaft speed n_d calculated from the desired thrust T_d is used to set the commanded motor torque Q_{cn} by for example a PID algorithm $f(n - n_d)$ (B.11). In torque control the commanded motor torque Q_{cq} is found by a direct mapping from the desired thrust T_d (B.12). In power control the desired power P_d is found from the desired torque (B.12) and the desired shaft speed (B.11), and the commanded motor torque Q_{cp} (B.13) is calculated from P_d using feedback from the shaft speed. The relationships (B.3) have been used to relate the desired thrust, torque, shaft speed and power to the nominal thrust and torque coefficients K_{Q0} and K_{T0}.

B.5.2 Combined Power/Torque Thruster Control

The combined power/torque controller presented in Smogeli, Sørensen & Fossen (2004) is formulated as:

$$Q_{cc} = \alpha_c(n)Q_{cq} + (1 - \alpha_c(n))Q_{cp}, \tag{B.14}$$

where Q_{cc} is the commanded motor torque, $\alpha_c(n)$ is a weight function of the type (B.10), and Q_{cq} and Q_{cp} are given by (B.12) and (B.13). The shape of $\alpha_c(n)$ defines the dominant regimes of the two control schemes, and can be used to tune the controller according to user specifications. The combined controller was shown to have smooth behavior with respect to n as long as $r > 1$ in the function $\alpha_c(n)$, and hence removes the singularity for zero shaft speed found in the power controller. The performance of the combined controller (B.14) was compared to the conventional shaft speed PID-controller (B.11) in Smogeli, Sørensen & Fossen (2004) by simulations of a ducted propulsor in the aft ship of a supply vessel in moderate seas. It was shown that the combined controller in absence of ventilation leads to less fluctuations in power and load torque, and also gives a more appropriate thrust production. The combined controller therefore is the preferred controller in normal conditions.

In extreme conditions however, ventilation incidents lead to severe deterioration of the performance of the combined controller, resulting in propeller spin and motor racing. This can be compared to loss of friction for a car wheel, resulting in wheel spin unless the motor torque is rapidly decreased. Propeller spin is an inherent problem also for the torque controller (B.12) and power controller (B.13), and motivates the introduction of anti-spin thruster control.

B.6 Anti-spin Control

The anti-spin control action is triggered by the ventilation detection algorithm. The basic concept is to lower the shaft speed once a ventilation situation is detected, i.e. $\zeta : 0 \rightarrow 1$, and increase the shaft speed to normal when the loss situation is considered over, i.e. $\zeta : 1 \rightarrow 0$. The primary anti-spin control action is to modify the controller torque output with a modification factor γ, giving the following anti-spin controller:

$$Q_{cas} = \gamma Q_{cc} = \gamma(\alpha_c(n)Q_{cq} + (1 - \alpha_c(n))Q_{cp}), \tag{B.15}$$

where Q_{cas} is the anti-spin commanded torque. The modification factor would naturally be chosen in the interval $\gamma \in [0, 1]$.

At a steady-state ventilation condition, the propeller load torque Q_p, motor torque Q_m, and commanded torque Q_{cas} are equal. Using $\gamma = \hat{\beta}_{Q,}$ and assuming that the shaft speed $n \neq 0$ and $|n|$ large enough to yield $\alpha_b(n) \approx 0$ such that $\hat{\beta}_Q \approx \hat{Q}_p/Q_{n0}$ and $Q_{n0} \neq 0$, the following relationship is established from (B.9) and (B.15):

$$Q_p = Q_m = Q_{cas} = \gamma Q_{cc} = \frac{\hat{Q}_p}{Q_{n0}} Q_{cc} = \frac{\hat{Q}_p}{sgn(n)K_{Q0}\rho D^5 n^2} Q_{cc}. \tag{B.16}$$

If it is further assumed that the estimated propeller torque is identically equal to the actual propeller torque, $\hat{Q}_p = Q_p$, and that the sign of n and Q_{cc} are equal, then the shaft speed n will be

given as:

$$n = sgn(Q_{cc})\sqrt{\frac{|Q_{cc}|}{K_{Q0}\rho D^5}}. \tag{B.17}$$

In order to investigate the resulting shaft speed, a pure torque and pure power controller are substituted for the combined controller in (B.17). If assuming that n is small enough to give $\alpha_c(n) \approx 1$ such that $Q_{cc} \approx Q_{cq}$, the combined controller becomes a torque controller. The shaft speed in (B.17) is then from (B.12) given as:

$$n = sgn(Q_{cq})\sqrt{\frac{|Q_{cq}|}{K_{Q0}\rho D^5}} = sgn(T_d)\sqrt{\frac{\frac{K_{Q0}}{K_{T0}} D\,|T_d|}{K_{Q0}\rho D^5}} = sgn(T_d)\sqrt{\frac{|T_d|}{\rho D^4 K_{T0}}}. \tag{B.18}$$

This is exactly the same as the desired shaft speed n_d given by the shaft speed feedback controller (B.11). If instead assuming that n is large enough to give $\alpha_c(n) \approx 0$ such that $Q_{cc} \approx Q_{cp}$, the combined controller becomes a power controller. The shaft speed in (B.17) is then from (B.13) given as:

$$sgn(n)n^2 = \frac{sgn(Q_{cp})\,|Q_{cp}|}{K_{Q0}\rho D^5} = \frac{1}{K_{Q0}\rho D^5} sgn(T_d) \frac{K_{Q0}}{\sqrt{\rho} D K_{T0}^{3/2}} \frac{|T_d|^{3/2}}{|n|}, \tag{B.19}$$

$$\Downarrow$$

$$n = \frac{sgn(T_d)|T_d|^{1/2}}{\rho^{1/2} D^2 K_{T0}^{1/2}} = sgn(T_d)\sqrt{\frac{|T_d|}{\rho D^4 K_{T0}}}. \tag{B.20}$$

This is again the desired shaft speed given by (B.11). It is therefore assumed that the combined controller (B.14) as used in (B.15) will give the same result, as it is a linear combination of the torque and power controllers. If requiring $Q_{cq} = Q_{cp}$ from (B.12) and (B.13), the resulting condition is (B.11), substantiating the assumption. Simulations further confirm this. Using $\gamma = \hat{\beta}_Q$ in (B.15) therefore leads to the same steady-state shaft speed as the shaft speed controller in (B.11). The following modification factor is proposed as primary anti-spin control action:

$$\gamma = \begin{cases} 1 & for \quad \zeta = 0, \\ \hat{\beta}_Q & for \quad \zeta = 1. \end{cases} \tag{B.21}$$

The transition between 1 and $\hat{\beta}_Q$ at ventilation detection and termination is done by requiring a rate limit κ, i.e. $|\partial\gamma/\partial t| < \kappa$, where κ typically would be of magnitude 1. When the detection flag changes from 1 to 0, and the commanded torque again is used directly as motor input, the power control part of the combined controller will assure that no significant power transients occur. In this paper the transient performance of the controller will be validated by simulations.

An additional reduction in shaft speed will be desired during a ventilation incident, calling for a secondary anti-spin control action. This may be done by modifying the thrust reference during ventilation, since the primary anti-spin control action assures that the shaft speed corresponding to (B.11) is kept. The desired shaft speed during ventilation n_{as} will be a thruster specific parameter which ideally should give the maximum achievable thrust during ventilation. This corresponds to $n/n_{\max} \approx 0.55$ in Fig. B.1 and $n/n_{\max} \approx 0.4$ in Fig. B.4, where the two propellers are

different. For thrust optimal control, it is a reasonable assumption that n_{as} may be modelled as a slowly-varying parameter and adapted according to an optimization criterion based on the estimated torque loss. Other optimization criteria may include the power peaks and the torque oscillations. This is subject to further research. The shaft speed n_d corresponding to the nominal thrust reference T_d should not be changed to n_{as} instantaneously, as this will lead to undesired transients. It is therefore proposed to add a low-pass filter and rate limiting algorithm to the change from n_d to n_{as} at ventilation detection and from n_{as} to n_d at ventilation termination. The output desired shaft speed from this algorithm is termed n_{das}. The modified thrust reference T_{das}, which constitutes the secondary anti-spin control action, is given as:

$$T_{das} = \begin{cases} T_d & for \quad \zeta = 0, \\ T_n(n_{das}) & for \quad \zeta = 1, \end{cases} \tag{B.22}$$

where $T_n(n_{das})$ is given by (B.3). The motivation for using the primary anti-spin action in (B.15) instead of a conventional shaft speed controller to assure that the secondary anti-spin action in (B.22) is fulfilled, i.e. $n \rightarrow n_{as}$ during ventilation, is twofold. Firstly, there is no need to switch between the combined controller and shaft speed controller when ventilation is detected, reducing the problem of ensuring bumpless transfer between the various controllers. Secondly, the combined controller gives smoother control action with rapidly changing inputs, reducing wear-and-tear and limiting power transients.

A simplified illustration of a ventilation incident with detection and anti-spin control action is sketched in Fig. B.2. The figure shows how the torque modification γ and the anti-spin shaft speed n_{das} evolves with the ventilation incident, including detection and transition. Fig. B.3 shows a block diagram of the resulting controller, where also a torque limiting function has been included to avoid commanding excessive motor power or torque, see Sørensen et al. (1997).

B.7 Simulation Results

Simulations of a heavily ventilating propeller were performed to validate the performance of the anti-spin controller given by (B.15) and (B.22). The simulated thruster was a ducted propeller of diameter $D = 4m$ installed in the aft ship of a typical supply vessel with main particulars $[L, B, T] = [80, 18, 5.6]m$ conducting DP operations in a sea state with significant wave height $H_s = 5m$. The thrust reference was $500kN$. Fig. B.4 shows the modelled ventilation loss β_Q as a function of relative submergence h/R and relative shaft speed $n/n_{\max}$, with the trace of a ventilating thruster with the anti-spin controller activated drawn as stars. The shaft speed of the propeller starts at $n/n_{\max} \approx 0.5$, and the ventilation incident starts when h/R is reduced such that it falls over the edge for $h/R \approx 1.2$. The loss of load torque leads to an increase in shaft speed until the ventilation is detected and the shaft speed is lowered to $n/n_{\max} \approx 0.35$. When ventilation is terminated, the shaft speed is increased to its original value.

Fig. B.5 shows the propeller shaft speed, propeller thrust, propeller torque, motor torque and motor power for three different controllers:

- The combined power/torque controller with no anti-spin control action from (B.14) (thin line),
- The PID shaft speed controller from (B.11) (dotted line),

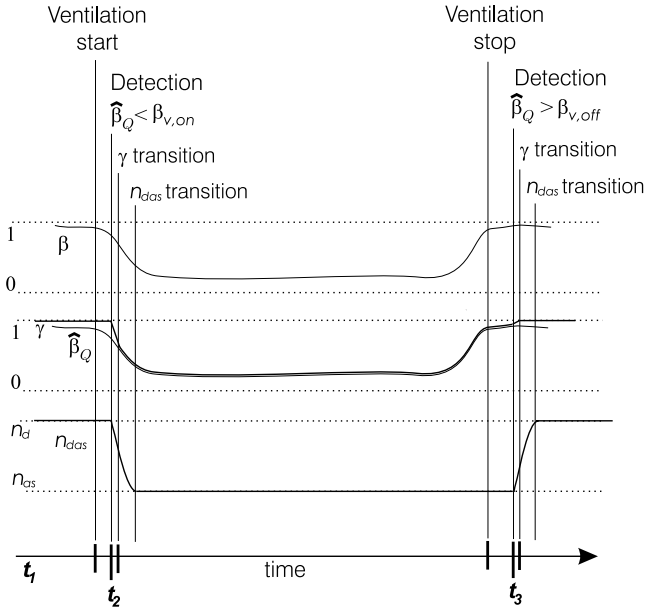

Figure B.2: Ventilation incident with detection and anti-spin control action.

- The anti-spin controller with primary and secondary anti-spin control action from (B.15) and (B.22) (thick line).

The simulations illustrate the good properties of the proposed anti-spin controller. During ventilation the shaft speed PID-controller has trouble with oscillations and engine racing, and the combined power/torque controller alone leads to severe engine racing. The anti-spin controller gives a less fluctuating and more responsive shaft speed than the PID-controller, and reduces the shaft speed additionally during the ventilation situation. The result is more thrust, reduced wear-and-tear due to less peaks in the propeller load torque and motor torque, and less peaks in the motor power as the propeller re-enters the water. Fig. B.6 shows details from the anti-spin controller for the same time series; actual torque loss β_Q, estimated torque loss $\hat{\beta}_Q$, torque modification γ, ventilation detection flag ζ and relative thrust reference T_{das}/T_d. The ventilation detection limits were set to $\beta_{v,on} = 0.6$ and $\beta_{v,off} = 0.9$.

The anti-spin controller has been tested in simulations of varying environmental conditions, varying thrust references and varying levels of measurement noise, and showed good performance in all situations.

B.8 Conclusion

A thrust optimal anti-spin controller for marine propulsion systems in extreme conditions has been developed and tested by simulations based on experimental results. The controller utilized

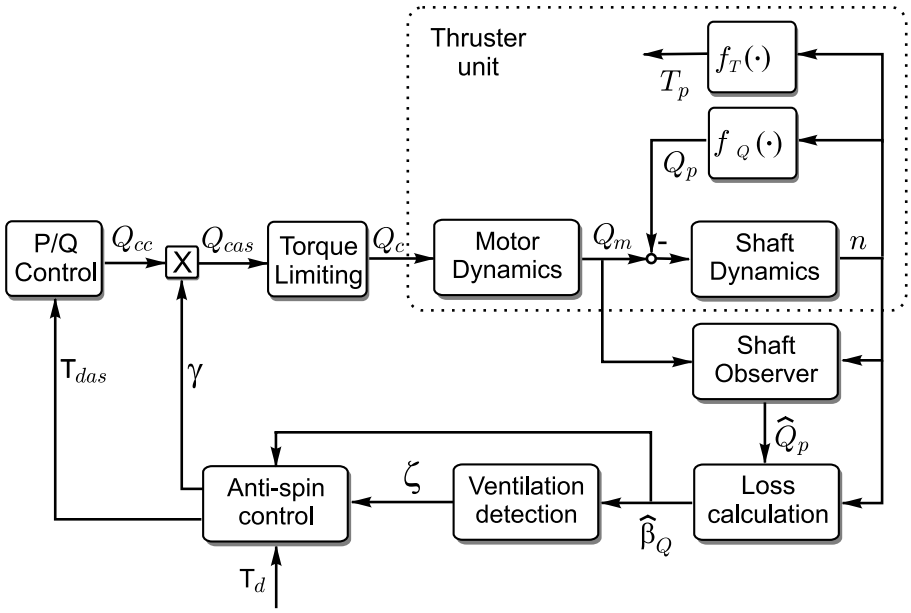

Figure B.3: The anti-spin control scheme, including combined power/torque controller, shaft observer, loss calculation, ventilation detection and anti-spin control.

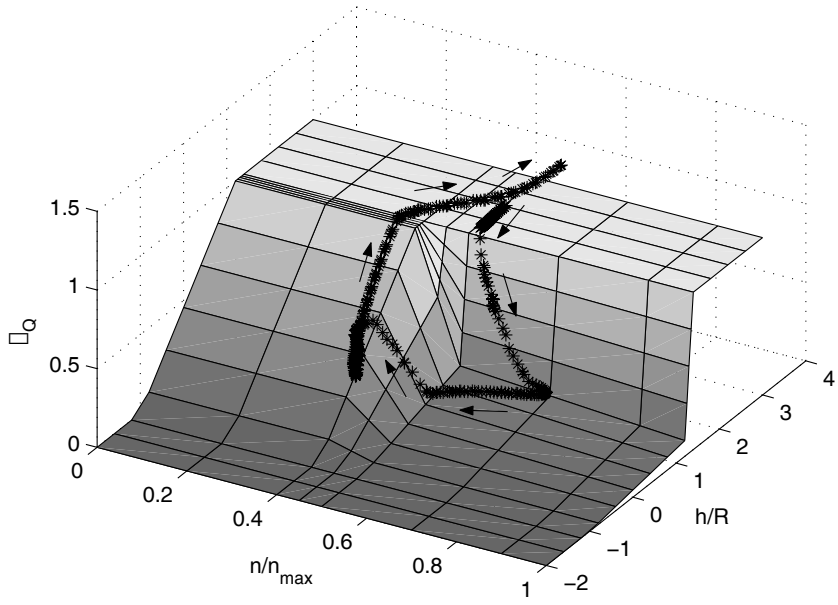

Figure B.4: Ventilation loss model with the trace of a ventilating propeller with anti-spin controller drawn as stars.

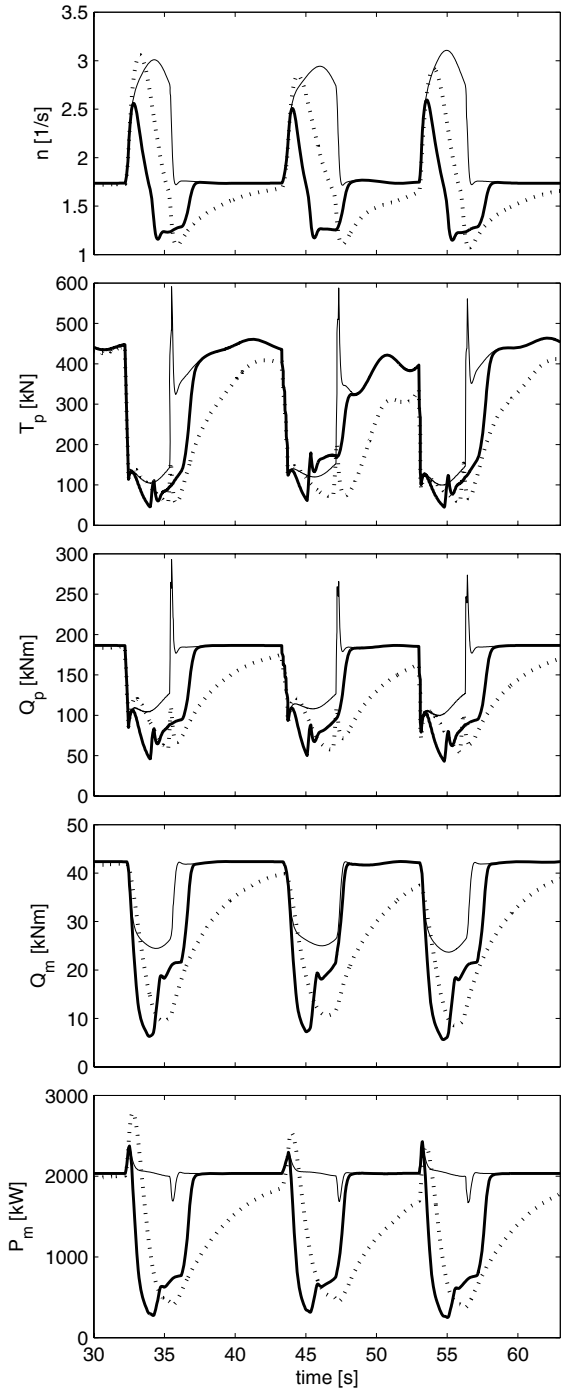

Figure B.5: Propeller shaft speed n, thrust T_p, load torque Q_p, motor torque Q_m and motor power P_m for the combined power/torque controller (thin line), the shaft speed PID-controller (dotted line) and the anti-spin controller (thick line) during three ventilation incidents.

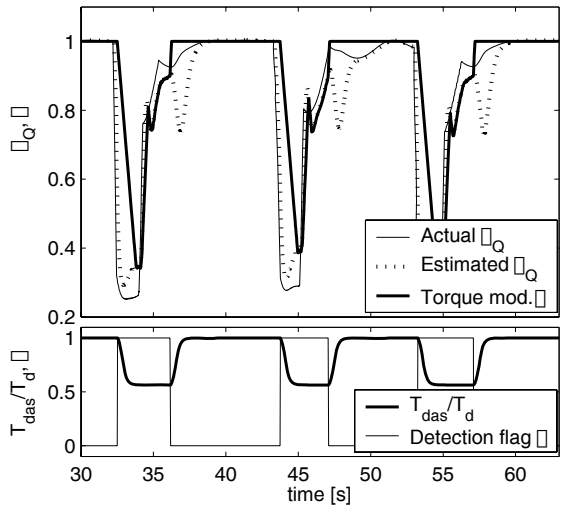

Figure B.6: Actual loss factor β_Q, estimated loss factor $\hat{\beta}_Q$, torque modification γ, loss detection flag ζ and relative thrust modification T_{das}/T_d for the anti-spin controller during three ventilation incidents.

an estimate of the torque loss to detect ventilation incidents, which triggered an anti-spin control action. The primary anti-spin control action was to modify the output torque from the combined power/torque controller in order to take control of the propeller shaft speed. The secondary anti-spin control action was to reduce the thrust reference in order to lower the shaft speed to some optimal value. Simulations showed that the anti-spin controller gave improved thrust production, limited transients in the power system and reduced mechanical wear-and-tear when compared to conventional thruster control schemes during ventilation. It has earlier been shown that the combined controller had better performance than the shaft speed controller in moderate seas. The combined controller with anti-spin control action has thereby been shown to be preferable for all operating conditions.

B.9 Acknowledgment

This work has been carried out at the *Centre for Ships and Ocean Structures* (CESOS) at NTNU in cooperation with the research project on *Energy-Efficient All-Electric Ship* (EEAES). The Norwegian Research Council is acknowledged as the main sponsor of CESOS and EEAES.

Appendix C

Alternative Anti-spin Controller in Transit Operation

This chapter presents the paper Pivano, Bakkeheim, Johansen & Smogeli (2008). The paper describes an alternative anti-spin strategy to the four-quadrant case in Chapter 5. The approaches are similar in way of modelling thruster dynamics and the way of handel nonzero advance speed by using a dynamic reference generator. The thruster model is divided into two separate parts; nominal dynamics and torque loss estimator. They are however distinct in handling the estimated torque loss. In Chapter 5 the thrust loss is used in a PI-controller with a Lyapunov-based resetting mechanism, while in this paper the torque loss is used as a feed forward term to a shaft speed PI-controller.

C.1 Abstract

In this paper a nonlinear thrust controller for a fixed pitch marine propeller with torque loss estimation and an anti-spin strategy is presented. The controller, designed to work in the four-quadrant plane composed by the shaft speed and the vessel speed, is a combination of a thrust controller designed for calm sea conditions and an anti-spin strategy to reduce power peaks and wear-and-tear in extreme sea conditions. The anti-spin algorithm lowers the shaft speed once high torque losses due to ventilation are detected and increases the shaft speed to normal when the loss situation is considered over. The ventilation incident is detected by monitoring the torque losses, estimated with a nonlinear observer. The performances of the proposed controller are validated by experiments carried out in a towing tank.

C.2 Introduction

In the last years there has been a growing number of works in the design of vessel control systems focusing on the low level thrusters controller, see Whitcomb & Yoerger (1999*a*), Fossen & Blanke (2000), Smogeli, Hansen, Sørensen & Johansen (2004), Guibert, Foulon, Aït-Ahmed &

Loron (2005), Smogeli (2006) and Pivano et al. (2007). The main difficulties to design effective propeller controllers lie in the modeling of the propeller's dynamics and in the problem of measuring the environmental state. A marine propeller is often affected by thrust losses due to in-line velocity variations, ventilation, in-and-out-of-water effects, wave-induced water velocities, interaction between the vessel hull and the propeller and interaction between propellers. The primary objective of the low level thruster controller is to obtain the desired thrust from the propeller regardless the environmental state. The knowledge of the propeller thrust and torque, together with the thrust induced pressure force on the hull, is fundamental to achieve high vessel control performance. Unfortunately a propeller system is not usually equipped with thrust and torque sensors therefore thrust losses are not directly measured.

As reported in Smogeli, Ruth & Sørensen (2005), today's industrial standard for FPPs is shaft speed control where the desired shaft speed is computed from the desired thrust through a static mapping. Also torque and power control and combination of those have been developed and implemented (see for example Blanke & Nielsen (1990) and Smogeli et al. (2005)). All the mentioned controllers do not use information about the propeller working condition, i.e. the controller performance may be poor when thrust losses occur.

In this paper a nonlinear thrust controller for FPPs that includes the estimation of the propeller working condition is derived. The proposed algorithm is effective both in calm seas and in extreme sea conditions. The controller is a combination of a thrust controller for calm seas and an anti-spin strategy to reduce the power peaks and wear-and-tear in extreme sea conditions.

The thrust controller for calm seas consists of a propeller shaft speed controller where the speed reference is computed from the requested thrust to the propeller by the high-level controller (e.g. a vessel speed controller) and the torque losses, estimated with a nonlinear observer. The controller is an enhancement of the one presented in Pivano et al. (2007) where the mapping to compute the desired shaft speed from the thrust reference and the torque losses has been improved. This is done in order to reduce the high control activity experienced in Pivano et al. (2007) for values of the shaft speed and the vessel speed in the 2^{nd} and 4^{th} quadrants. Moreover, in harsh sea state, high thrust losses are experienced and the controller designed in Pivano et al. (2007) increases the desired shaft speed to large values in order to counteract the losses due to ventilation. For this reason an anti-spin strategy has been implemented, reducing the shaft speed once high thrust losses due to ventilation are detected. When the ventilation is considered over, the desired shaft speed is set to normal values. The anti-spin algorithm for marine propellers was first introduced in Smogeli et al. (2003) and further developed in Smogeli, Hansen, Sørensen & Johansen (2004) and Smogeli (2006). The cited anti-spin controllers were designed for DP operations where the vessel speed is small and for positive values of the shaft and vessel speed. In the present work the controller is designed for the full four-quadrant range of the propeller shaft speed and the vessel speed and also for maneuvering and transit operations where the vessel speed is larger than in DP operations.

The effectiveness of the controller has been validated by experimental tests carried out in a towing tank where the proposed scheme has been tested in simulated calm and harsh sea state.

C.3 Propeller Model

Fig. C.1 shows the propeller system composed of an electric motor attached to a shaft and to a propeller through a gear-box.

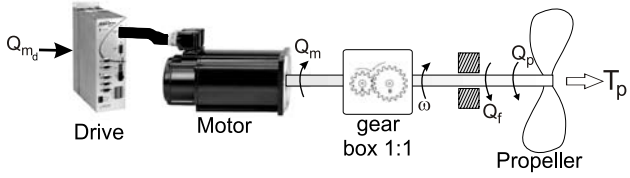

Figure C.1: Propeller system scheme.

The shaft rotates at the angular speed ω. Its dynamics can be written as

$$J_m\dot{\omega} = Q_m - Q_p - Q_f(\omega), \tag{C.1}$$

where J_m is shaft moment of inertia, $Q_f(\omega)$ is the shaft friction torque which depends on the shaft speed, Q_m is the motor torque which is controlled by the motor drive based on the reference Q_{m_d} and Q_p is the propeller load torque. The friction torque is modeled as a Coulomb plus a linear and nonlinear viscous effect. This model, motivated by experiments presented in Pivano, Smogeli, Johansen & Fossen (2006), is written as

$$Q_f(\omega) = k_{f_1}\frac{2}{\pi}\arctan\left(\frac{\omega}{\epsilon}\right) + k_{f_2}\omega + k_{f_3}\arctan(k_{f_4}\omega), \tag{C.2}$$

where the coefficients k_{f_i} and ϵ are constant and positive. In order to avoid the singularity in zero, the Coulomb effect, usually written as a $\mathrm{sign}(\omega)$, has been replaced by the function $\frac{2}{\pi}\arctan(\frac{\omega}{\epsilon})$ with a small positive ϵ. The friction coefficients can be determined measuring the motor torque in steady-state conditions during test with the propeller in air. In this case the propeller torque is zero and the friction torque corresponds to the motor torque. The propeller load torque Q_p is represented by the torque produced at zero advance speed, that is the propeller is deeply submerged and not subjected to losses, plus a term Δ_q that incorporates losses of torque:

$$Q_p = \begin{cases} G_{Q_p}\,|\omega|\,\omega + \Delta_q & \omega \geq 0 \\ G_{Q_n}\,|\omega|\,\omega + \Delta_q & \omega < 0. \end{cases} \tag{C.3}$$

The terms $G_{Q_p}$and G_{Q_n} are positive constants and of different magnitudes due to the propeller asymmetry with respect to the shaft speed ω. Neglecting the dynamics of the electrical part of the system (frequency converter, stator and rotor), usually faster than the shaft dynamics, the control input is represented by $Q_m = Q_{m_d}$. Both Q_m and ω are measured. The term Δ_q is represented by a Markov like process with time constant τ driven by a bounded noise signal w :

$$\dot{\Delta}_q = -\frac{1}{\tau}\Delta_q + w. \tag{C.4}$$

The noise w represents the contribution of all the phenomena that can generate torque losses. Grouping the nonlinearities in the function $\psi(\omega)$, the system can be rewritten as:

$$J_m\dot{\omega} = Q_m - \psi(\omega) - k_{f_2}\omega - \Delta_q \tag{C.5}$$

where Δ_q is given by (C.4),

$$\psi(\omega) = G_{Q_{p,n}}\,|\omega|\,\omega + k_{f_1}\frac{2}{\pi}\arctan\left(\frac{\omega}{\epsilon}\right) + k_{f_3}\arctan(k_{f_4}\omega), \tag{C.6}$$

and

$$G_{Q_{p,n}} = \begin{cases} G_{Q_p}, & \omega \geq 0 \\ G_{Q_n}, & \omega < 0. \end{cases} \tag{C.7}$$

A block diagram of the overall control system is shown in Fig. C.2.

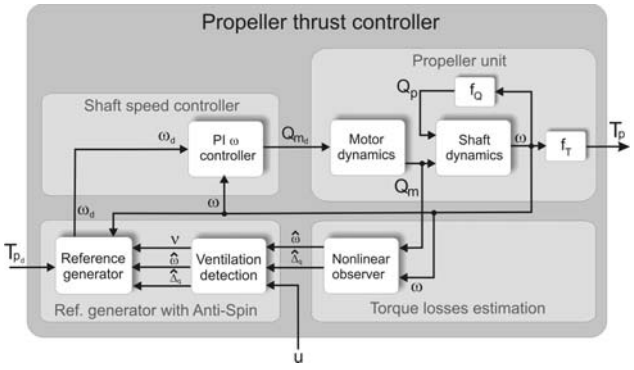

Figure C.2: Block diagram of the overall system.

C.4 Observer for Torque Loss Estimation

A nonlinear observer with gain l_1 and l_2 is designed to estimate the torque loss $\hat{\Delta}_q$ and the shaft speed $\hat{\omega} = \hat{y}$:

$$J_m\dot{\hat{\omega}} = Q_m - \psi(\hat{\omega}) - k_{f_2}\hat{\omega} - \hat{\Delta}_q + l_1(y - \hat{y}) \tag{C.8}$$

$$\dot{\hat{\Delta}}_q = -\frac{1}{\tau}\hat{\Delta}_q + l_2(y - \hat{y}) \tag{C.9}$$

$$y = \omega. \tag{C.10}$$

Defining the observer error variables as $\tilde{\omega} = \omega - \hat{\omega}$ and $\tilde{\Delta}_q = \Delta_q - \hat{\Delta}_q$, from the model in (C.4), (C.5), (C.6) and (C.7) and the observer in (C.8), (C.9) and (C.10), the observer error

dynamics becomes:

$$J_m\dot{\tilde{\omega}} = -\left(\psi(\omega) - \psi(\hat{\omega})\right) - l_1\tilde{\omega} - k_{f_2}\tilde{\omega} - \tilde{\Delta}_q \tag{C.11}$$

$$\dot{\tilde{\Delta}}_q = -\frac{1}{\tau}\tilde{\Delta}_q - l_2\tilde{\omega} + w. \tag{C.12}$$

Proposition C.1 *If there exist* a_{11}, $a_{22}>0$ *and the gains* l_1 *and* l_2 *are chosen such that*

A1 $l_1 > -k_{f_2}$,

A2 $\left|\frac{a_{11}}{J_m} + a_{22}l_2\right| < 2\sqrt{a_{11}a_{22}\left(\frac{k_{f_2}+l_1}{\tau J_m}\right)}$,

then the error dynamics (C.11) and (C.12) is GES when $w = 0\ \forall t$, and input-to-state stable (ISS) with respect to w.

Proof. See Pivano et al. (2007). ■

The estimates $\hat{\omega}$ and $\hat{\Delta}_q$ can be used to compute an estimate of the propeller torque from

$$\hat{Q}_p = G_{Q_{p,n}}\left|\hat{\omega}\right|\hat{\omega} + \hat{\Delta}_q. \tag{C.13}$$

C.5 Thrust Controller

C.5.1 Controller for Calm Sea

We design a shaft speed controller which is derived as follows: first a desired torque Q_{p_d} is computed from the desired thrust T_{p_d} using the standard propeller characteristics; second a desired shaft speed is computed from Q_{p_d} and the estimated losses $\hat{\Delta}_q$.

The standard propeller characteristics is measured in steady-state conditions and is usually presented in the form of the non-dimensional thrust and torque coefficients K_T and K_Q, identified by towing the propeller at different velocities. The coefficients are plotted as a function of the advance number J, given from:

$$J = \frac{2\pi u_a}{\omega D}, \tag{C.14}$$

where D is the propeller disc diameter and u_a is the advance speed, i.e. the speed of the inlet water to the propeller disc. The thrust and torque coefficients are computed from Van Lammeren, Manen & Oosterveld (1969) as:

$$K_T = \frac{4\pi^2 T_p}{\rho\left|\omega\right|\omega D^4}, \tag{C.15}$$

$$K_Q = \frac{4\pi^2 Q_p}{\rho\left|\omega\right|\omega D^5}. \tag{C.16}$$

Using the relations (C.15) and (C.16) in combination with the desired propeller thrust, the desired propeller torque Q_{p_d} is computed as:

$$Q_{p_d} = \frac{1}{G_{QT}(\hat{J})}T_{p_d}, \tag{C.17}$$

where

$$G_{QT}(\hat{J}) = \frac{T_p}{Q_p} = \frac{K_T|_{\hat{J}}}{DK_Q|_{\hat{J}}}. \tag{C.18}$$

To compute $G_{QT}(\hat{J})$, the value of $\hat{J}$, an estimate of the advance number, is derived employing the estimated propeller torque. Using $\hat{Q}_p$ instead of Q_p in (C.16) we compute the estimate $\hat{K}_Q$. Combining the value of $\hat{K}_Q$ with the K_Q curve, see Fig. C.3 (a), we can derive the value of $\hat{J}$. As shown in Fig. C.3 (a), the K_Q curve is not invertible in the all plotted range. The problem of not being able to invert the K_Q curve is solved by approximating the value of $G_{QT}(J)$ by $G_{QT}(0)$ in zone 1.

When the propeller works at negative values of J (2^{nd} and 4^{th} quadrants), the advance speed u_a and the shaft speed ω have opposite signs. The propeller tries to reverse the inlet flow and a recirculation zone, often called a ring vortex, occurs, see Vysohlid & Mahesh (2004). This is due to the interaction between the inlet flow and the reversed flow. The flow then becomes unsteady and can cause quick variations of the propeller load, see Pivano et al. (2006), and consequently oscillations of the value K_Q and $\hat{K}_Q$. In this situation, even a constant value of the desired thrust could result in quick variation on the reference signal Q_{p_d}. This, in turns, may produce the shaft speed reference with high frequency content, resulting in thrust oscillations as experienced in Pivano et al. (2007). That may cause wear-and-tear of the mechanical parts of the system. This is avoided by approximating $G_{QT}(J)$ by a constant in zone 1.

The advance number J is limited in the range $[-1.5, 1.1]$ for positive ω and $[-1.5, 1.0]$ for negative ω, the usual working range for the tested propeller.

Fig. C.3 (b) shows the ratio between the propeller thrust and torque $G_{QT}(J)$ computed from the propeller characteristics and its approximation $G_{QT}(\hat{J})$. The plot refers to positive shaft speed ω; the plot for negative speed is similar but the K_Q and $G_{QT}(J)$ curves present smaller magnitude due to the propeller asymmetry.

In order to track the desired propeller torque Q_{p_d}, a shaft speed controller is designed. Given the desired propeller torque Q_{p_d}, the desired shaft speed $\bar{\omega}_d$ is computed by inverting (C.3) and using the estimated torque loss $\hat{\Delta}_q$:

$$\bar{\omega}_d = \sqrt{\frac{\left|Q_{p_d} - \hat{\Delta}_q\right|}{G_{Q_{p,n}}}}\,\text{sign}(Q_{p_d} - \hat{\Delta}_q). \tag{C.19}$$

We design a controller to track the desired shaft speed $\bar{\omega}_d$. To generate a smooth reference signal ω_d and $\dot{\omega}_d$, we employ a second order low pass filter with cutoff frequency equal to ω_c and relative damping factor ξ:

$$\ddot{\omega}_d + 2\omega_c\xi\dot{\omega}_d + \omega_c^2\omega_d = \omega_c^2\bar{\omega}_d. \tag{C.20}$$

The filter is also needed because the time derivative of $\bar{\omega}_d$, used in the feed-forward term of the controller, is infinity when $Q_{p_d} - \hat{\Delta}_q = 0$.

We employ the following control law that includes a feed-forward part, a proportional action and an integral action to ensure convergence in presence of constant disturbances:

$$\begin{aligned} Q_m = \quad & J_m\dot{\omega}_d + \hat{\Delta}_q + \psi(-\gamma e_1 + \omega_d) + k_{f_2}\omega_d \\ & - (k_I + \gamma k_P)\, e_1 - k_P e_2. \end{aligned} \tag{C.21}$$

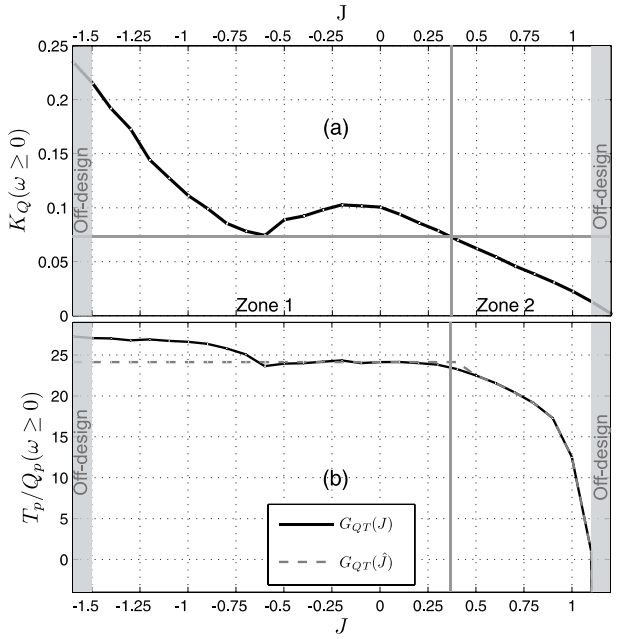

Figure C.3: K_Q characteristic for $\omega \geq 0$ and the ratio between thrust and torque for $\omega \geq 0$.

Defining the control error $e_1 = \int_0^t (\omega(\tau) - \omega_d(\tau))d\tau$ and $e_2 = \omega - \omega_d$, the control error dynamics becomes:

$$\begin{aligned} \dot{e}_1 &= e_2 \\ \dot{e}_2 &= -\tfrac{k_{f_2}}{J_m} e_2 - \tfrac{1}{J_m}\left[\psi(\omega) - \psi(-\gamma e_1 + \omega_d)\right] - \tfrac{k_P}{J_m} e_2 \\ &\quad -\tfrac{1}{J_m}\left(k_I + \gamma k_P\right) e_1 - \tfrac{1}{J_m}\tilde{\Delta}_q. \end{aligned} \tag{C.22}$$

Proposition C.2 *If the gains γ, k_I and k_P are chosen such that*

B1 $\gamma > 0$,
B2 $k_P > 0$, $k_P > \gamma J_m - k_{f_2}$,
B3 $k_I > 0$, $k_I > -J_m\gamma^2 + \gamma k_{f_2}$,
then the origin of the overall error dynamics (observer + controller) is ISS with respect to w.

Proof. See Pivano et al. (2007). ■

Furthermore, as proved in Pivano et al. (2007), the bound of the control error decreases by increasing the control gains. The resulting propeller thrust is bounded and converges to a ball around the desired thrust.

C.5.2 Anti-Spin Strategy

When the propeller is deeply submerged, losses of thrust are mainly caused by variations of advance speed, interaction between the propeller and the vessel hull or between propellers and cross flows. The losses sensed through the torque loss observer are compensated by the controller by changing the shaft speed to fulfill the required thrust. When the propeller spins close to the water surface the shaft load decreases due to ventilation and a drop of thrust and torque occurs, as documented by experimental test in Pivano et al. (2006) and Bakkeheim et al. (2006). When the ventilation incident occurs high thrust losses are experienced and the calm sea controller, in order to compensate them, increases the value of desired shaft speed to large values. In Smogeli et al. (2003) it has also been experimentally demonstrated that during ventilation a reduction of the shaft speed may increase the propeller thrust. These considerations motivate the use of an anti-spin strategy that also reduces the power peaks and wear-and-tear of the mechanical parts due to large shaft speeds. The anti-spin algorithm avoids an excessive increase of the shaft speed when high torque losses are detected by setting desired shaft speed to a constant value. When the loss situation is considered over the desired shaft speed is set to normal values.

Ventilation Detection

The ventilation incident is detected monitoring the ratio between the estimated propeller torque given by (C.13) and the nominal torque Q_{p_n} computed from the K_Q coefficient through (C.16). The ratio, often termed as the torque reduction coefficient, is written as

$$\hat{\beta}_Q = \alpha(\omega) + (1 - \alpha(\omega)) \frac{\hat{Q}_p}{Q_{p_n}}, \tag{C.23}$$

where

$$\alpha(\omega) = e^{-k|\omega|^p} \tag{C.24}$$

and

$$Q_{p_n} = K_Q \frac{\rho \, |\omega| \, \omega D^5}{4\pi^2}. \tag{C.25}$$

The weighting function $\alpha(\omega)$ with positive tuning gains k and p is used to avoid the singularity of $\hat{Q}_p/Q_{p_n}$ at $\omega = 0$. The nominal value of K_Q in (C.25) is derived from the K_Q characteristic using the nominal value of J computed from (C.14) using the steady-state relation

$$u_a = (1 - w_f)u, \tag{C.26}$$

where $|w_f| < 1$ is the *wake fraction number,* often identified from experimental tests (see e.g. Lewis (1988)) and u is the vessel speed. The wake fraction number accounts for the reduction of the water velocity to the propeller caused by the vessel hull.

The ventilation is detected when the value of $\hat{\beta}_Q$ becomes smaller than a threshold value $\beta_{v,on}$. It is considered terminated when the value of $\hat{\beta}_Q$ becomes larger than $\beta_{v,off}$. The ventilation state, described by the variable ν, is defined as follows:

$$\begin{aligned}
\hat{\beta}_Q \geq \beta_{v,on} \quad &\Rightarrow \quad \nu = 0, \text{ no ventilation} \\
\hat{\beta}_Q < \beta_{v,on} \quad &\Rightarrow \quad \nu = 1, \text{ ventilation on} \\
\hat{\beta}_Q \geq \beta_{v,off} \quad &\Rightarrow \quad \nu = 0, \text{ ventilation off}
\end{aligned}$$

The hysteresis in the ventilation detection is included in order to increase its robustness with respect to measurement noise that could affect the $\hat{\beta}_Q$ estimate. When the propeller works in the 2nd or 4th quadrant of the plane (u_a, ω), the nominal torque model (C.25) may be inaccurate (see Pivano et al. (2006) for example) leading to jumps in the ventilation state. For this reason a ventilation detection is held on for a minimum time T_{hold}.

Anti-spin Action

When the ventilation is detected, the desired shaft speed is defined as follows:

$$\omega_d = \begin{cases} \omega_{v_{opt}} & \text{if } \nu = 1 \text{ and } \omega_d \geq \omega_{v_{opt}} \\ \omega_d & \text{otherwise} \end{cases}$$

The value of $\omega_{v_{opt}}$ is chosen such that the thrust produced by the propeller at $\omega_{v_{opt}}$ is equal or larger than for higher shaft speeds. It may also be chosen according to an optimization criterion based on the estimate of torque loss. Other criteria may include power peaks and the torque oscillations. This is subject to further research.

C.6 Experimental Results

The tests were performed at the MCLab, an experimental laboratory equipped with a towing carriage that can reach a maximum speed of 2 m/s. The rig with motor, underwater housing, shaft and propeller was attached to the towing carriage in order to move it through the water. The propeller was a FPP with diameter 25cm. The real-time system Opal RT-Lab® was used to interface the Matlab/Simulink® environment to the motor drive and the sensors. We employed a three phase brushless motor commanded by a drive equipped with a built-in torque controller sufficiently fast to consider its dynamics neglectable. The thrust was measured with an inductive transducer and the torque was measured with a strain gauge transducer placed on the propeller shaft. A sketch of the setup is shown in Fig. C.4.

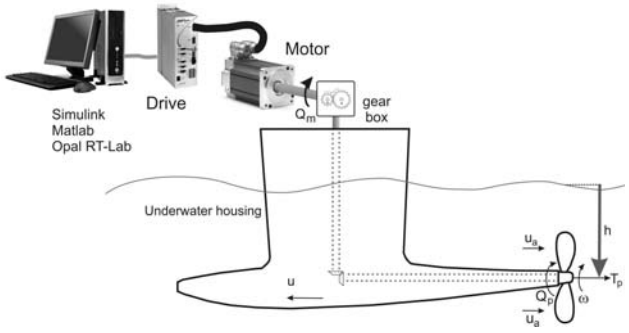

Figure C.4: Sketch of the experimental setup.

The results reported describe one experiment carried out in calm water (to reproduce calm sea conditions) and two conducted in order to reproduce the motion that the propeller may experience

in harsh sea conditions. In all three tests the propeller works in the all four quadrants of the plain (u_a, ω). In order to simulate a realistic scenario the towing carriage speed is first positive when the thrust is positive and then become negative when the thrust is reversed. The advance speed u_a is considered equal to towing carriage speed since the propeller housing does not create a significant wake. The measured propeller thrust and torque, the shaft speed, the motor power and the submergence signals have been filtered with a low pass filter with cut-off frequency of 10Hz.

Fig. C.5 shows data from the calm sea test where the produced thrust T_p tracks well the desired one T_{p_d} despite the changes in the advance speed. Also the shaft speed tracking error is very small. The highest errors occur when reversing the thrust. The flow around the propeller becomes irregular and very fast changes in the torque losses are not captured by the observer. The estimated torque and the measured one are not presented due to lack of space. The commanded motor torque Q_{m_d} is depicted in Fig. C.5 (e).

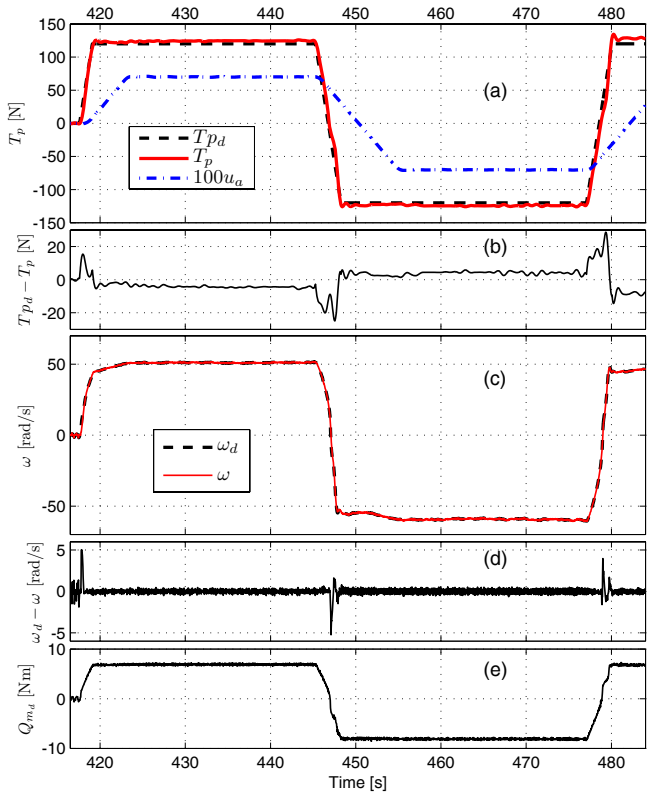

Figure C.5: Undisturbed water test: propeller thrust and advance speed (a), thrust error (b), shaft speed (c), shaft speed error (d) and desired motor torque (e).

Fig. C.6 is relative to the test where the propeller was also moved along its vertical axis. This is done in order to reproduce the flow variations that a propeller may encounter in harsh sea

state due to the motion of the vessel when traveling in waves. In this test, the anti-spin algorithm was employed. The value of $\omega_{v_{opt}}$ has been set equal to 45 rad/s for positive ω and 54 rad/s for negative ω. This choice is done since the produced thrust is asymmetric with respect to the shaft speed. In Fig. C.6 (a) the measured propeller torque and its estimate are plotted showing good agreement. Part (b) of the same figure shows the torque loss reduction used for the ventilation detection. The ventilation state is plotted in Fig. C.6 (c) together with the propeller submergence. The propeller submergence h is defined equal to zero when the center of the propeller is at the water level and positive when the propeller is submerged, as shown in Fig. C.4. The ventilation incident is detected when the propeller moves toward the water surface and the propeller torque has a drop. In Fig. C.6 (e) we can notice that before the ventilation is detected, the controller increases the shaft speed to compensate for the torque loss but when the ventilation is detected the desired speed is set to the $\omega_{v_{opt}}$ value. Also in this situation, despite the shaft load variation, the shaft speed controller furnishes very good performances.

Fig. C.7 shows data from a test similar to the second one where the anti-spin algorithm was disabled. During the ventilation incident the shaft speed increases quickly to the maximum value which was set to 75 rad/s. Comparing these results with the test employing the anti-spin, we can notice that without anti-spin the propeller thrust fluctuates more and, even if the shaft speed is almost double, the produced thrusts when the propeller rotates close to the water surface is practically equal to the one obtained when the anti-spin is enabled. Fig. C.8 shows the measured motor power P_m for the three tests. The controller without anti-spin presents large power peaks that may not be tolerated by the power generators. Also, without employing the anti-spin strategy, the mean power consumption is larger. Tab. C.1 presents the mean values of the propeller thrust and the consumed power and an energy efficiency number. The mean thrust produced without the anti-spin strategy is slightly larger than with the anti-spin. This is due to the thrust spikes that occur when the ventilation incident is terminating, where the shaft speed is at the maximum value and the propeller submergence increases toward deeply submerged values. The energy efficiency number is given by the ratio between the mean power generated by the propeller and the mean motor power:

$$\eta_E = \frac{mean(T_p \cdot u_a)}{mean(P_m)}. \tag{C.27}$$

The controller with anti-spin increases the energy efficiency of about 20% with respect the case where the anti-spin is not employed.

Table C.1: Mean thrust and power and efficiency number.

Controller	$T_p\ [N]$	$P_m\ [W]$	η_E
Anti-spin	79.2	290	0.151
No anti-spin	89.1	378	0.123

C.7 Conclusion

In this paper a nonlinear thrust controller for a fixed pitch marine propeller with torque loss estimation and anti-spin strategy has been presented. The controller is able to work in the four-

quadrant plane composed by the shaft speed and the vessel speed and is a combination of a thrust controller designed for calm seas and an anti-spin strategy to reduce power peaks and wear-and-tear in extreme sea conditions. The anti-spin algorithm lowers the shaft speed once high torque losses due to ventilation are detected and increases the shaft speed to normal when the loss situation is considered over. The ventilation incident is detected by monitoring the torque losses, estimated with a nonlinear observer. Experiments showed that when large thrust losses occur, the controller that employs the anti-spin algorithm increases the energetic efficiency and reduces the power fluctuation with respect the controller without anti-spin.

C.8 Acknowledgments

The Research Council of Norway is acknowledged as the main sponsor of this project.

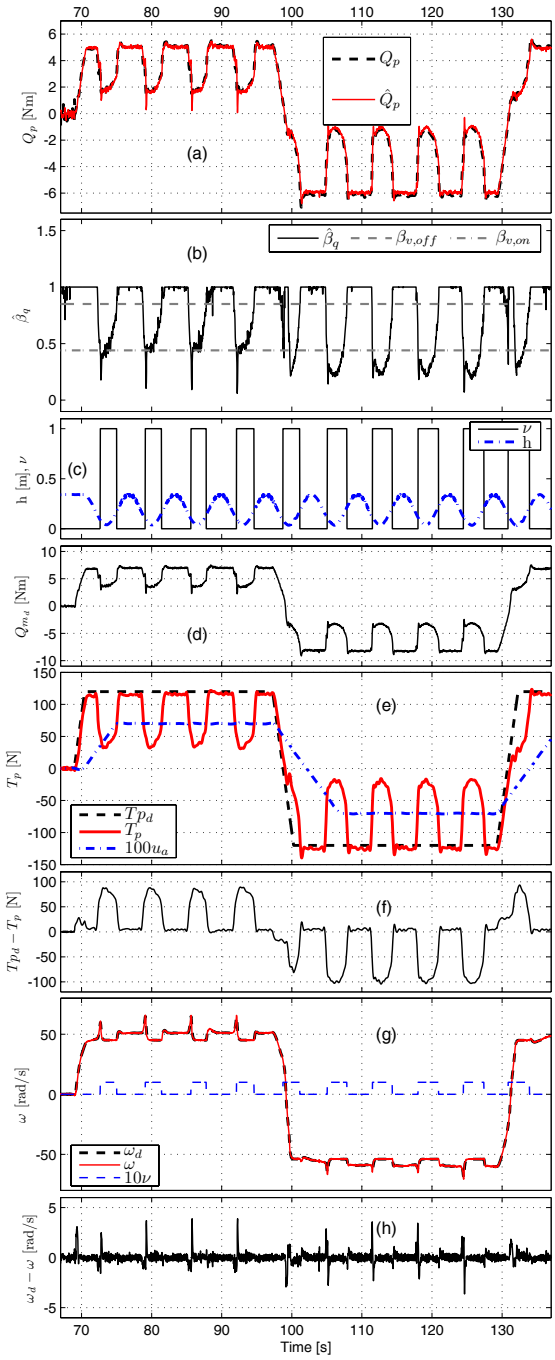

Figure C.6: Test with large thrust losses and anti-spin: propeller torque and its estimate (a), ventilation detection (b) and (c), desired motor torque (d), propeller thrust and advance speed (e), thrust error (f), shaft speed (g) and shaft speed error (h).

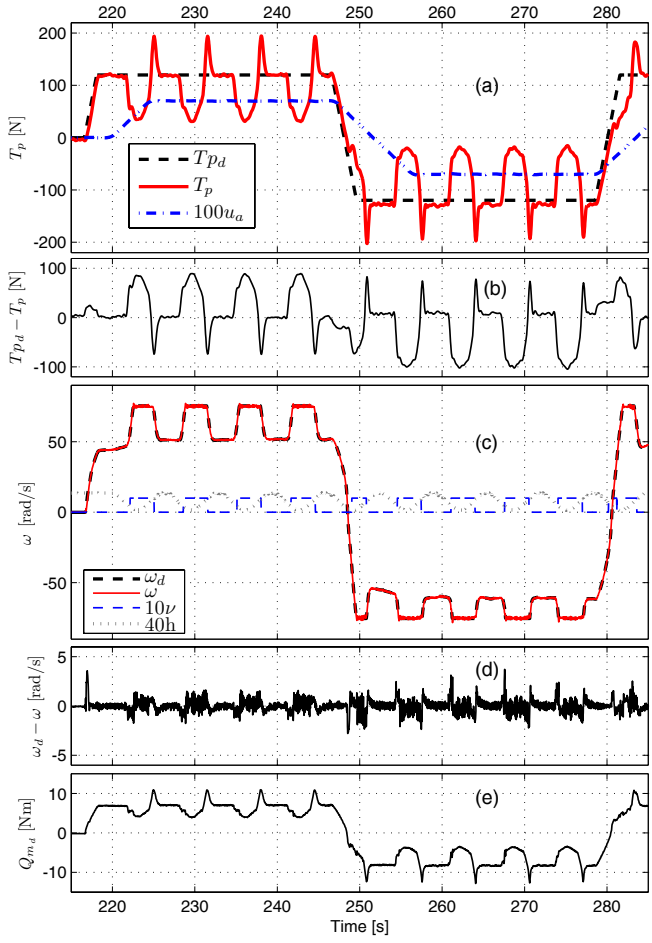

Figure C.7: Test with large thrust losses and without anti-spin: propeller thrust and advance speed (a), thrust error (b), shaft speed (c), shaft speed error (d) and desired motor torque (e).

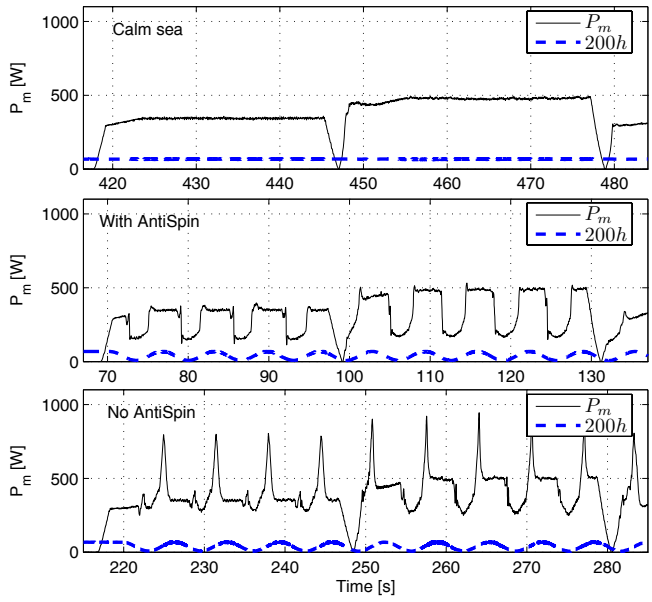

Figure C.8: Motor power in calm water and with large thrust losses (with and without the anti-spin algorithm).

Bibliography

Anderson, B. D. O., Brinsmead, T., Liberzon, D. & Morse, S. (2001), 'Multiple Model Adaptive Control with Safe Switching', *International Journal of Adaptive Control and Signal Processing* **15**, 445–470.

Anderson, B. D. O. & Moore, J. B. (1989), *Optimal Control - Linear Quadratic Methods*, Prentice-Hall.

Artstein, Z. (1983), 'Stabilization with Relaxed Controls', *Nonlinear Analysis* **7**(11), 1163–1173.

Athans, M., Castañon, D., Dunn, K.-P., Greene, C. S., Lee, W. H., Sandell Jr., N. R. & Willsky, A. S. (1977), 'The Stochastic Control of the F-8C Aircraft Using a Multiple Model Adaptive Control (MMAC) Method-Part I: Equilibrium Flight', *IEEE Transactions on Automatic Control* **22**(5), 768–780.

Bakkeheim, J. & Johansen, T. A. (2006), 'Transient Performance, Estimator Resetting and Filtering in Nonlinear Multiple Model Adaptive Backstepping Control', *IEE Proceedings - Control Theory & Applications* **153**(5), 536–545.

Bakkeheim, J., Johansen, T. A., Smogeli, Ø. N. & Sørensen, A. J. (2008), 'Lyapunov-based Integrator Resetting with Application to Marine Thruster Control', *IEEE Transactions on Control Systems Technology* . Accepted.

Bakkeheim, J., Murray-Smith, R. & Johansen, T. A. (2005), Nonparametric Identification of Linearizations and Uncertainty using Gaussian Process Models - Application to Robust Wheel Slip Control, *in* 'Preceedings of the IEEE Conference on Decision and Control (CDC'05)', Seville, Spain.

Bakkeheim, J., Pivano, L., Johansen, T. A. & Smogeli, Ø. N. (2007), Integrator Reset Anti-spin for Marine Thrusters Operating in Four-Quadrants and Extreme Sea Conditions, *in* 'Proceedings of the IFAC Conference on Control Applications in Marine Systems (CAMS'07)', Bol, Croatia.

Bakkeheim, J., Smogeli, Ø. N., Johansen, T. A. & Sørensen, A. J. (2006), Improved Transient Performance by Lyapunov-based Integrator Reset of PI Thruster Control in Extreme Seas, *in* 'Proceedings of the IEEE Conference on Decision and Control (CDC'06)', San Diego, USA.

Bakker, E., Nyborg, L. & Pacejka, H. B. (1987), Tyre Modelling for Use in Vehicle Dynamic Studies, Technical Report 870421, Society of Automotive Engineers, Warrendale PA.

Beker, O., Hollot, C. V. & Chait, Y. (2004), 'Fundamental Properties of Reset Control Systems', *Automatica* **40**(6), 905–915.

Blanke, M. & Nielsen, P. B. (1990), The Marine Engine Governor, *in* 'Proceedings of the 2nd International Conference on Maritime Communications and Control', London, UK, pp. 11–20.

Branicky, M. S. (1998), 'Multiple Lyapunov Functions and Other Analysis Tools for Switched and Hybrid Systems', *IEEE Transactions on Automatic Control* **43**(4), 475–482.

Burckhardt, M. (1993), *Fahrwerktechnik: Radschlupf-Regelsysteme*, Vogel Verlag.

Carlton, J. S. (1994), *Marine Propellers & Propulsion*, Butterworth-Heinemann Ltd.

Cezayirli, A. & Ciliz, K. (2004), Multiple Model Based Adaptive Control of a DC Motor under Load Changes, *in* 'Proceedings of Mechatronics, ICM '04', Istanbul, Turkey, pp. 328 – 333.

Cezayirli, A. & Ciliz, K. (2006), Adaptive Tracking for Nonlinear Plants Using Multiple Identification Models and State-Feedback, *in* 'Proceedings of IEEE Industrial Electronics (IECON'06)', Paris, France, pp. 19–24.

Chaudhuri, B., Majumder, R. & Pal, B. (2004), 'Application of Multiple-Model Adaptive Control Strategy for Robust Damping of Interarea Oscillations in Power System', *IEEE Transaction on Control Systems Technology* **12**(5), 727–736.

Chen, L. & Narendra, K. S. (2001), 'Nonlinear Adaptive Control using Neural Networks and Multiple Models', *Automatica* **37**(8), 1245–1255.

Ciliz, M. K. & Cezayirli, A. (2006), 'Increased Transient Performance for the Adaptive Control of Feedback Linearizable Systems Using Multiple Models', *International Journal of Control* **79**(10), 1205–1215.

Clegg, J. C. (1958), 'A Nonlinear Integrator for Servomechanisms', *Transactions A.I.E.E., Part II, Applications and Industry* **77**, 41–42.

Daiss, A. & Kiencke, U. (1996), Estimation of Tyre Slip During Combined Cornering and Braking Observer Supported Fuzzy Estimation, *in* 'Proceedings of the 13th IFAC World Congress', San Francisco, USA, pp. 41–46.

Decarlo, R. A., Branicky, M. S., Pettersson, S. & Lennartson, B. (2000), Perspectives and Results on the Stability and Stabilizability of Hybrid Systems, *in* 'Proceedings of IEEE, Special Issue on Hybrid Systems', Vol. 88, pp. 1069–1082.

Dougherty, D., Arbogast, J. & Cooper, D. (2003), A Multiple Model Adaptive Control Strategy for DMC, *in* 'Proceedings of the American Control Conference (ACC'03)', Denver, Colorado.

Fossen, T. I. (2002), *Marine Control Systems*, 1st edn, Marine Cybernetics.

Fossen, T. I. & Blanke, M. (2000), 'Nonlinear Output Feedback Control of Underwater Vehicle Propellers Using Feedback From Estimated Axial Flow Velocity', *IEEE Journal of Oceanic Engineering* **25**(2), 241–255.

Garulli, A., Tesi, A. & Vicino, A., eds (1999), *Robustness in Identification and Control*, Springer-Verlag. Number 245 in Lecture notes in Control and Information Sciences.

Girard, A., Rasmussen, C. E., Candela, J. Q. & Murray-Smith, R. (2003), Gaussian Process Priors with Uncertain Inputs – Application to Multiple-Step Ahead Time Series Forecasting, *in* S. T. S. Becker & K. Obermayer, eds, 'Advances in Neural Information Processing Systems 15', MIT Press, Cambridge, MA, pp. 529–536.

Goebel, R., Hespanha, J., Teel, A. R., Cai, C. & Sanfelice, R. (2004), Hybrid Systrems: Generalized Solutions and Robust Stability, *in* 'Proceedings of the IFAC Symposium on Nonlinear Control Systems', Stuttgart, Germany.

Guibert, C., Foulon, E., Aït-Ahmed, N. & Loron, L. (2005), 'Thrust Control of Electric Marine Thrusters', *Industrial Electronics Society. IECON 2005. 32nd Annual Conference of IEEE* .

Hansen, J. & Johansen, T. A. (2004), Transient Performance, Resetting and Filtering in Nonlinear Multiple Model Adaptive Control, *in* 'Proceedings of the American Control Conference (ACC'04)', Boston, Massachusetts.

Haskara, I., Özgüner, U. & Winkelman, J. (2000), 'Wheel Slip Control for Antispin Acceleration via Dynamic Spark Advance', *Control Engineering Practice* **8**, 1135–1148.

Hespanha, J. (2003), 'Hysteresis-based Switching Algorithms for Supervisory Control of Uncertain Systems', *Automatica* **39**, 263–272.

Hespanha, J. P. (1998), Logic-Based Switching Algorithms in Control, PhD thesis, Dept. of Electrical Eng., Yale University, New Haven, CT.

Hespanha, J. P. & Morse, A. S. (1999), Stability of switched systems with average dwell-time, *in* 'Proceedings of the IEEE Conference on Decision and Control (CDC'99)', pp. 2655–2660.

Horowitz, I. & Rosenbaum, P. (1975), 'Non-linear Design for Cost of Feedback Reduction in Systems with Large Parameter Uncertainty', *International Journal of Control* **21**(6), 977–1001.

Ioannou, P. & Sun, J. (1996), *Robust Adaptive Control*, Prentice Hall.

Jiang, F. & Gao, Z. (2001), An Application of Nonlinear PID Control to a Class of Truck ABS Problems, *in* 'Proceedings of the IEEE Conference on Decision and Control (CDC'01)', Orlando.

Johansen, T. A., Hunt, K., Gawthrop, P. J. & Fritz, H. (1998), 'Off-equilibrium Linearisation and Design of Gain Scheduled Control with Application to Vehicle Speed Control', *Control Engineering Practice* **6**, 167–180.

Kalkkuhl, J., Johansen, T. A. & Lüdemann, J. (2002), 'Improved Transient Performance of Nonlinear Adaptive Backstepping Using Estimator Resetting Based on Multiple Models', *IEEE Transactions on Automatic Control* **47**(1), 136–140.

Kalkkuhl, J., Johansen, T. A., Lüdemann, J. & Queda, A. (2001), Nonlinear Adaptive Backstepping with Estimator Resetting Using Multiple Observers, *in* 'Proceedings of Workshop on Hybrid Systems, Computation and Control', Rome, Italia.

Khalil, H. K. (2002), *Nonlinear Systems*, 3rd edn, Prentice-Hall, New Jersey.

Kocijan, J., Murray-Smith, R., C.Rasmussen & Girard, A. (2004), Gaussian Process Model Based Predictive Control, *in* 'Proceedings of the American Control Conference (ACC'04)', Boston, Massachusetts.

Krishnan, K. R. & Morowitz, I. M. (1974), 'Synthesis of a Non-linear Feedback System with Significant Plant-ignorance for Prescribed System Tolerance', *International Journal of Control* **19**(4), 689–706.

Krstic, M., Kanellakopoulos, I. & Kokotovic, P. (1995), *Nonlinear and Adaptive Control Design*, John Wiley & Sons, Inc, New York.

Lauvdal, T. & Ådnanes, A. K. (2000), 'Power Management System with Fast Acting Load Reduction for DP Vessels', *Dynamic Positioning Conference* .

Leith, D. J., Leithead, W. E., Solak, E. & Murray-Smith, R. (2002), Divide & Conquer Identification: Using Gaussian Process Priors to Combine Derivative and Non-derivative Observations in a Consistent Manner, *in* 'Proceedings of the Conference on Decision and Control (CDC'02)'.

Leith, D. J., Murray-Smith, R. & Leithead, W. E. (2000), Nonlinear Structure Identification: A Gaussian Process Prior/Velocity-based Approach, *in* 'Proceedings of Control 2000, Cambridge'.

Lewis, E. V. (1988), *Principles of Naval Architecture Vol II: Resistance, Propulsion and Vibration*, 3rd edn, Society of Naval Architects and Marine Engineers, New York.

Liberzon, D. (2003), *Switching in Systems and Control*, 1st edn, Birkhuser.

Liberzon, D. & Morse, A. (1999), 'Basic Problems in Stability and Design of Switched Systems', *IEEE Control Systems Magazine* **19**(5), 59–70.

Lüdemann, J. (2002), Heterogeneous and Hybrid Control with Application in Automotive Systems, PhD thesis, University of Glasgow.

Maciejowski, J. M. (2002), *Predictive Control with Constraints*, Prentice-Hall, England.

Mårtensson, B. (1986), Adaptive Stabilozation, PhD thesis, Lund Institute of Technology.

Middleton, R. H., Goodwin, G. C., Hill, D. J. & Mayne, D. Q. (1988), 'Design Issues in Adaptive Control', *IEEE Transactions on Automatic Control* **33**(1), 50–58.

Minsaas, K. J., Thon, H. J. & Kauczynski, W. (1987), Estimation of Required Thruster Capacity for Operation of Offshore Vessels under Severe Weather Conditions, *in* 'Proceedings of the 3rd International Symposium on Practical Design of Ship and Mobile Units (PRADS'87)', Trondheim, Norway, pp. 411–427.

Morse, A. S. (1996), 'Supervisory Control of Families of Linear Set-point Controllers-Part1: Exact Matching', *IEEE Transactions on Automatic Control* **41**(10), 1413–1431.

Morse, A. S., Mayne, D. Q. & Goodwin, G. C. (1992), 'Applications of Hysteresis Switching in Parameter Adaptive Control', *IEEE Transactions on Automatic Control* **37**(9), 1343–1354.

Murray-Smith, R. & Girard, A. (2001), Gaussian Process Priors with ARMA Noise Models, *in* 'Proceedings of the Irish Signals and Systems Conference, Maynooth', pp. 147–152.

Murray-Smith, R., Johansen, T. A. & Shorten, R. (1999), On Transient Dynamics, Off-equilibrium Behaviour and Identification in Blended Multiple Model Structures, *in* 'Proceedings of the European Control Conference (ECC'99)', Karlsruhe, Germany.

Murray-Smith, R. & Sbarbaro, D. (2002), Nonlinear Adaptive Control using Non-parametric Gaussian Process Prior Models, *in* 'Proceedings of the 15th IFAC World Congress on Automatic Control', Barcelona.

Murray-Smith, R. & Shorten, R. (2005), *Proceedings of the Hamilton Summer School on Switching and Learning in Feedback Systems*, Vol. 3355, Springer-Verlag, Lecture Notes in Computing Science.

Narendra, K. S. & Balakrishnan, J. (1994), 'Improving Transient Response of Adaptive Control Systems Using Multiple Models and Switching', *IEEE Transactions on Automatic Control* **39**(9), 1861–1866.

Narendra, K. S. & Balakrishnan, J. (1997), 'Adaptive Control Using Multiple Models', *IEEE Transactions on Automatic Control* **42**(2), 171–187.

Narendra, K. S., Balakrishnan, J. & Ciliz, M. K. (1995), 'Adaptation and Learning Using Multiple Models, Switching, and Tuning', *IEEE Control Systems Magazine* **15**(3), 37–51.

Narendra, K. S. & George, K. (2002), Adaptive Control of Simple Nonlinear Systems Using Multiple Models, *in* 'Proceedings of the American Control Conference (ACC'02)', pp. 1779–1784.

O'Hagan, A. (1978), 'On Curve Fitting and Optimal Design for Regression (with Discussion)', *Journal of the Royal Statistical Society B* **40**, 1–42.

O'Hagan, A. (1992), Some Bayesian Numerical Analysis, *in* J. M. Bernardo, J. O. Berger, A. P. Dawid & A. F. M. Smith, eds, 'Bayesian Statistics 4', Oxford University Press, pp. 345–363.

Pacejka, H. B. & Sharp, R. S. (1991), 'Shear Force Developments by Pneumatic Tyres in Steady-State Conditions: A review of Modeling Aspects', *Vehicle Systems Dynamics* **29**, 409–422.

Parks, P. C. (1966), 'Lyapunov redesign of mode reference adaptive control systems', *IEEE Transactions on Automatic Control* **11**(3), 362–367.

Petersen, I. (2003), Wheel Slip Control in ABS Brakes using Gain Scheduled Optimal Control with Constraints, PhD thesis, Norwegian University of Science and Technology.

Pivano, L., Bakkeheim, J., Johansen, T. A. & Smogeli, Ø. N. (2008), A Four-Quadrant Thrust Controller for Marine Propellers with Loss Estimation and Anti-Spin, *in* 'Proceedings of the 17th IFAC World Congress', Seoul, Korea. Accepted.

Pivano, L., Johansen, T. A., Smogeli, Ø. N. & Fossen, T. I. (2007), Nonlinear Thrust Controller for Marine Propellers in Four-quadrant Operations, *in* 'Proceedings of the American Control Conference (ACC'07)', New York, USA.

Pivano, L., Smogeli, Ø. N., Johansen, T. A. & Fossen, T. I. (2006), Experimental Validation of a Marine Propeller Thrust Estimation Scheme, *in* 'Proceedings of the 7th IFAC Conference on Manoeuvring and Control of Marine Craft (MCMC'06)', Lisbon, Portugal.

Radan, D., Smogeli, Ø. N., Sørensen, A. J. & Ådnanes, A. K. (2006), Operating Criteria for Design of Power Management Systems on Ships, *in* 'Proceedings of the 7th IFAC Conference on Manoeuvring and Control of Marine Craft (MCMC'06)', Lisbon, Portugal.

Radan, D., Sørensen, A. J., Ådnanes, A. K. & Johansen, T. A. (2007), 'Reducing Power Load Fluctuations on Ships using Power Redistribution Control', *Marine Technology Journal-SNAME* . Accepted.

Rasmussen, C. E. (1996), Evaluation of Gaussian Processes and other Methods for Non-Linear Regression, PhD thesis, Graduate department of Computer Science, University of Toronto.

Rasmussen, C. E. (2003), Gaussian Processes to Speed up Hybrid Monte Carlo for Expensive Bayesian Integrals, *in* J. M. Bernardo, J. O. Berger, A. P. Dawid, D. Heckerman, A. F. M. Smith & M. West, eds, 'Bayesian Statistics 7', Oxford University Press, pp. 651–659.

Reinelt, W., Garulli, A. & Ljung, L. (2002), 'Comparing Different Approaches to Model Error Modelling in Robust Identification', *Automatica* **38**(5), 787–803.

Rugh, W. (1991), 'Analytical Framework for Gain Scheduling', *IEEE Control Systems Magazine* **11**(1), 79–84.

Sciavicco, L. & Siciliano, B. (2000), *Modelling and Control of Robot Manipulators*, Springer-Verlag, London.

Skogestad, S. & Postlethwaite, I. (1996), *Multivariable Feedback Control: Analysis and Design*, John Wiley & Sons.

Slotine, J.-J. E. & Li, W. (1991), *Applied Nonlinear Control*, Prentice Hall.

Smogeli, Ø. N. (2006), Control of Marine Propellers: from Normal to Extreme Conditions, PhD thesis, Norwegian University of Science and Technology, Trondheim, Norway.

Smogeli, Ø. N., Aarseth, L., Overå, E. S., Sørensen, A. J. & Minsaas, K. J. (2003), Anti-Spin Thruster Control in Extreme Seas, *in* 'Proceedings of the 6th IFAC Conference on Manoeuvring and Control of Marine Craft (MCMC'03)', Girona, Spain, pp. 221–226.

Smogeli, Ø. N., Hansen, J., Sørensen, A. J. & Johansen, T. A. (2004), Anti-spin Control for Marine Propulsion Systems, *in* 'Proceedings of the IEEE Conference on Decision and Control (CDC'04)', Bahamas.

Smogeli, Ø. N., Ruth, E. & Sørensen, A. J. (2005), Experimental Validation of Power and Torque Thruster Control, *in* 'Proceedings of the IEEE 13th Mediterranean Conference on Control and Automation (MED'05)', Limassol, Cyprus, pp. 1506–1511.

Smogeli, Ø. N. & Sørensen, A. J. (2006), 'Anti-spin Thruster Control for Ships', *Automatica* . Accepted.

Smogeli, Ø. N., Sørensen, A. J. & Fossen, T. I. (2004), Design of a Hybrid Power/Torque Thruster Controller with Thrust Loss Estimation, *in* 'Proceedings of the IFAC Conference on Control Applications in Marine Systems (CAMS'04)', Ancona, Italy.

Smogeli, Ø. N., Sørensen, A. J. & Minsaas, K. J. (2006), 'The Concept of Anti-spin Thruster Control', *Control Engineering Practice* . To appear.

Solak, E., Murray-Smith, R., Leithead, W. E., Leith, D. J. & Rasmussen, C. E. (2003), Derivative Observations in Gaussian Process Models of Dynamic Systems, *in* S. T. S. Becker & K. Obermayer, eds, 'Advances in Neural Information Processing Systems 15', MIT Press, Cambridge, MA, pp. 1033–1040.

Solyom, S. (2004), Control of Systems with Limited Capacity, PhD thesis, Lund Institute of Technology.

Sontag, E. D. (1983), 'A Lyapunov-like Characterization of Asymptotic Controllability', *SIAM J. Control and Optimization* **21**(3), 462–471.

Sontag, E. D. (1989), 'A 'Universal' Construction of Artstein's Theorem on Nonlinear Stabilization', *Systems & Control Letters* **13**(2), 117–123.

Sørensen, A. J. (2005), 'Structural Issues in the Design and Operation of Marine Control Systems', *IFAC Journal of Annual Reviews in Control* **29**(1), 125–149.

Sørensen, A. J., Ådnanes, A. K., Fossen, T. I. & Strand, J. P. (1997), A New Method of Thruster Control in Positioning of Ships based on Power Control, *in* 'Proceedings of the 4th IFAC Conference on Manoeuvring and Control of Marine Craft (MCMC'97)', Brijuni, Croatia, pp. 172–179.

Utkin, V. (1977), 'Variable Structure Systems with Sliding Modes', *IEEE Transactions on Automatic Control* **22**(2), 212–222.

Utkin, V., Guldner, J. & Shi, J. (1999), *Sliding Mode Control in Electromechanical Systems*, Taylor & Francis, London.

Van Lammeren, W. P. A., Manen, J. D. V. & Oosterveld, M. W. C. (1969), 'The Wageningen B-Screw Series', *Transactions of SNAME* .

Vysohlid, M. & Mahesh, K. (2004), 'Large-Eddy Simulation of Propeller Crashback', *APS Meeting Abstracts* .

Wang, Y., Schmitt-Hartmann, T., Schinkel, M. & Hunt, K. J. (2001), A New Approach to Simultanious Stabilisation and Strong Simultanious Stabilisation with D Stability and its Application to ABS Control Systems Design, *in* 'Proceedings of the IEEE European Control Conference (ECC'01)', Porto, Portugal.

Whitcomb, L. L. & Yoerger, D. (1999*a*), 'Developement, Comparison, and Preliminary Experimental Validation of Nonlinear Dynamic Thruster Models', *IEEE Journal of Oceanic Engineering* **24**(4), 481–494.

Whitcomb, L. L. & Yoerger, D. R. (1999*b*), 'Preliminary Experiments in Model-Based Thruster Control for Underwater Vehicle Positioning', *IEEE Journal of Oceanic Engineering* **24**(4), 495–506.

Williams, C. K. I. (1998*a*), 'Computation with Infinite Neural Networks', *Neural Computation* **10**, 1203–1216.

Williams, C. K. I. (1998*b*), Prediction with Gaussian Processes: From Linear Regression to Linear Prediction and Beyond, *in* M. I. Jordan, ed., 'Learning and Inference in Graphical Models', Kluwer, pp. 599–621.

Xiushan, C., Xiaodong, W. & Haoran, Z. (2007), 'Universal Construction of control Lyapunov Functions for a Class of Nonlinear Systems', *Journal of Systems Engineering and Electronics* **18**(3), 598–602.

Zhivoglyadov, P. V., Middleton, R. H. & Fu, M. (2000), 'Localization Based Switching Adaptive Control for Time-varying Discrete-time Systems', *IEEE Transactions on Automatic Control* **45**(4), 752–755.

Zhou, K., Doyle, J. & Glover, K. (1996), *Robust and Optimal Control*, Prentice-Hall.